2017

Multiple input multiple output modified positive position feedback control for an excited liquid impounding plate

Joshua Bradley Mervyn Cox
University of Wollongong

Multiple Input Multiple Output Modified Positive Position Feedback Control for an Excited Liquid Impounding Plate

A Thesis Submitted in fulfilment of the requirements for the award of the degree

Master of Philosophy (Mechatronics)

From

University of Wollongong

By

Joshua Bradley Mervyn Cox, B.Eng. (Mechatronics)

Faculty of Engineering and Information Sciences,

School of Mechanical, Materials and Mechatronic Engineering

January 2017

Acknowledgements

I would like to thank my supervisor and co-supervisor Professor Gursel Alici, and Doctor Shahid Hussain respectively, for their feedback and assistance in the preparation and writing of this thesis, and for spending time in assisting me whenever needed.

I would like to thank Tanju Yildirim, for his assistance in my learning of essential software components such as LabVIEW and Comsol, assisting in my preliminary understanding of the dynamics involved, and assisting in any experimental issues that may have arisen throughout this thesis.

I would also like to thank my former supervisor Doctor Mergen HajGhayesh for granting me a professional experience position as a researcher, wherein I learned and completed work that would become the foundation of the research conducted for this thesis.

I express my gratitude to the examiners of this thesis, and thank them for their valuable time and any forthcoming comments or feedback.

Abstract

A new modified positive position feedback (M-PPF) controller is proposed as an improved alternative to the positive position feedback controller for use in circumstances where greater control over the damped frequency range is required.

An experimental investigation was conducted using a system consisting of a fully clamped thin aluminium plate mounted to the front face of a cubic steel tank, which was filled with 9 varying amounts of water. The plate was excited via an electromagnetic shaker, and the controller was implemented to attempt to reduce amplitudes for the first four modal frequencies of the plate using an array of sensor/actuator pairs of piezoelectric patches.

It is shown that the M-PPF method can effectively control the first four modes of the system for various water levels, and it is shown in comparison within the literature, that it can be tuned more accurately and precisely than traditional PPF controllers as hypothesised. The overall average amplitude reduction was seen to be 14.8%.

Plate modal frequency and amplitude effects due to changing levels of water were explored. It is found that, in general, modal frequencies follow an overall linear decreasing trend as the water level increases, due to the damping effect the water has on the plate. Strain amplitudes were seen to follow a decreasing trend for the first and fourth mode, and a less prominent, increasing trend for the second and third modes. Amplitude for all modes after the first seems to vary somewhat sporadically, as oscillation at lower amplitudes, as is the case for these modes, is more readily influenced by the movement of the fluid.

List of Abbreviations

BF	Bandpass filter
CAD	Computer aided design
DMA	Direct memory access
DVF	Direct velocity feedback
FIFO	First in first out
FPGA	Field programmable gate array
MFC	Macro Fibre Composite
MIMO	Multiple input multiple output
M-PPF	Modified positive position feedback
NI-cRIO	National Instruments compact real time input / output
NI-DAQ	National Instruments data acquisition
PID	Proportional integral derivative control
PPF	Positive position feedback
PVDF	Polyvinylidene fluoride
PZT	Lead zirconate titanate
SISO	Single input single output
VCM	Voice coil motor
VI	Virtual instrument (LabVIEW)

List of Figures

List of Tables

Contents

Chapter 1 Introduction

Control of undesirable vibration is a recurrent issue in dynamic systems; generally, the most effective solution is to design the system with appropriate levels of damping to avoid such motion, however, this is not always possible or plausible, due to weight, size or space restrictions. In such circumstances, it is beneficial to use semi-active and active motion suppression methods. In systems such as these, including; precision manufacturing equipment, such as CNC machines and 3D printers, sensitive marine and aerospace equipment, and containers holding delicate or volatile substances, the addition of a relatively small and non-intrusive motion controllers to the main structural components can significantly reduce the unwanted motion [1]. In this study, a new modified positive position feedback control method is proposed and tested experimentally to control vibrations in a fully clamped, fluid impounding plate, with varying levels of fluid.

1.1 Dynamics of plates in contact with fluid

The dynamics of vibrating plates in contact with and/or impounded by a fluid has been studied extensively, both theoretically [2-5], and experimentally[6, 7]. In most cases, including the focus of this study, the expected first four eigenmode shapes for a fully clamped thin plate are expected to be; (1-1), (2-1), (1-2), and (2-2), respectively [7] as shown in Figure 1.1.

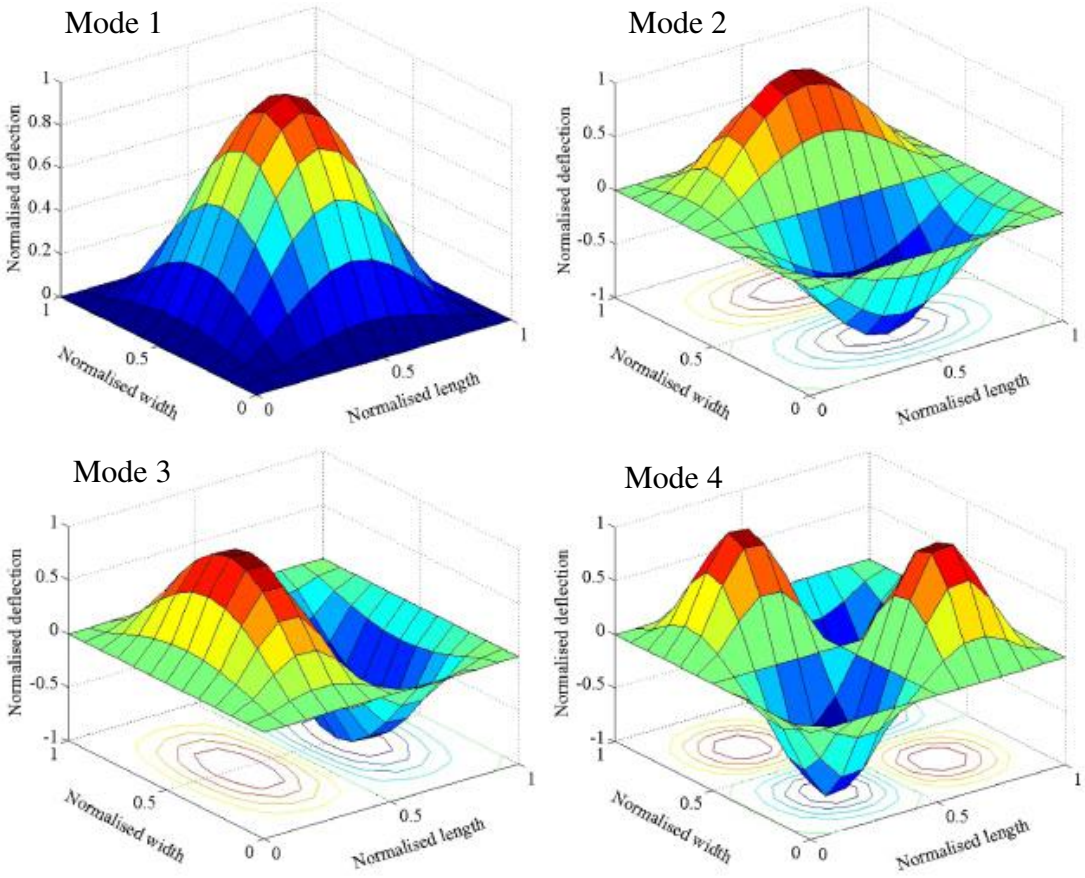

Figure 1.1 – First 4 modes of a fully clamped plate [8]

In the case where the plate is not in contact with fluid, and the plate is square, such as in the initial case of the current study, it is seen that the second and third modes will occur at the same frequency [6, 9], this is expected and can be seen from the equation of the natural frequency of an isotropic plate in the absence of in plane stress [10]:

$$\omega_{mn} = \pi \sqrt{\frac{D}{\hat{m}}} \left(\frac{m^2}{a^2} + \frac{n^2}{b^2} \right)^2 \qquad (1.1)$$

From eq. (1.1) it can be seen that when length and width (*a* and *b*) are equal, mode shapes (*m*-*n*) that are inversed, i.e. (1-2) and (2-1), will have the same natural frequency. As more fluid is added and impounded by the plate, the frequency locations of the eigenmodes are expected to change, [4] and the 2nd and 3rd modes will become more distinct. This is due to the changing dynamics of the plate caused by the added mass, and damping, introduced by the fluid structure interaction and the subsequent hydrostatic forces [7]. It has been shown that the shapes of the modes vary only slightly when changing fluid levels, which means optimal sensor/actuator placement can be determined for the initial case and then used for any fluid level [7].

1.2 Methods of Sensing and Actuation for Vibration Control

Many sensing and actuation methods for controlling systems in oscillatory motion have been used in the past, common sensors include; strain gauges, optical sensors, and piezoelectric stacks and patches. Commonly used actuators include; electromagnetic actuators and various types of piezoelectric stacks, composites and patches.

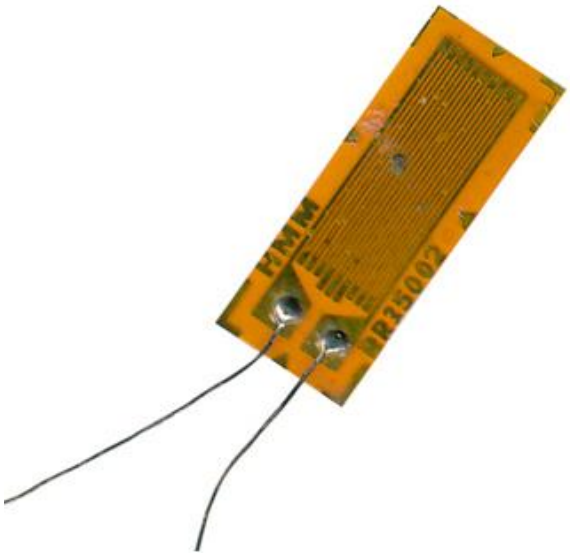

Figure 1.2 – Metal-foil resistance strain gauge [11, 12]

Metal-foil resistance strain gauges are a very common, cheap and relatively inconspicuous method of measuring strain, or in some cases by derivation, displacement. Strain gauges are advantageous as they are a cheap, compact, and simple way to measure strain. When correctly calibrated, they have a fairly high resolution of around 5μ strain [13]. They have seen extensive usage in slow moving dynamic or static systems, as sensing is not effected by a low rate of strain, due to their resistor like properties. The disadvantages of strain gauges however, are that they are highly susceptible to environmental factors, including humidity, and especially heat, and are highly susceptible to signal noise, due to their low signal voltage, commonly in the order of mV or even μV [14]. Strain gauges have been effectively used as the primary sensor in many vibration control systems [15, 16], and have even seen usage in studying piezoelectric strain sensors [17].

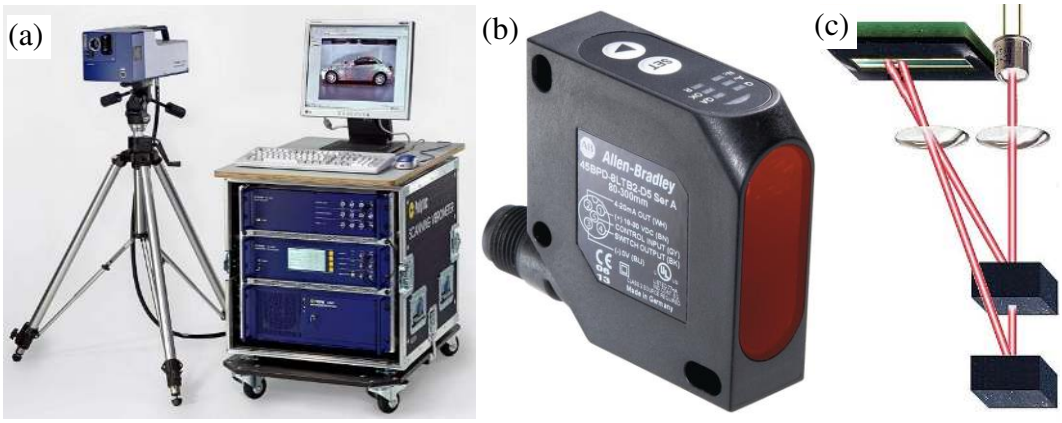

Figure 1.3 – Optical sensors: a) vibrometer[18] b) distance sensor[19] c) operation[20]

Optical sensors, such as laser distance sensors and laser vibrometers are a common, highly accurate and unobtrusive method of sensing vibrations. This style of sensing has major advantages in its superior precision, with resolutions up to 1nm [21], and its low impact on the system in question, due to their non-contact nature. Optical sensors also, in general have vastly longer life cycles, due to their detachment from the dynamic system, and lack of moving parts. These sensors are highly useful for extremely precise systems that require highly detailed data, for example, in depth studies on the dynamics of a system [22]. The disadvantages of optical sensors are that that they are generally expensive, relatively large and bulky devices, that require a relatively large amount of power compared to other sensors. It is also necessary to place these sensors separate from the system to be measured, and the system has to be observable from the sensor. These requirements prevent or inhibit their usage in any systems where space is an issue, or if the system is optically enclosed.

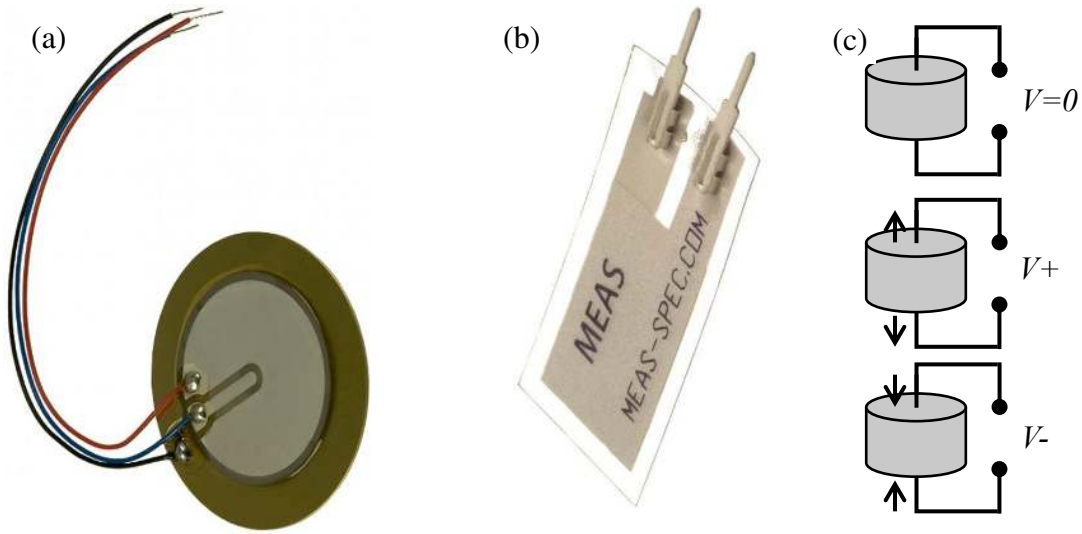

Figure 1.4 – PZT(a)[23], PVDF(b)[24], and operation(c) of piezoelectric Sensors

Piezoelectric materials have seen extensive usage as numerous types of sensors to measure pressure, force, strain and many other environmental properties, they are highly energy efficient and precise. For sensing strain, there are two main types of piezoelectric sensors; monolithic lead zirconate titanates (PZT) and polyvinylidene fluoride (PVDF). PZT has much higher piezoelectric coefficients, in the order of around 10 times more than PVDF, however PVDF is much more flexible, having a Young's modulus of around 5GPa, which is about a twelfth of monolithic PZT, making it a better choice as a sensor in systems that could be influenced by the sensor's stiffness [17]. Piezoelectric strain sensors tend to have a strain resolution similar to that of conventional foil strain gauges, but much better noise to signal ratios, due to their relatively high signal voltage, in the range of multiple to tens of volts, and in the case of PZT, less variation from environmental factors [17]. Piezoelectric sensors are very effective at sensing highly dynamic behaviour in systems, which makes them ideal for vibration control systems such as that in the current study. Piezoelectric strain sensors, however are detrimental in relatively static systems, as they act theoretically similar to capacitors, in that the induced energy will discharge from the sensor, and give inaccurate results if strain rate is too gradual [25].

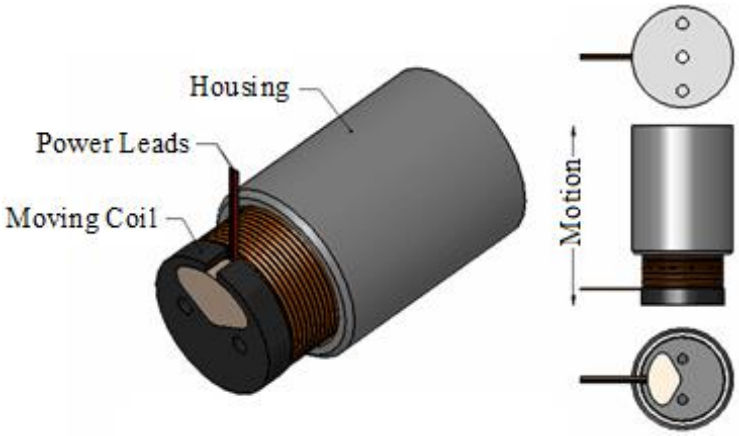

Figure 1.5 – Voice coil linear motor [26]

Electromagnetic actuation for active vibration control has seen extensive use in the past, most commonly, voice coil linear motors (VCMs) [27]. VCMs have the advantages of high accuracy, very fast response times, and high forcing, making them highly effective for motion control [28]. VCMs, however tend to be relatively large, which could interfere with the controlled system, and add undesirable mass. They are also less energy efficient that pure transducers such as piezoceramics, due to heat induced by eddy currents [29].

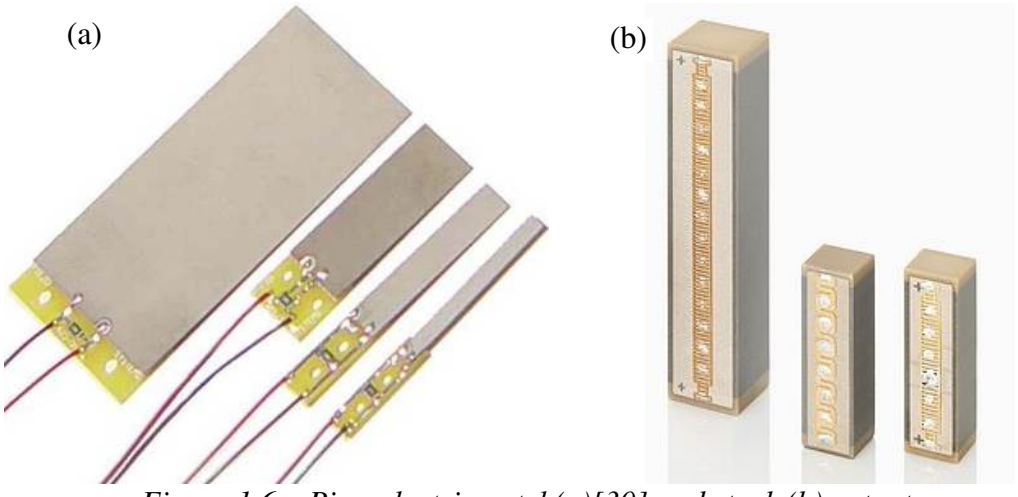

Figure 1.6 – Piezoelectric patch(a)[30] and stack (b) actuators

Piezoelectric actuators in various forms have seen extensive use in vibration control, especially in smaller systems, due to their relatively high forcing to size ratio.

Piezoelectric actuators are highly energy efficient, due to them being close to true transducers, in that practically all electrical energy in converted into mechanical contraction or expansion [14]. Piezoelectric actuators are disadvantageous in larger systems, due to their short travel length, and they also require relatively high voltages compared to other actuators, up to thousands of volts, so specially designed amplifiers are required for effective usage [31].

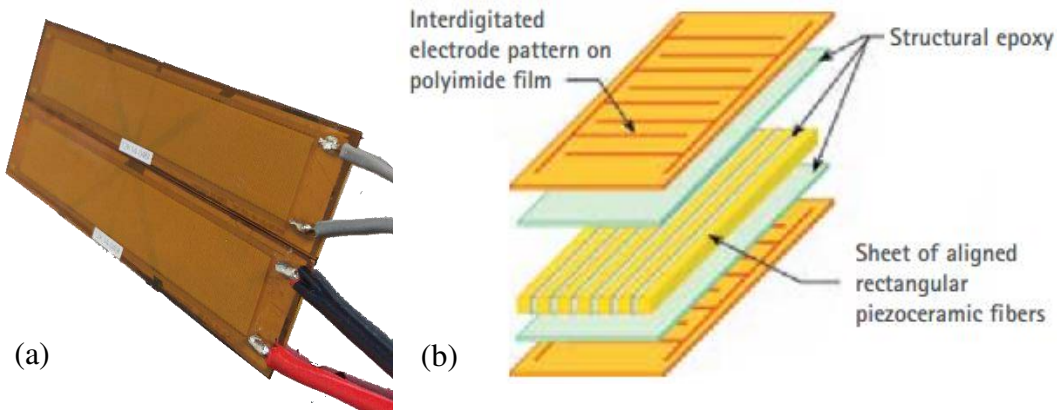

Figure 1.7 – Macro Fibre Composite (MFC): patch(a) construction(b) [32]

Macro fibre composite (MFC) is a combination piezoelectric sensor and actuator, originally proposed by Wilkie et al.[33] and constructed at NASAs Langley research centre as a flexible, high force piezoelectric actuator. MFC was first explored as a dynamic motion sensor by Sodano et al. and was found to be an exceptional sensor [34]. MFC consists of a composite of axially aligned wafers of PZT fibres which are polled and consequently actuated by interlocked electrodes aligned perpendicular to the fibres [33, 35]. The wafer and electrodes are coated by a polyimide resin to strengthen and environmentally seal the MFC. This construction allows for MFC to be much more flexible than standard monolithic PZT, having a modulus of elasticity of ~15Gpa, which makes it four times as flexible, while still retaining the high piezoelectric coefficient typical of PZTs. MFC is more effective than most other piezoelectric actuators, utilising the longitudinal d33 effect, which is about twice the magnitude of the commonly

utilised transversal d31 effect [36]. As an actuator, tests have shown that MFC is powerful and durable capable of large high strains on the order of 2000με at 4000V with no performance reduction for 90 million cycles [33]. MFC is also highly useful as a sensor; compared to other piezoelectric sensors it has the benefits of having a higher piezoelectric coefficient compared to PVDF, and is more flexible than PZT. Due to its light weight, sensitivity, flexibility and high blocking force, MFC has seen extensive usage as an actuator and sensor in light systems [35, 37-40]. It has been chosen in this study as both the sensor and actuator in the system due to its proven effectiveness as both of these in lightweight systems.

1.3 Methods of Vibration Control

Proportional integral derivative (PID) controllers are a very common, and relatively simple control method. The PID controller is a type of feedback method governed by the transfer function [41]:

$$H_{PID}(s) = k_p + \frac{k_i}{s} + k_d s \qquad (1.2)$$

As can be seen in (1.2) the PID controller is regulated by three terms, which are: k_p, the gain proportional to the error, k_i, the integral gain, which will reduce steady state error, but increase overshoot, and k_d, the derivative gain, which will slow the control action but reduce overshoot. PID has seen to be effective in vibration control applications [37], however other more suited control methods are more commonly used.

Direct velocity feedback control (DVF) is another common vibration control method, that has been used extensively before it was surpassed by positive position feedback control [42-44]. DVF is seen as a highly stable controller, capable of high

damping and resistant to changes in system dynamics [44]. It is stable as long as velocity sensor actuator pairs are collocated, and the number of sensor and actuators are equal [43, 45]. DVF is a relatively simple method for implementing active damping. The velocity signal is measured then passed through a gain, then fed back into an actuator [46].

Positive position feedback (PPF) is a prominent and widely used method used for active motion control of dynamic systems [1, 38, 39, 47, 48]. A PPF controller is fundamentally a second order filter, represented by the transfer function [49, 50]:

$$H_{PPF}(s) = \frac{\omega_n^2}{s^2 + 2\zeta\omega_n s + \omega_n^2} \quad (1.3)$$

From (1.3), ω_n represents the desired frequency at which signals should be attenuated, and ζ denotes the desired damping ratio of the controller. In PPF the displacement response (or related) is positively fed back from the sensor through the controller system to give desired displacement which can be applied via a controlled actuator. The control method was first proposed by Goh and Caughey [51] and then explored and tested by Fanson and Caughey [49] as a superior method of dynamic motion stabilisation compared to direct velocity feedback control; the primary advantage of this method is that it is not sensitive to the spill-over phenomenon wherein energy is transferred from low order to higher order modes which can cause unwanted residual motion [1, 49]. The controller also has the ability to dampen specific modes without affecting others due to the rapid roll off of the transfer function at higher frequencies than that it is tuned to, as such they are well suited to controlling the first mode of a structure with well separated modes as the controller is insensitive to disturbances from higher frequency modes. PPF control is also highly stable, so long as controlled modes are well defined and do not overlap [1, 52].

1.4 Control of Excited Plates in Contact with Fluid

Active motion control of plates using piezoelectric materials and in contact with fluids have been successfully explored in the past. Multi position control of plates using PPF control has also been successfully implemented on free plates by Zippo et al [38]. and Ferrari et al. who concluded that a multiple input multiple output (MIMO) configuration was the most effective, compared to single input single output (SISO) or multi SISO [39].

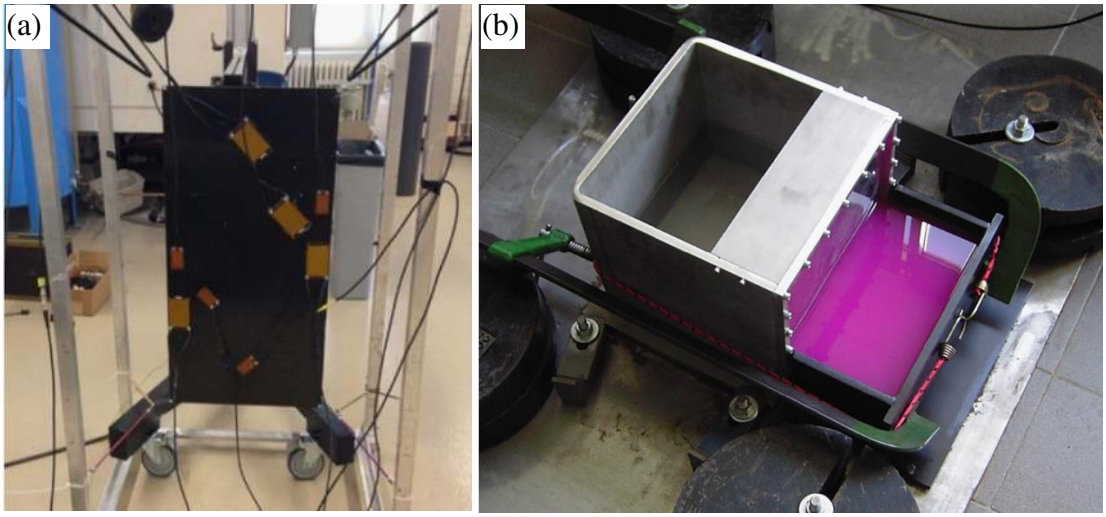

Figure 1.8 – Similar experimental systems: MFC controlled plate(a)[39] liquid impounding tank(b)[7]

The PPF control method has also seen success in control of cantilever plates in contact with fluid in research by Kwak et al. wherein two actuator sensor pairs were used successfully to control the first four modes using a MIMO configuration, however it is generally more effective to have as many actuators as desired modes to control, if such an option is viable [53]. It has been shown that the usage of non-collocated sensor actuator pairs can increase effectiveness of attenuation of a free plate [39]. However, collocated sensor actuator pairs are used in the current study due to the asymmetrical dynamics introduced by adding water to the systems, making non-collocated control non-viable. A cantilever plate in contact with fluid, controlled by PZT wafers was

successfully implemented by Kwak et al., showing that damping using piezoelectric materials is effective for plate in contact with air and fluid [53].

1.5 Objectives, Scope, & Limitations

In the present study, a modified PPF algorithm is employed in order to improve its multi-modal control, bandwidth tuning and overall energy efficiency. This new modified PPF algorithm (M-PPF) is tested on a multiple input multiple output (MIMO) array of MFC patches which are adhered to an excited fully clamped plate system impounded by varying levels of water. The system dynamics, and effectiveness of the active damping of the first four modes, under the varying conditions described utilising M-PPF are explored.

The scope of this thesis encompasses the development and introduction of the proposed M-PPF control method as an alternative in some systems where the PPF method is traditionally used. The M-PPF was tested in one system, as described above, and is applied using a LabVIEW FPGA. This thesis aims to show experimental results of the operational effectiveness of the M-PPF for the designed system, and results in comparative effectiveness will be drawn between experimental results and results from literature.

This study will not cover direct experimental comparisons between M-PPF and PPF control methods, or the effectiveness of the M-PPF for other systems outside the scope of the experimentation.

1.6 Organisation of Thesis

From the beginning of this chapter, the thesis is organised in the following way:

Chapter 1: Introduces the thesis, and reviews the literature on the topics of plate dynamics, sensing and actuating methods, vibration control methods, and control of similar plate systems.

Chapter 2: Explores the theory behind the thesis, including;

Positive position feedback, and the basis of the proposed modified positive position feedback method.

Calculation of ideal placement of sensors and actuators based on plate dynamics

Calculation of voltages required and given to create or interpret the desired actuator and sensor effects.

Chapter 3: Describes experimental method, and how experimentation was conducted. Shows and explores hardware and software used and created for experimentation.

Chapter 4: Analyses results observed in the varying of water levels as described in chapter 3, particularly in how modal frequencies and amplitudes are effected.

Chapter 5: Analyses effectiveness of proposed modified positive position feedback controller

Chapter 6: Conclusion presented and future research proposed

Chapter 2 Theoretical Derivations and Background

In this, the proposed modified positive position feedback control method (M-PPF) is be explored in detail. Plate, actuator and sensor dynamics and equations are defined.

2.1 Modified Positive Position Feedback Controller

The traditional positive position feedback controller (PPF), centrally consists of a second order low pass filter, that follows the transfer function [49, 50]:

$$H_{PPF}(s) = \frac{g\omega_n^2}{s^2 + 2\zeta\omega_n s + \omega_n^2} \quad (2.1)$$

where g, ω_n and ζ are the gain, tuned frequency, and damping ratio of the controller respectively. The PPF controller is highly effective at controlling the first mode of a system. However, it is somewhat difficult to accurately tune, especially for multi-modal control. The proposed M-PPF controller aims to improve the multi-modal effectiveness of the controller, while giving better tuning control. The new M-PPF consists fundamentally of a second order band pass filter, defined by [54]:

$$H_{BP}(s) = \frac{g2\zeta\omega_n s}{s^2 + 2\zeta\omega_n s + \omega_n^2} \quad (2.2)$$

For the bandpass filter, the bandwidth of the controller can be controlled precisely by using [55]

$$f_c = 2\zeta f_n \quad (2.3)$$

This equation relates the damping and tuned frequency of the controller to the half power bandwidth, or 3dB point, which is known as the cut-off frequency of the controller.

Given that the equation relating frequency to angular frequency is:

$$f = \frac{\omega}{2\pi} \tag{2.4}$$

Damping can be expressed as a function of angular control frequency and cut-off frequency by combining Eqs. (2.3) and (2.4):

$$\zeta = \frac{\pi f_c}{\omega_n} \tag{2.5}$$

By combining Eqs. (2.2), (2.4) and (2.5), and summing for x controllable modes, the M-PPF is then defined as:

$$H_{MPPF}(s) = \sum_{i=1}^{x} \frac{g\omega_{c_i} s}{s^2 + \omega_{c_i} s + \omega_{n_i}^2} \tag{2.6}$$

Note that the gain must be kept constant for all modes, or else the control signal of lesser gain modes will gravitate towards higher gain modes and cause undesirable input and output phase shifts.

For x channels, a full multi-input multi-output (MIMO) M-PPF system is then defined as a diagonal matrix of

$$\overline{H}_{MPPF}(s) = \begin{bmatrix} H_{MPPF_1} & \cdots & 0 \\ \vdots & \ddots & \vdots \\ 0 & \cdots & H_{MPPF_x} \end{bmatrix} \tag{2.7}$$

Figures 2.3 and 2.4 show the block diagrams of the proposed MPPF and PPF respectively, where ω_{xy} is the transfer function derived in Eq. 2.6, and ω is the PPF transfer function given in Eq. 2.1.

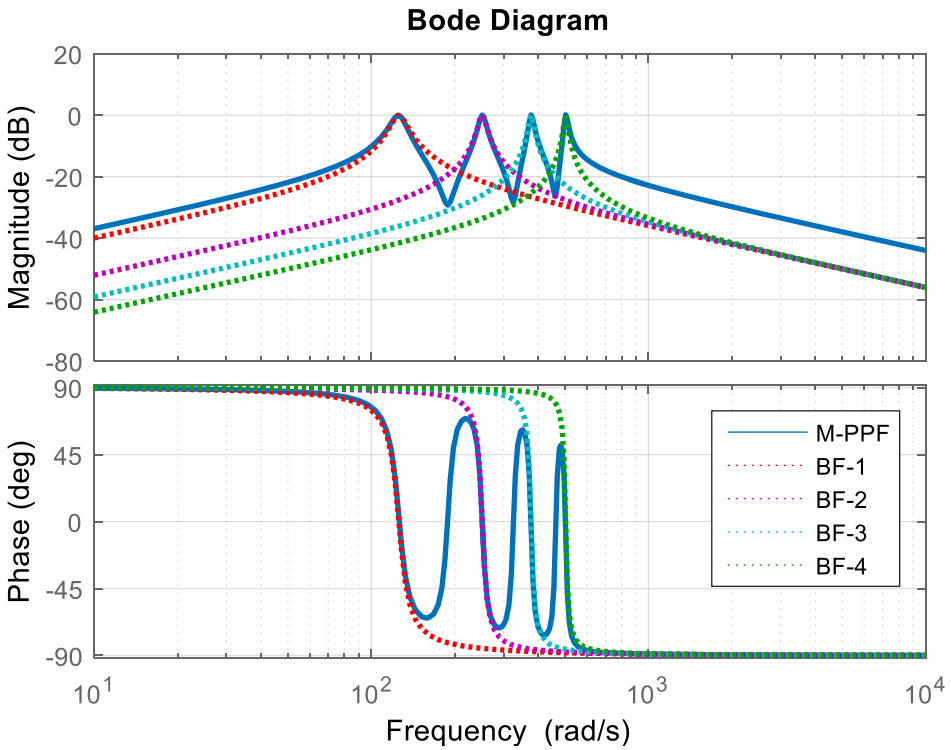

Figure 2.1 – Bode Plot of M-PPF and individual BFs

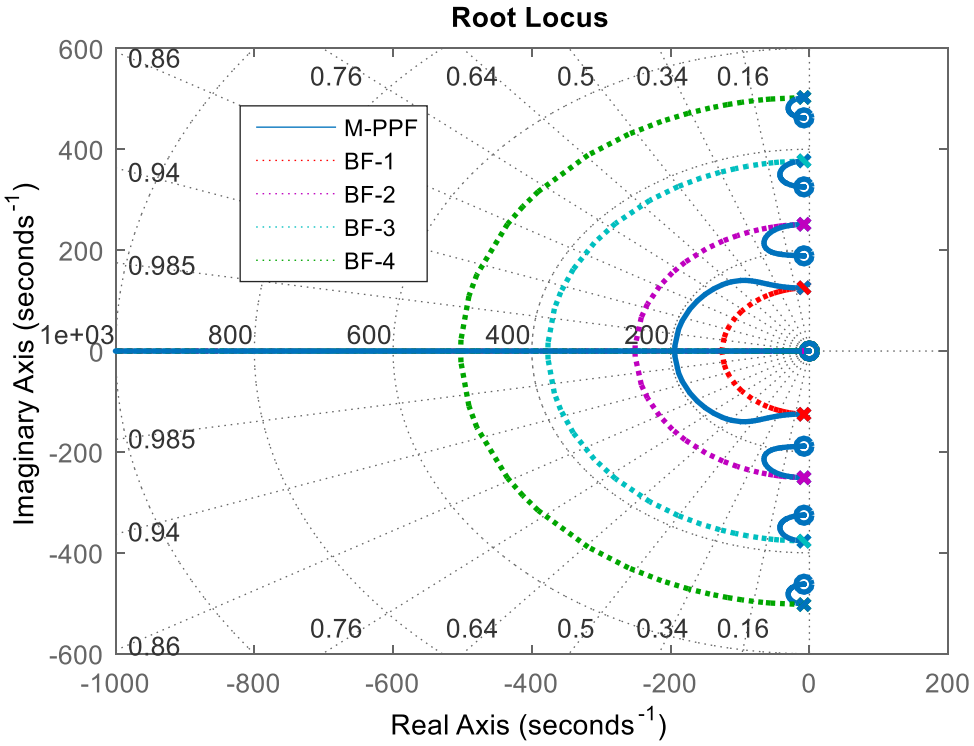

Figure 2.2 – Root locus stability plot

Figure 2.1 shows the Bode diagram of a M-PPF controller optimised for 4 modes, which are for examples sake, 20Hz (~125rad/s) apart with 2.5Hz (~16rad/s) bandwidth. The four constituent bandpass filter (BF) bode plots are superimposed onto the plot for comparison. From the magnitude plot it can be seen that the peaks of the M-PPF align with their component bandpass filters, which is advantageous for tuning. It can be seen that for the M-PPF, in between modes, steep roll off at a constant negative gradient occurs until the central point between the modes where the gradient increases at the same rate until the peak. A possible disadvantage of the M-PPF can be seen for frequencies outside the tuned range, where initial and final roll off levels out at a higher magnitude than the individual bandpass filters. As seen from figure 2.2 the system is seen to be stables as all poles lie to the left of the imaginary axis in the root locus plot.

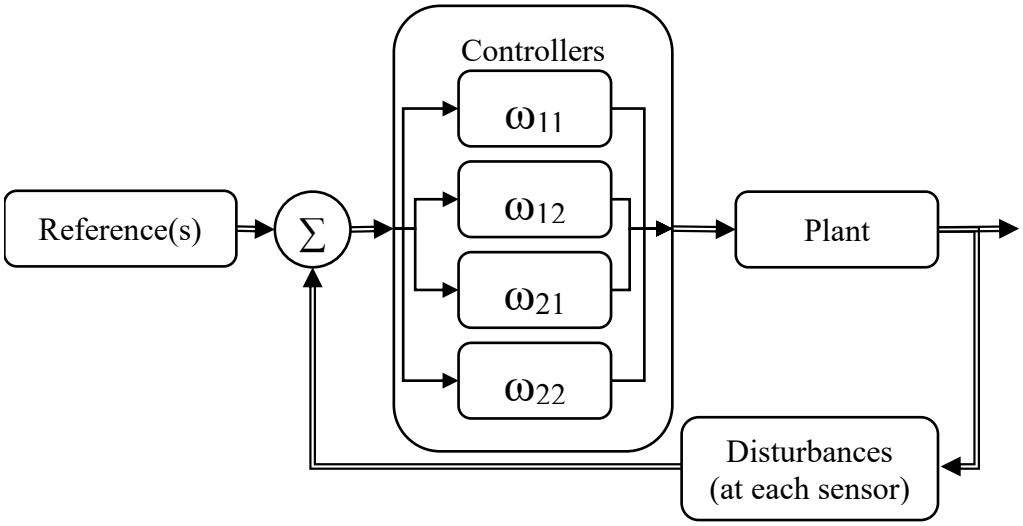

Figure 2.3 – Block Diagram of MPPF

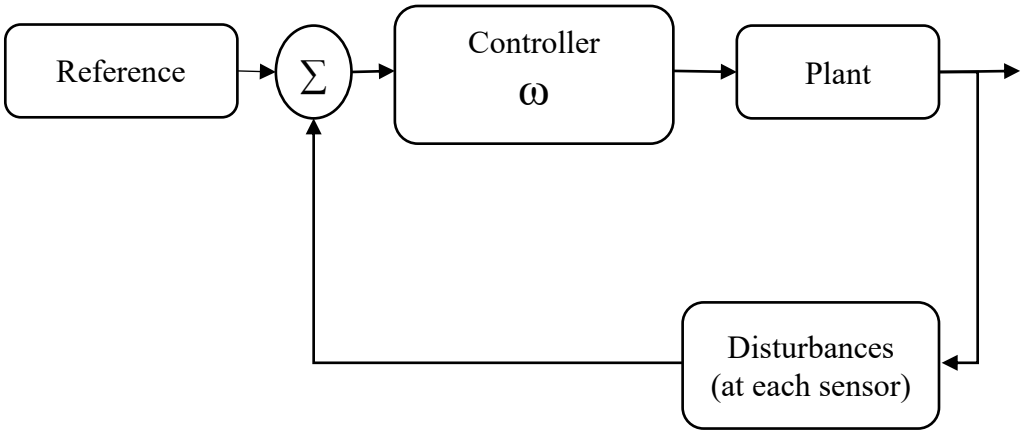

Figure 2.4 – Block Diagram of PPF

2.2 Calculation of plate dynamics and actuator placement

The optimal placement of the actuators and sensors is an important step in the current study. Traditionally, two types of setups are used to determine their positions; collocated and non-collocated setups. Collocated setups constitute of sensors and actuators placed in the same location (or as close to each other as possible); this method is the most widely used. In non-collocated control setups, the sensors and actuators are placed away from each other; in particular, sensors and actuators are placed diametrically opposed around the focal point of the vibration so that they are sensing and actuating the same displacement. This method has been found to be more effective than comparable experiments done using the collocated control. However, in the present study, the collocated control method was chosen as it has more practical applications in asymmetrical systems, which is the case when fluid is added at varying levels to the system.

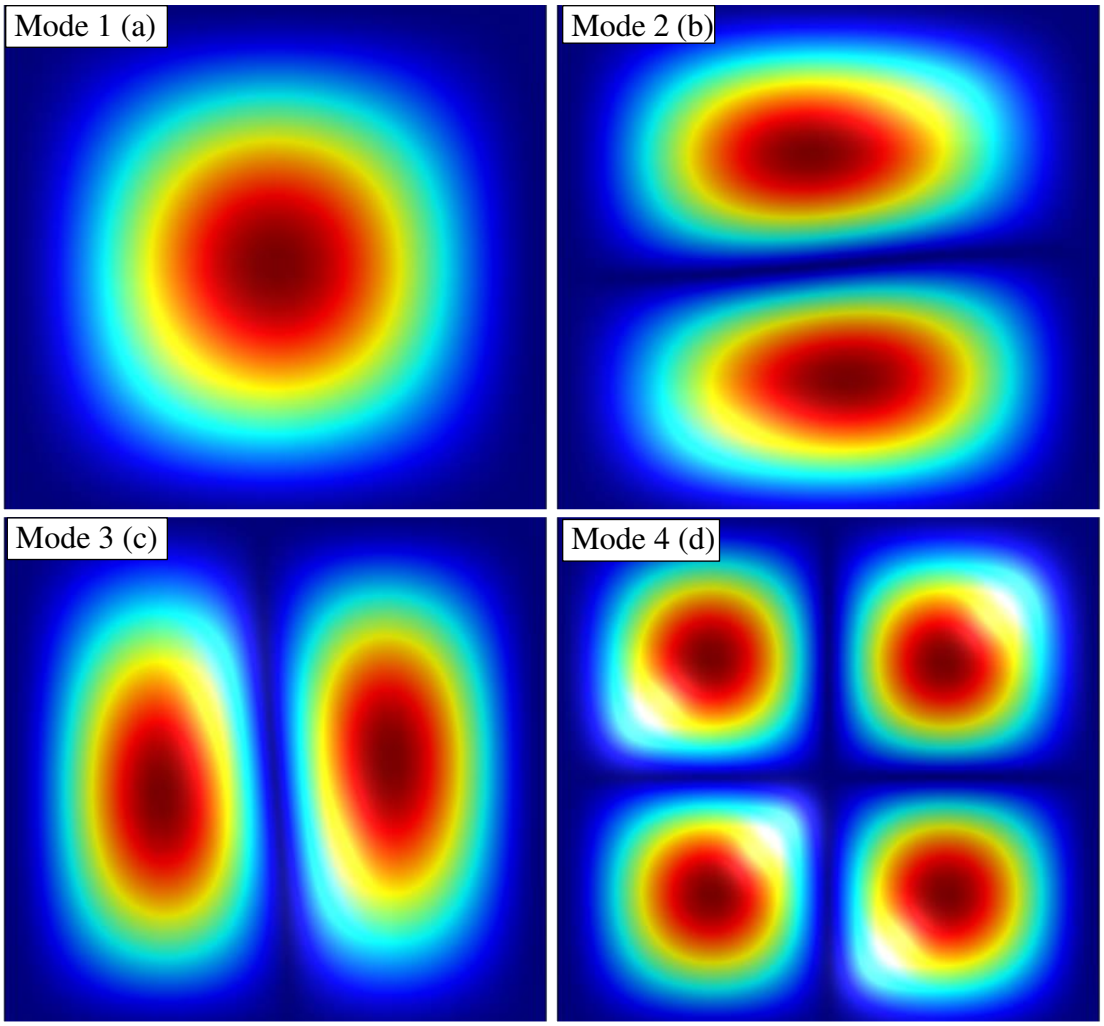

Figure 2.5 – Mode shapes of a square 0.6mm aluminium plate

The exact positions of sensor/actuator pairs are determined utilising a Comsol simulation of the first four modes of a 368x368x0.6mm aluminium plate. Figure 2.5 shows the results of the simulation with redder spectral colours showing higher displacement, from this, it is seen that the predicted mode shapes are 1-1 (a), 2-1 (b), 1-2 (c), and 2-2 (d).

Table 2-1 - Optimal sensor and actuator position

Mode	Shape	Optimal Co-ordinates (mm)		Positions	Angle
		x	y		
1	1-1	184	184	1	any
2	1-2	184	184±73.5	2	0°
3	2-1	184±73.5	184	2	90°
4	2-2	184±73.5	184±73.5	4	any

For optimal control of each mode, a sensor/actuator pair must be placed on one of the maxima of each mode, which correspond to the positions given in Table 2-1. For modes 2-1 and 1-2, the most beneficial angle of the sensor/actuator pair is to align it with the longer dimension of the mode, for the other two modes, angle is insignificant, as they are circular. Each mode only requires one actuator in order to be successfully controlled, even if there are more than one maxima present, which is the case for all but the first mode. This is because all the maxima in a given mode shape are dynamically related, thus affecting one peak will affect all the others for that mode.

2.3 Piezoelectric actuation and sensing

For optimal control of the system, a ratio of applied voltage, to actuation strain must be defined for the MFC actuator used.

From the MFC datasheet [32] the piezoelectric constant of the material is:

$$\mathrm{d}_{33} = 400 * 10^{-12}\, mV^{-1}\ if\ |E| < 1 * 10^{6}\, Vm^{-1} \qquad (2.8)$$

Electric field of a piezoelectric material is defined as [56]

$$E = \frac{\varepsilon}{d_{33}} \quad (2.9)$$

Therefore, given Eq. (2.9), it can be seen that the statement in Eq. (2.8) holds true so long as strain is kept below 400 με. For accuracy and simplicity of the system, both actuation and sensing should be kept below this limit for this experiment, and all material constants chosen assuming this.

From the MFC datasheet [32], strain produced per volt is given from the equation

$$\varepsilon_a = 0.75 * 10^{-6} V_a \quad (2.10)$$

where V_a is applied voltage, and ε_a is produced strain. However as Eq. (2.10) does not take into account the capacitance of the material, it can be assumed that this equation only holds true for sufficiently dynamic systems wherein capacitive discharge is negligible. This equation is used in order to calculate the voltage to apply to the system in order to counter the strain, and thus control the system.

As a sensor, the strain can be calculated from the following equation [17]:

$$\varepsilon_s = \frac{V_s C}{d_{33} Y A} \quad (2.11)$$

where ε_s is strain measured, V_s is voltage measured, C is MFC capacitance, Y is Young's modulus and A is the sensor area. This equation is used to in order to calculate the strain of the system at the site of the piezoelectric sensor which is used for control.

Chapter 3 Methods and Experimental Design

The experimental setup consists of two distinct sections; software and hardware. The software section encompasses the LabVIEW programs used to collect data and run the controller and the shaker, via the NI-cRIO (compact reconfigurable input output) and NI-DAQ (data acquisition) systems respectively.

The hardware section consists of the tank, sensor, and actuator subsystem, the electromagnetic shaker subsystem and circuitry subsystem. Figure 3.1 shows a flowchart of system interconnections, where arrows represent electrical and circles physical connections. Displacement is applied to the tank from the shaker through the force sensor, and measured through the piezoelectric sensor, a reaction force is then applied through the actuators. All other equipment facilitates this control.

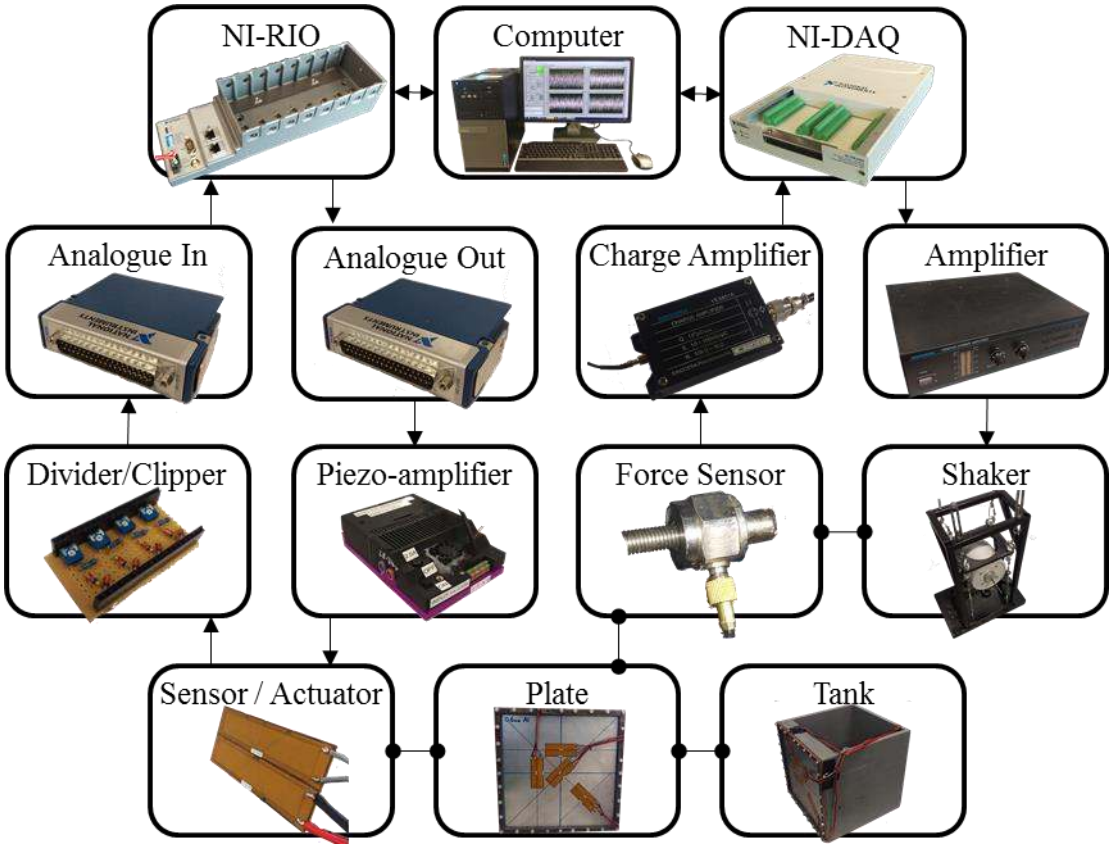

Figure 3.1 – System flowchart

3.1 Hardware Overview

The hardware setup consists of three sections; the tank, plate and actuators, the electromagnetic shaker system, and the sensing and actuating circuitry. Figure 3.2 and Table 3-1 show and describe the entire experimental setup.

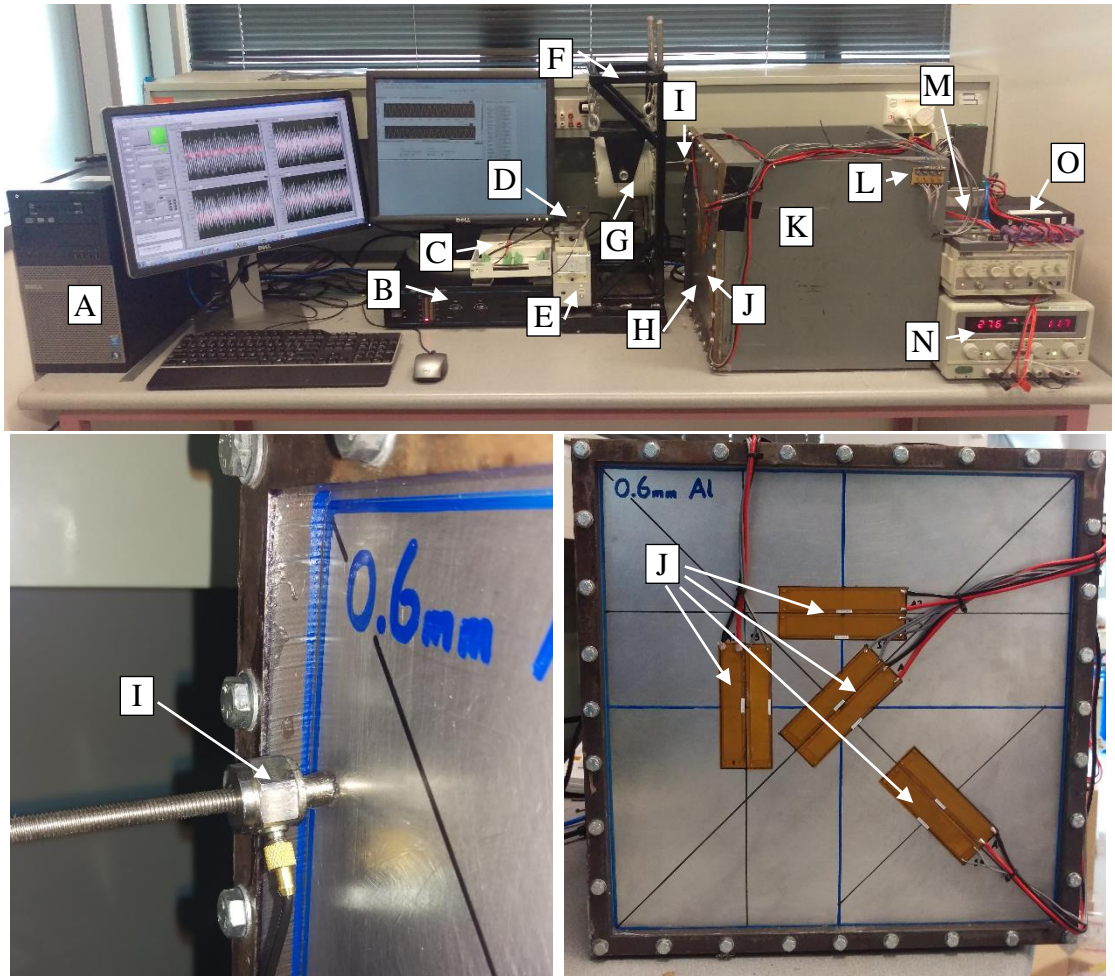

Figure 3.2 – System layout, (detailed in Table 3-1)

Table 3-1 – List of hardware shown in Figure 3.2

I.D.	Name	Part #	Description
A	Computer	Dell OptiPlex 9020	controls DAQ board and reads data from cRIO
B	Power amplifier	Sinocera YE5872H	Amplifies signal between DAQ board and shaker
C	DAQ board	NI-USB-6251	Handles inputs from force sensor and outputs to shaker
D	Charge amplifier	Sinocera YE851A	Amplifies signal from force sensor for DAQ board
E	Power supply		Powers charge amplifier
F	Shaker stand	N/A	Supports shaker
G	Shaker	Sinocera JZK-5	Provides disturbance force to the system
H	Aluminium plate	N/A	Fully clamped aluminium plate
I	Force sensor	CLD Y303	Used to control shaker force
J	MFC	Smart Material M-8514-P1	Used to sense and control plate modes
K	Steel tank	N/A	Steel tank with plate mounted to front face
L	Clipper/divider	N/A	Keeps sensor signal within acceptable range for cRIO
M	cRIO & Modules	NI cRIO-9074 NI-9205 NI-9264	Runs control system and MFC sensor/actuators
N	Power supply		Powers cRIO and Piezo amplifier
O	Power amplifier	N/A	Amplifies cRIO signal to desired voltage for actuator

3.1.1 Tank, plate, and actuators

This part of the experimental system is fundamentally a cubic tank with a thin plate attached in lieu of the front most surface. The actuator and sensor patches are attached to this plate.

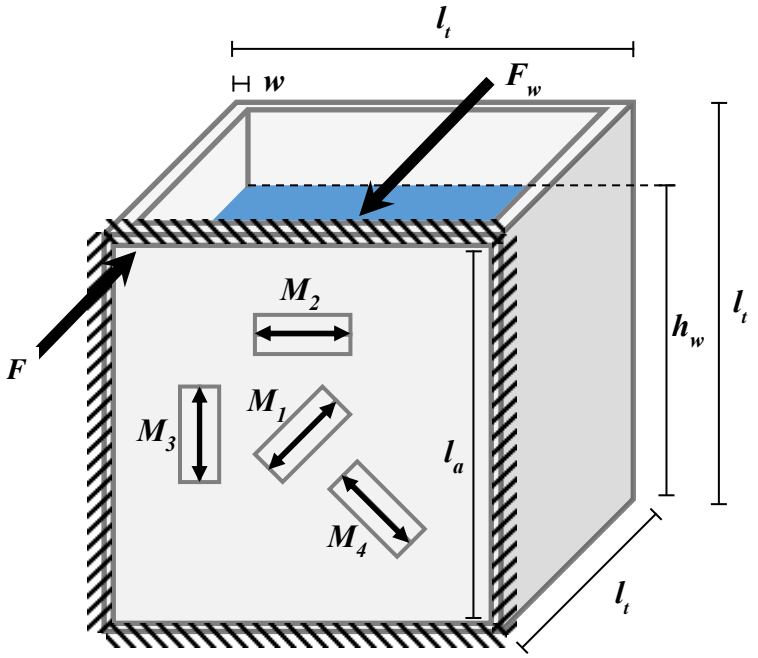

Figure 3.3 – Simplified system diagram

The testing platform consists of a 400x400x400mm (l_t) steel box with 16mm (w) thick walls and one open face, on which a 400x400x0.6mm aluminium plate is bolted via a 16mm thick flange. The exposed size of the plate, and thus its practical dimension is then expressed as a fully clamped 368x368mm (l_a) 0.6mm thick plate. The box is then filled with an experimentally variable amount of water, at levels from 0 to 200mm (h_w) of water. The tank is not filled all the way as the weight of the water would buckle the plate, effecting experimental repeatability. The plate is excited by a force (F) and controlled by surface forces (M_1 to M_4) applied by the MFC actuators.

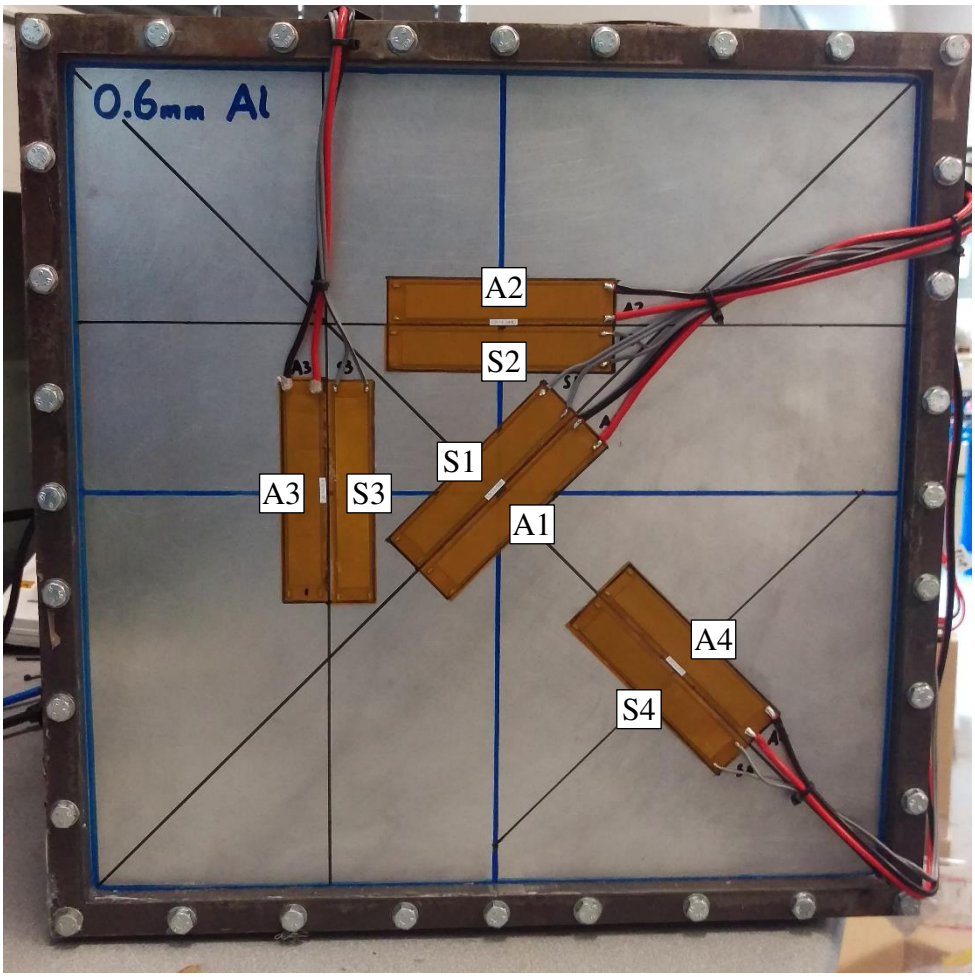

Figure 3.4 – Optimal positioning of sensors (S1-S4) and actuators (A1-A4)

Attached to the aluminium plate are four pairs of Smart Material M-8514 MFC piezoelectric patches which are used as both sensors and actuators for the control system. This is viable as piezoelectric materials will both provide a potential difference when strained, according to its d_{33} coefficient [36], and will also predictably strain when an external potential difference is applied [17, 57] which is described in section 2.3. The MFC patches are bonded via a cyanoacrylate adhesive in the positions shown in Figure 3.4 and detailed in Table 2-1 which correspond to their positions of maximum effect for their corresponding mode shapes. The chosen actuators are capable of applying large blocking forces up to 202N under a potential difference of 1000V which is a large enough force for the current study. While it is predicted that the sensors and

actuators will have slight geometric effects on the plate, it is assumed these are negligible due to the relatively small overall weight and size of the patches, as well as the fact they are highly flexible and thus would not add stiffness to the plate. It is not anticipated that this will contribute to or detriment the effectiveness of the controller.

3.1.2 Sensing and Actuating circuitry

The sensing and actuating circuitry is centralised around a National Instruments NI cRIO-9074 and the attached input and output modules, which are an NI-9205 and a NI-9264 respectively. The MFC sensor outputs a signal to the input module via a divider clipper circuit, which is then processed by the FPGA (field programmable gate array) on the cRIO and an input signal is created for the MFC actuators, which is amplified by a specially designed amplifier.

The output signal of the sensor MFC patches is filtered through a clipper divider circuit, in order to both attenuate the signal to within a readable range, and prevent any unwanted voltage spikes from damaging any downstream components. The voltage divider is used as the input module can only safely interpret signals up to ±10V, whereas the output voltage of the MFC can be close to or higher than this limit. The variable resistor also allows the four channels to be tuned accurately to be identical. The clipping part of the circuit is important as the MFC can produce large voltages in the order of tens of volts if the system is accidently knocked or excited by impulse, which could cause damage to the measuring equipment. This clipping does not affect results as any normal inputs will be within this range.

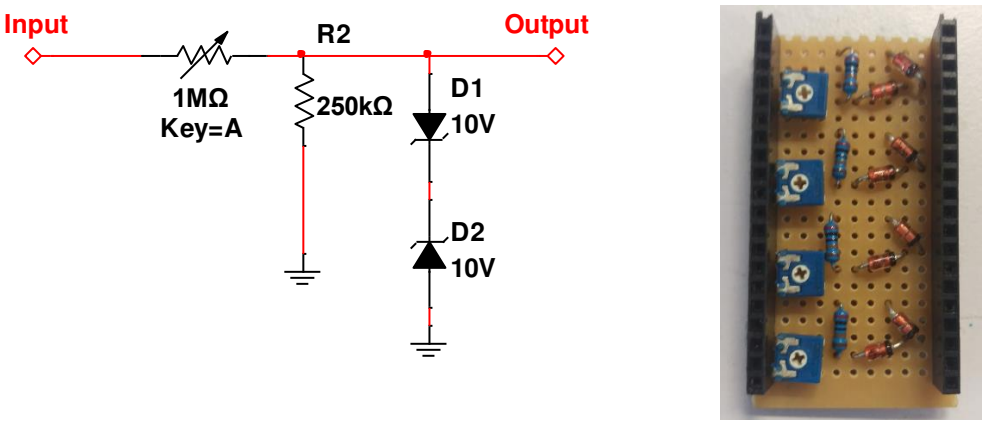

Figure 3.5 –Clipper/divider circuit diagram and board

An amplifier was designed to provide an acceptable bipolar voltage to the MFC actuators, from the given ±10V control signal generated by the output module. Using Eq. (2.10) given the maximum strain value of 400 με chosen in Section 2.3, the maximum voltage calculated is 533V, and as the actuators' rated voltage is -500V to +1000V [32], ±500V was decided as the output voltage swing.

For power calculation purposes, piezoelectric materials can be modelled as capacitors [58], which in the case of the 'Smart Material M-8514-P1' have a value of 3nF according to their datasheet [32] which was confirmed experimentally (via multimeter). Reactive power dissipation can then be given using the following equation [59].

$$P = \frac{V^2}{X_C} = V^2 2\pi f C \qquad (3.1)$$

The amplifier was designed so that each of the 4 channels is capable of effectively providing maximum swing voltage of ±500V for frequencies up to ~400Hz. Using Eq. (3.1), it can be seen that maximum reactance is ~2VAR which gives a maximum power dissipation of ~2W. This limit is chosen as it is approximately twice the maximum expected modal frequencies of the system, which gives an ample overhead to allow for effective usage in all conducted experiments.

The amplifier is constructed from two main systems; an oscillator to transformer to rectifier, and a common emitter amplifier. The oscillator transformer rectifier system provides the 1000V supply required by the amplifier by oscillating a 20V peak to peak supply between +10 and -10V at ~60kHz which is transformed to a ±1000V 60kHz signal, which is then rectified to the required 1000V.

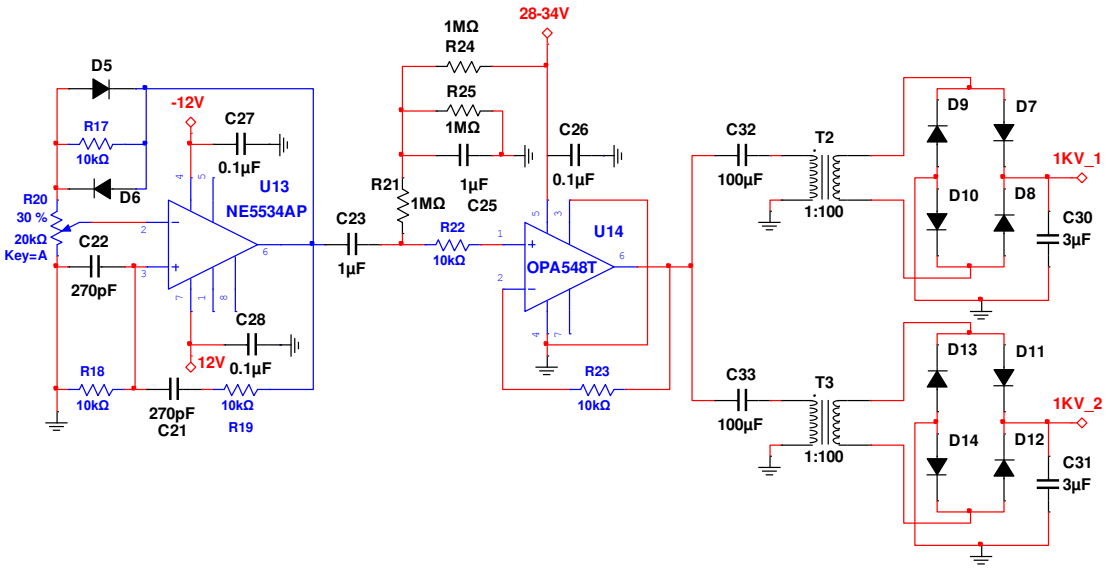

Figure 3.6 – Circuit diagram of oscillator - transformer - rectifier system

The common emitter amplifier circuit fundamentally consists of an NPN style bipolar junction transistor with the input signal connected at the base and the output at the collector [60]. The amplifier is biased so that the output oscillates from 0-1000V about a 500V reference, when a ±10V signal is applied, resistors were selected so that a 50 times amplification is obtained between the input and output. The 500V bias is removed via a blocking capacitor which gives the amplifier its ±500V range.

scope

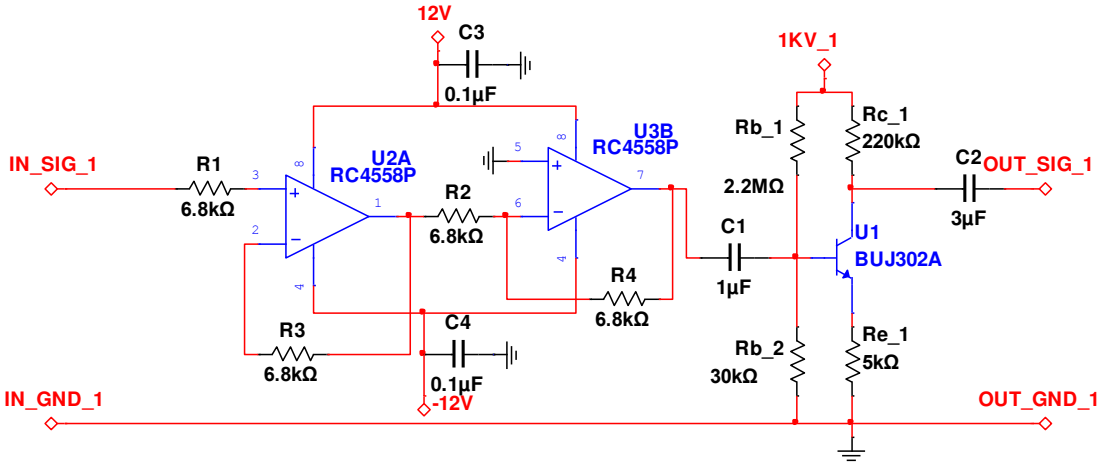

Figure 3.7 – Circuit diagram of common emitter amplifier system

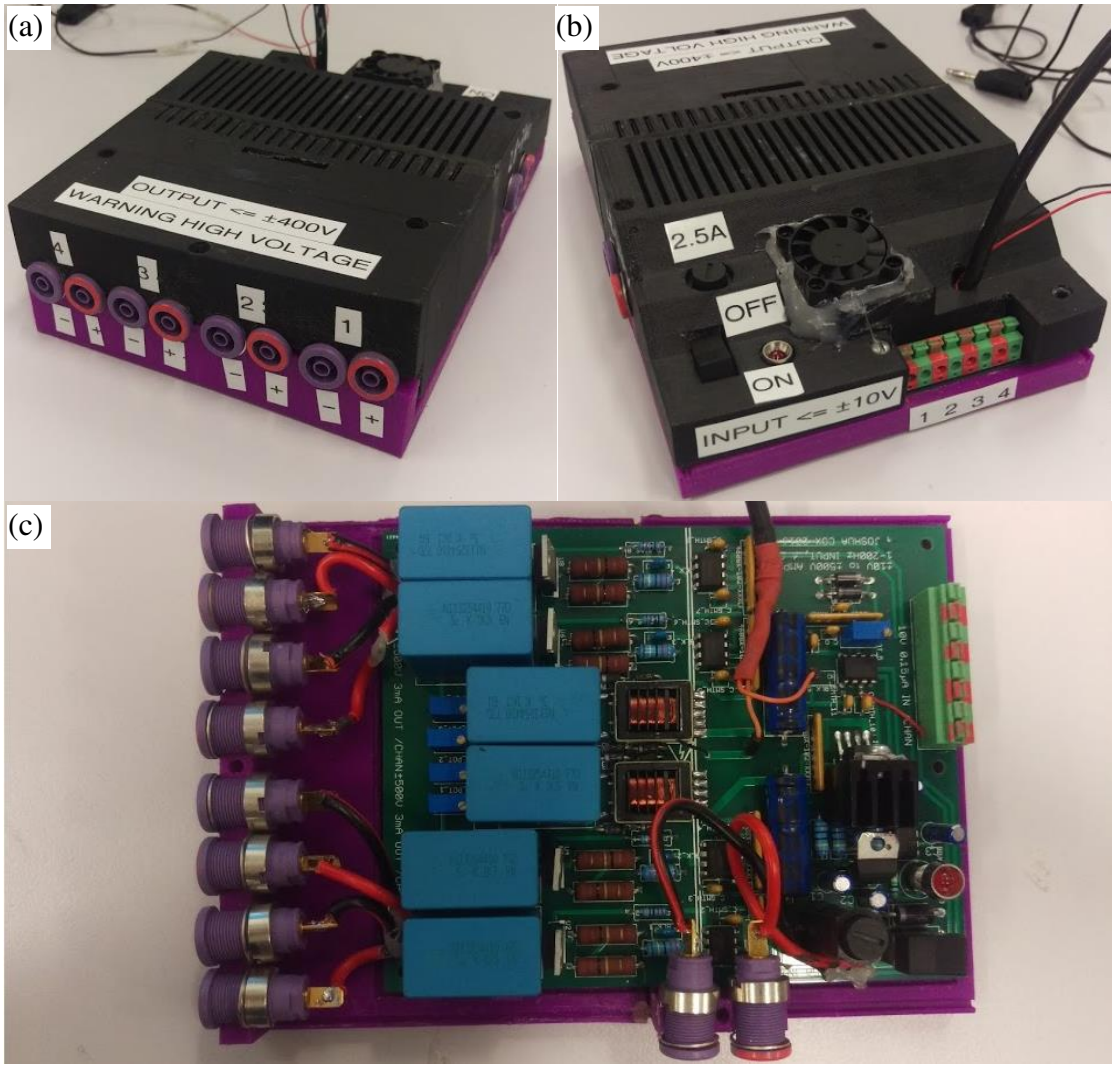

Figure 3.8 – Amplifier front(a) back(b) and PCB(c)

3.1.3 Electromagnetic Shaker System

The electromagnetic shaker, which is suspended within a frame, applies a constant force varied frequency disturbance to the edge of the plate via a stinger with a force sensor tip. The electromagnetic shaker is used to apply a disturbance signal to the system which is to be damped by the controller.

The shaker setup consists of a Sinocera JZK-5 modal shaker which is suspended by steel cables in a rigid steel frame. The shaker is suspended to minimise the shakers impact on the system, and allows the shaker to apply a constant disturbance.

The shaker is powered using a Sinocera YE5872H power amplifier which is controlled using an NI DAQ-6251. The stinger of the shaker is bolted to a force sensor at the tip (CLD Y303) which is then bonded to the plate via a cyanoacrylate adhesive to ensure constant contact. The position of the stinger was chosen to be as far to one side of the plate as possible without causing obstruction between the tank flange and force sensor. This is to minimise system interference as a result of forces exerted by the shaker. The force sensor is connected to an NI-USB-6251 DAQ board via a Sinocera YE851A charge amplifier, to provide force data to the shaker control software.

3.2 Software Overview

The control software was written using NI LabVIEW, and is designed to apply the modified PPF controller. The software reads in data collected from the four MFC sensors which is then fed into the control algorithm. The output signal is then fed into the actuators via an amplifier.

The electromagnetic shaker which is used to apply a disturbance to the system is also controlled by LabVIEW code that is designed to apply a constant forcing frequency sweep to the system. The software employs a PID controller and input from the force sensor, in order to keep forcing at a constant amplitude. Forcing is applied in a sinusoidal manner, at a linearly increasing frequency, in order to sweep through the desired number of modes for the system.

The M-PPF control system consists of two parts, the FPGA software, and the data acquisition software. The FPGA software runs on board the cRIO's inbuilt FPGA, which interfaces with the physical inputs and outputs of the system via the relevant I/O modules and applies the algorithm. As the full MIMO M-PPF algorithm is too complex to map on to the FPGA chip, and run in real time, an iterative controller was designed which cycles through the four input channels, then cycles each input through each of the four constituent transfer functions, then sums the result, and recombines the channel data, effectively applying the controller. While this iterative method seems more time consuming, the greatly reduced load and complexity on the FPGA consequently causes the software to run much faster, with full system execution speed found to be ~17us per cycle, which is acceptable given that the FPGA I/O read/write rate is limited by the hardware to 25kHz, or 40us per cycle.

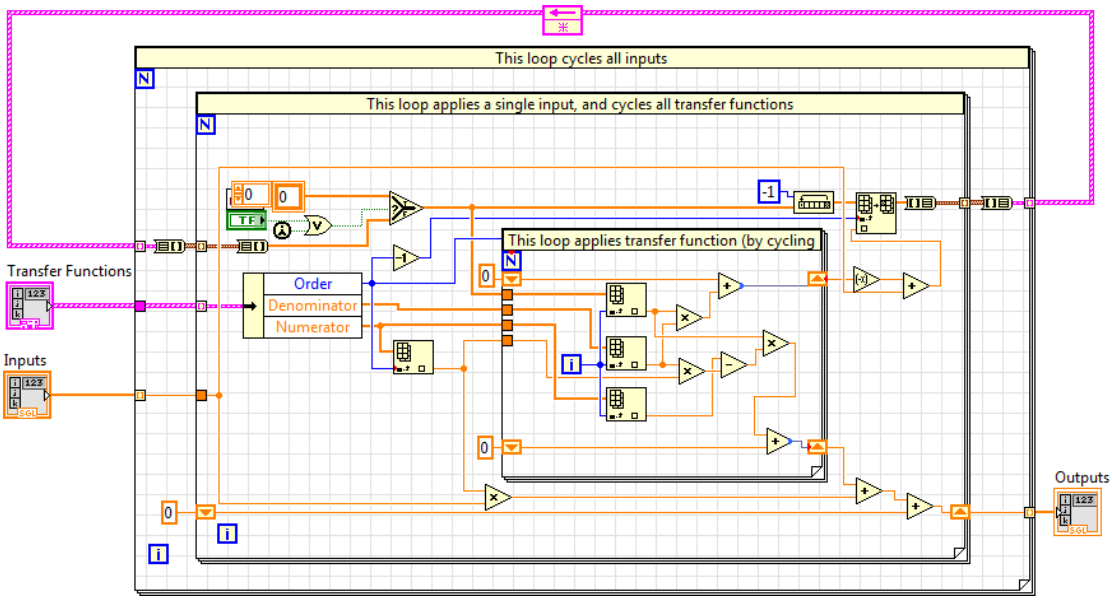

Figure 3.9 – Iterative M-PPF implementation

Data read into the FPGA is also streamed into a FIFO DMA buffer which is then read by the control computer. The data is displayed on various graphs for real time monitoring, and is saved in a file for future post processing and graphing via MATLAB.

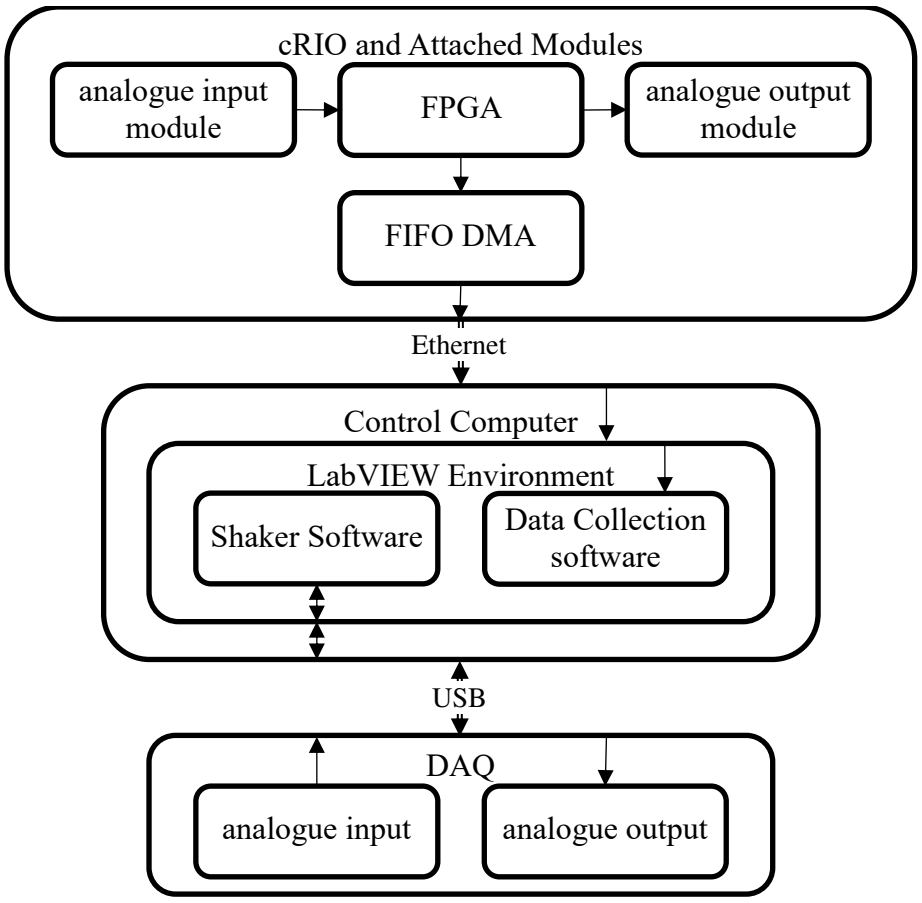

Figure 3.10 – Dataflow throughout system

3.3 Experimental Procedure

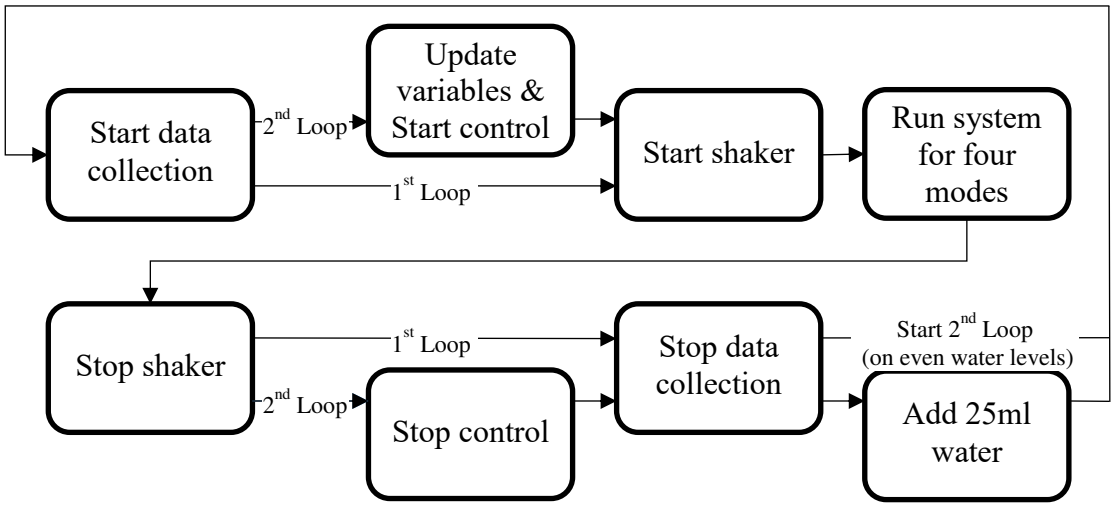

Figure 3.11 – Flow chart of experimental procedure

Experiments were conducted for 9 levels of water from 0mm to 200mm at 25mm intervals. The disturbance signal consisted of a swept frequency sinusoidal forcing at a varying range of frequencies in order to capture the first four modes of the system for each given water level. The signal was held at a constant 10N forcing, with the sine wave having a resolution of 2.5kHz. The frequency step resolution was 0.25Hz with one step incrementing every 250ms. For each water level the uncontrolled dynamics of the system was measured and recorded, and then at each even water level, a second test with the control system active and tuned to the appropriate modal frequencies was conducted, resulting in 9 total sets of results for system dynamics and 5 sets of results depicting the controlled system.

Chapter 4 System Dynamics Analysis Results

The dynamics of the plate for each of the nine water levels were consequently observed in the process of testing the control system. Results were checked against existing literature, and interesting phenomena were explored.

4.1 Experimental Results

Table 4-1 – Mode 1 dynamics data

Level (mm)	**0**	**25**	**50**	**75**	**100**	**125**	**150**	**175**	**200**
Modal frequency (Hz)	51.9	51.1	50.8	50.1	49.0	48.7	48.5	47.8	45.6
Peak strain (με)	2.32	1.71	1.82	1.36	0.61	0.50	0.54	0.63	0.74

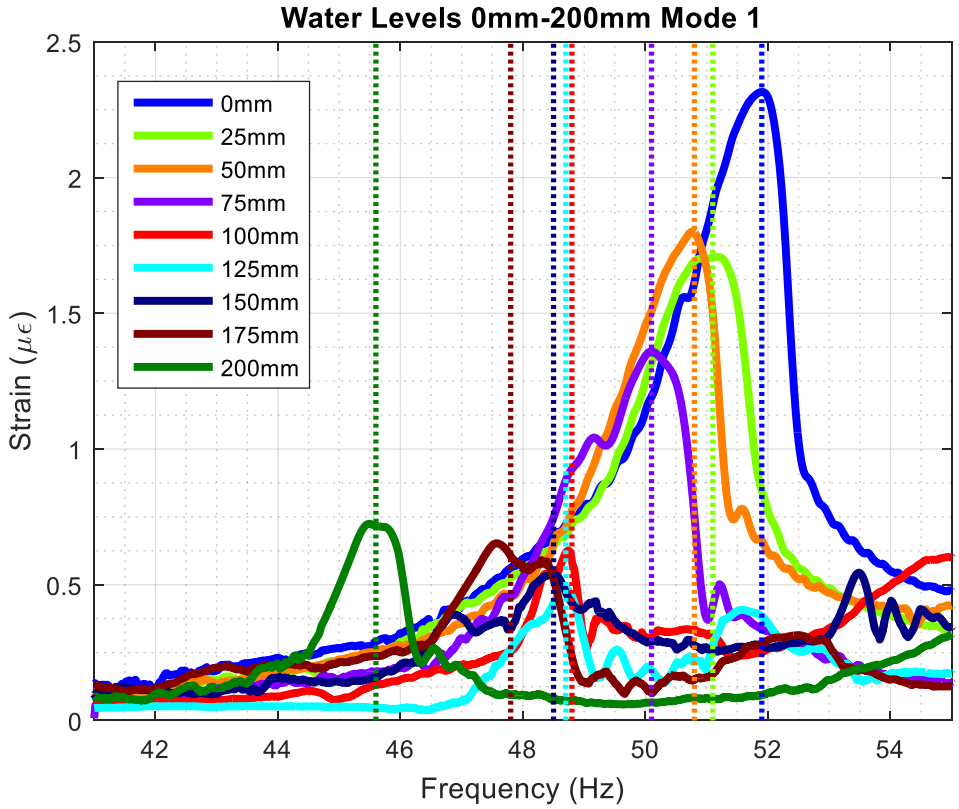

Figure 4.1 – Dynamics of mode 1 at water levels 0-200mm

For the first mode, a clear decreasing trend was seen for modal frequency. Frequency was seen to decrease as water level increases, which is expected due to the added damping as a result of fluid-structure interactions [7]. Frequency was seen to decrease fairly linearly, at an average rate of $-2.74*10^{-2}$ Hz/mm with a coefficient of determination of 0.94. The amplitude of resonance is seen to decrease from 2.32με to 0.50με at a fairly consistent average rate of $-1.47*10^{-3}$ με/mm up until 125mm, where it starts to increase up to 0.74 at a slower average rate of $3.24*10^{-3}$ με/mm.

Table 4-2 – Mode 2 dynamics data

Level (mm)	**0**	**25**	**50**	**75**	**100**	**125**	**150**	**175**	**200**
Modal frequency (Hz)	76.5	73	82	75.4	71.0	67.8	59	68.1	62.5
Peak strain (με)	0.68	0.68	0.73	0.53	1.11	0.57	0.68	0.56	1.45

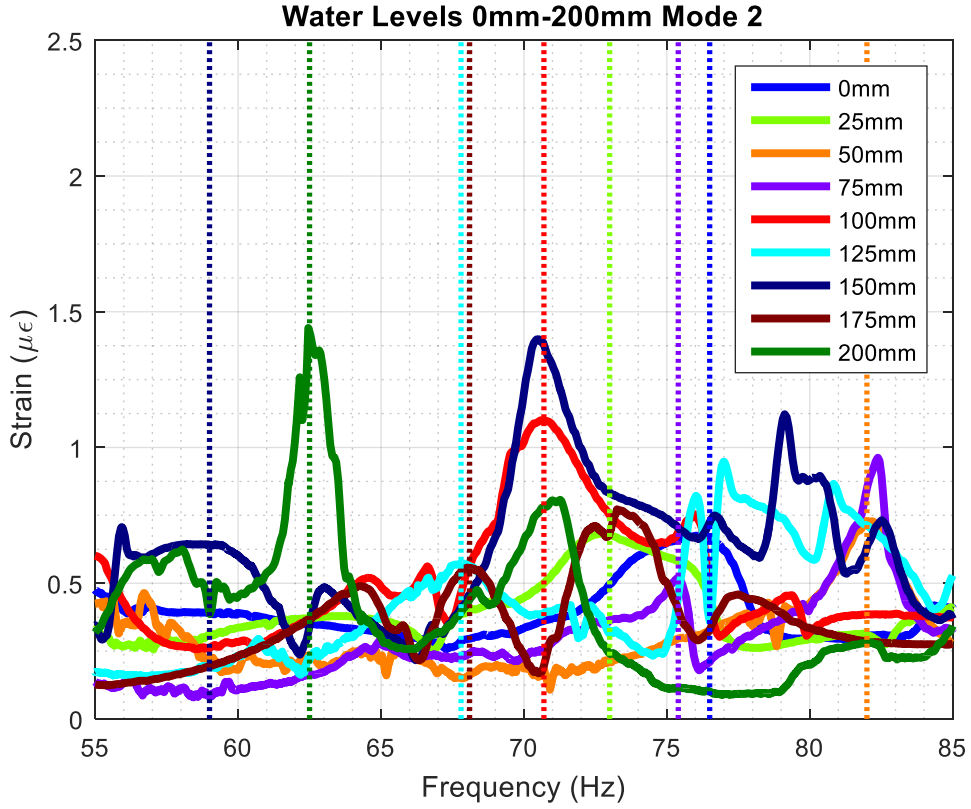

Figure 4.2 – Dynamics of mode 2 at water levels 0-200mm

Second mode frequencies follow a slight overall decrease in value, at an average decrease of $-8.29*10^{-2}$ Hz/mm following a roughly linear trend with a coefficient of determination of 0.63. The linearity of this relationship is mainly skewed by the first 3 values, which follow an overall increasing trend. Second mode strain amplitudes seem to fluctuate throughout experimentation, however a weak increasing trend is observed at an average rate of $1.77*10^{-3}$ με/mm. Data collected at the second and third modes also tends to have many other smaller surrounding modes caused by fluid movement, which could be effecting the measured modes, causing a degree of unpredictability.

Table 4-3 – mode 3 dynamics data

Level (mm)	**0**	**25**	**50**	**75**	**100**	**125**	**150**	**175**	**200**
Modal frequency (Hz)	76.5	73	82	82.4	76.1	77	70.5	73.4	70.9
Peak strain (με)	0.68	0.68	0.73	0.97	0.75	0.95	1.41	0.77	0.81

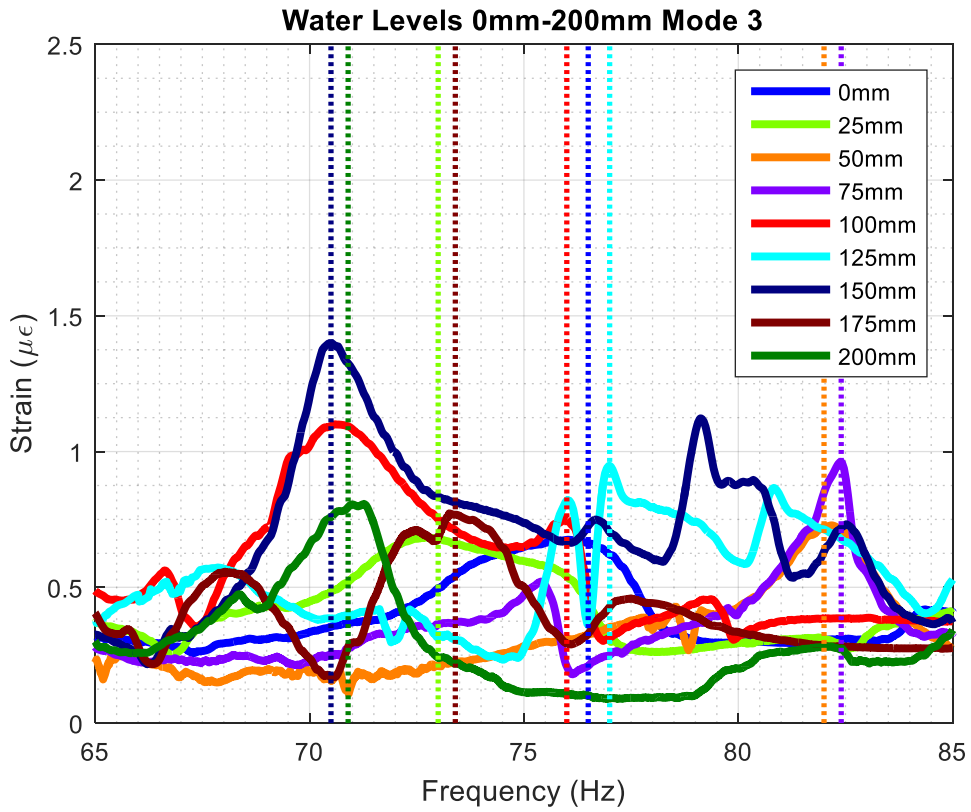

Figure 4.3 – Dynamics of mode 3 at water levels 0-200mm

The third mode follows a less prominent decreasing trend than the second mode, also skewed by the same 3 first values. The trends are similar due to the fact that as the plate is square, the 2 modes occur at the same frequency until sufficient water is added causing asymmetrical damping on the plate, triggering them to separate as symmetry decreases. Strain values again are seen to fluctuate in a similar manner to the previous mode with a weak increasing trend, following an average increase of $1.77*10^{-3}$ με/mm.

Table 4-4 – Mode 4 dynamics data

Level (mm)	**0**	**25**	**50**	**75**	**100**	**125**	**150**	**175**	**200**
Modal frequency (Hz)	107.0	103.5	99.5	97.8	96.2	95	94.7	91.9	87
Peak strain (με)	1.61	1.17	1.03	0.92	1.52	0.77	1.22	1.05	0.9

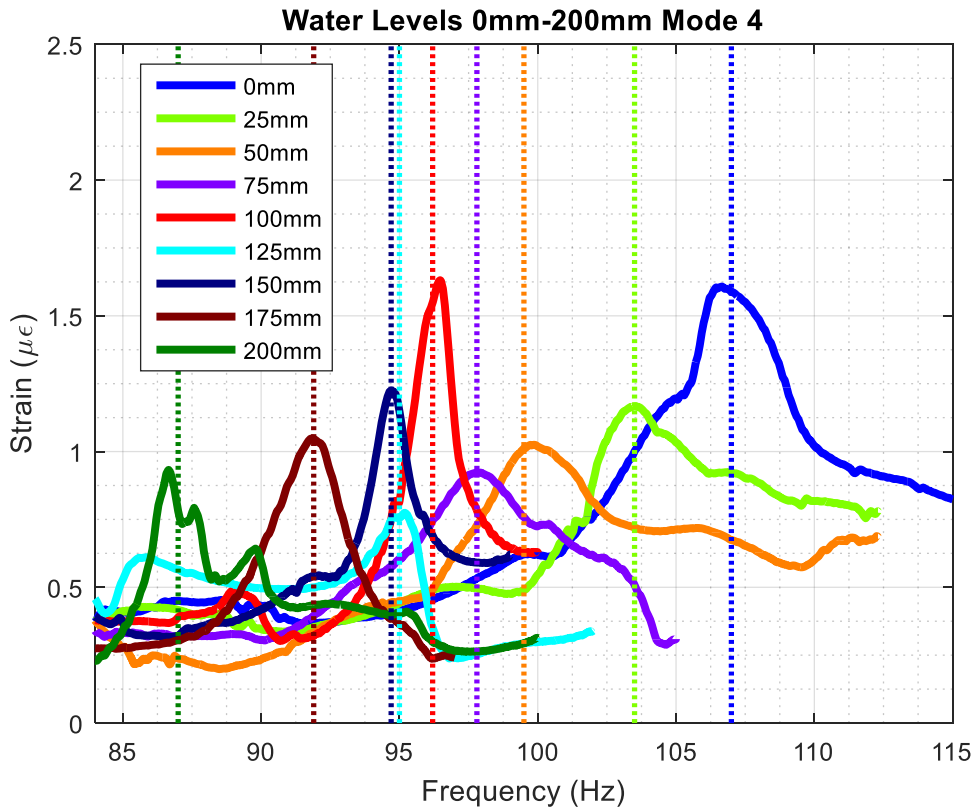

Figure 4.4 – Dynamics of mode 4 at water levels 0-200mm

Fourth Mode dynamics follow a similar trend to the first mode, with resonant frequency decreasing fairly linearly at a rate of $-8.61*10^{-2}$ Hz/mm as water level increases. Amplitude follows a roughly decreasing trend, with similar variance as seen in the previous 2 modes, and an average decrease of $-1.98*10^{-3}$ με/mm.

4.2 Overall Trends

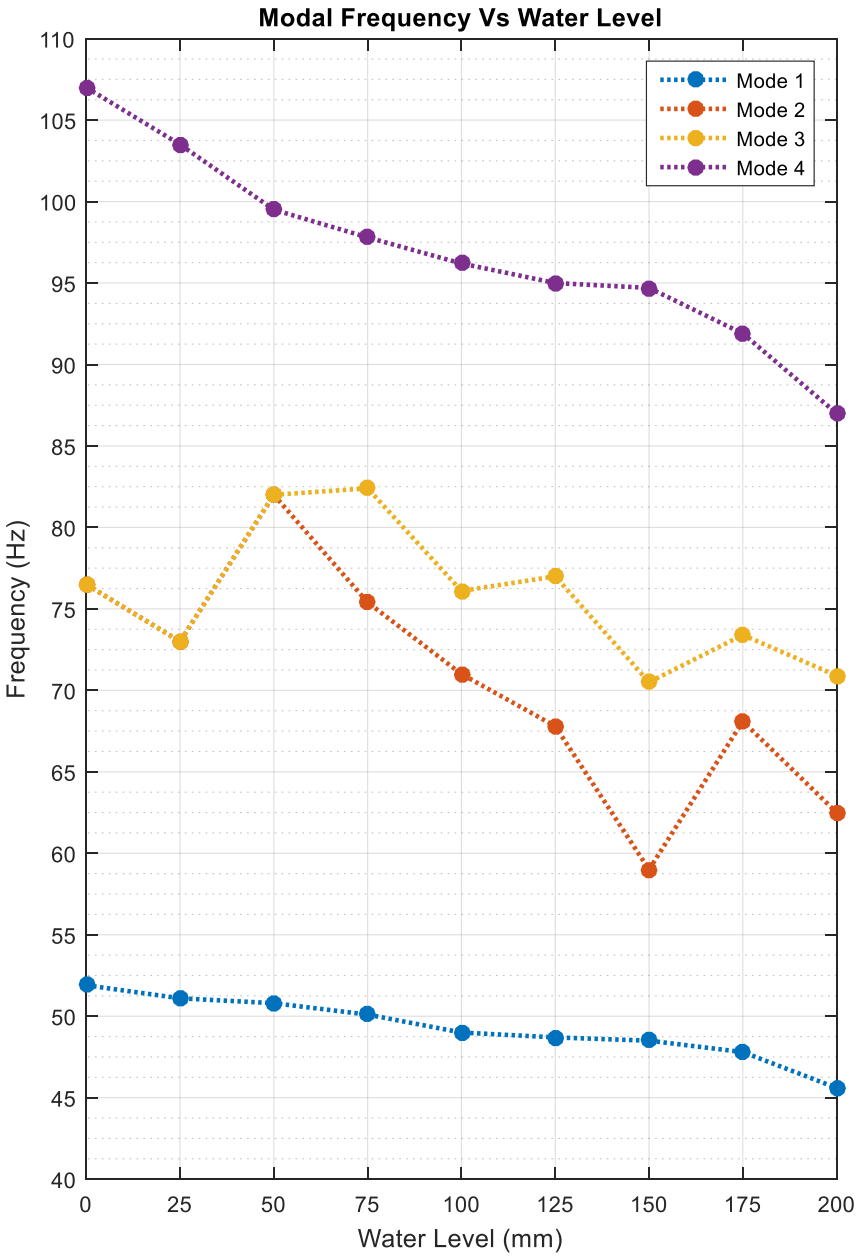

Figure 4.5 – Modal frequency vs. water level

Overall it is seen that modal frequencies tend to decrease in a generally linear fashion as water levels increases. For the first and fourth modes a clear trend is visible, however for the second and third, data trends are less clear. We postulate that this inconsistency or fluctuation in some results for modes 2 and 3 is due to experimental errors associated with the measurement system, requiring further investigation and repeat of the experiments and/or interference from resonances caused by fluid

interactions. Having said, the overall trend for both modes is down like the trend of first and fourth modes.

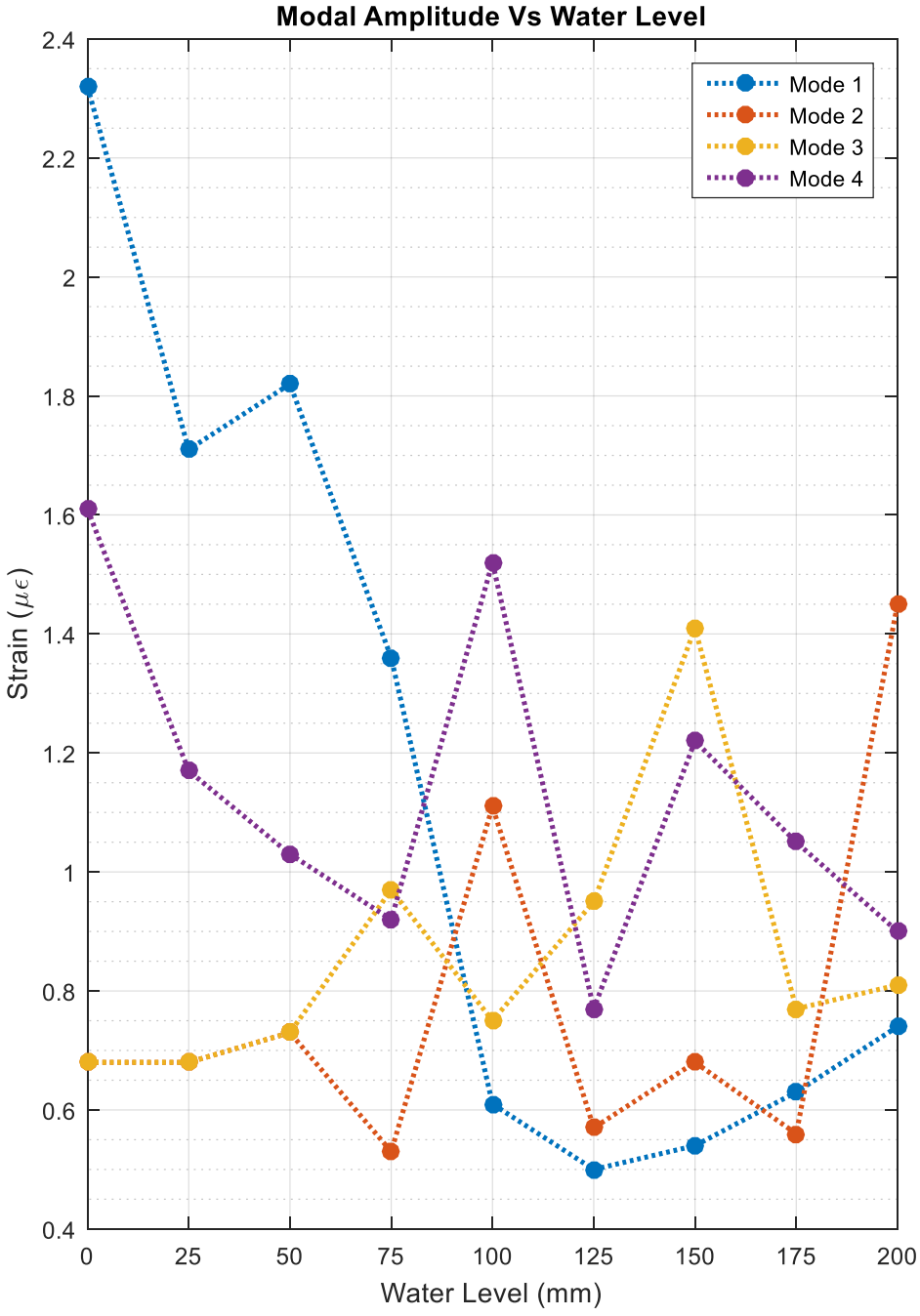

Figure 4.6 – Modal amplitude vs. water level

Amplitudes of vibration, expressed as strain, overall follow a decreasing trend for the first and fourth mode, and a less prominent, increasing trend for the second and third. Amplitude for all modes after the first seems to vary somewhat sporadically,

however values are consistently within 0.5-1.5μ strain which suggests that for smaller amplitudes, oscillation is more readily influenced by the movement of the fluid.

4.3 Comparison of Results with Literature

A fully clamped fluid impounding plate system was simulated at various water levels for the first three modes by Cho et al. [3]. The study shows that the natural frequency of the first mode decreases as water level increases, which is confirmed in experimentation conducted in this thesis, and for the first mode, by Khorshid and Farhadi [5]. For the second and third modes, Cho et al. indicated that natural frequencies decrease, however only slightly after the initial water level, results in this thesis, indicate a slightly overall downward trend, however results obtained fluctuate more than expected. First to fourth mode natural frequencies were shown to decrease as water level increases up to the half full point in experiments conducted by Jeong and Kim [61], which is supported by experimentation conducted in this thesis.

Damping due to the water is expected to increase as water level increases, thus decreasing amplitude. Results from experiments conducted reflect this trend clearly for the first mode, and to a lesser degree for the fourth mode. Second and third mode amplitudes are seen to vary sporadically, suggesting that fluid movement is also affecting amplitude [62].

Chapter 5 System Control Results

The system was tested with control for 5 water levels, and the overall controlled reduction percentage, and reduction of each mode and water level was observed.

5.1 Reduction Effectiveness at Each Water Level

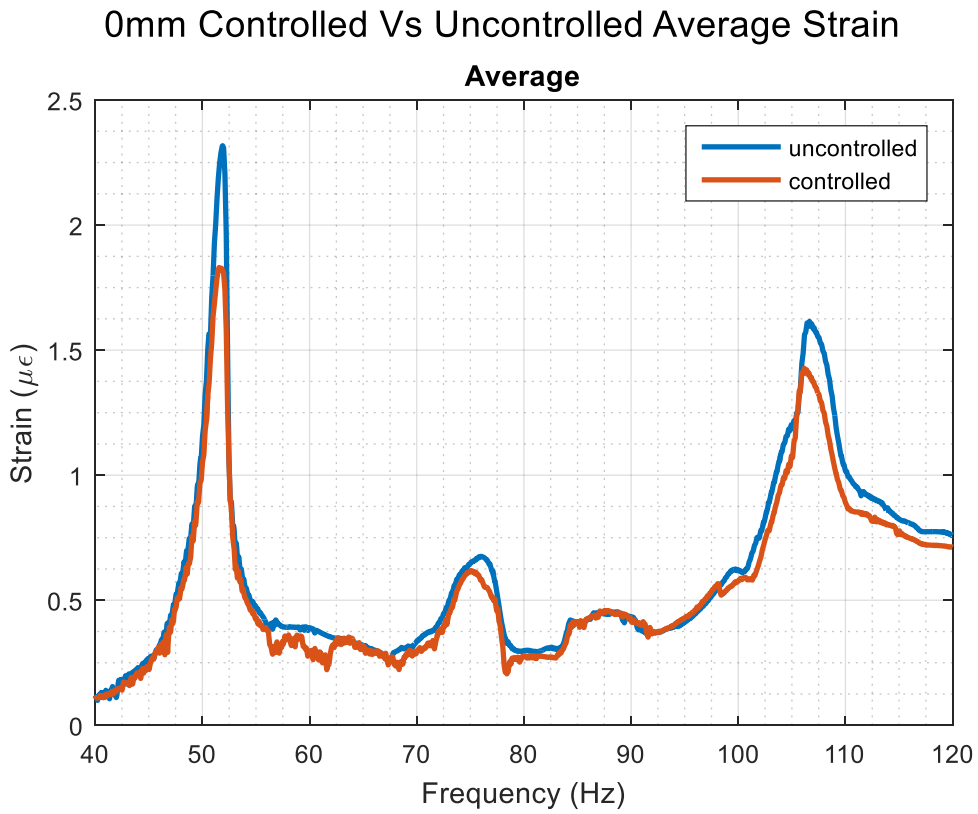

Figure 5.1 – 0mm controlled vs. uncontrolled

At the 0mm water level, while the tank is empty, more magnitude reduction is seen for the first mode, with the other 3 modes somewhat less controlled. As the plate is square, the second and third modes are also completely superimposed onto each other. Modes are well defined and the controller was seen to reduce peaks at an average 17.3%.

Table 5-1 – 0mm controller effectiveness

	Mode 1	Mode 2	Mode 3	Mode 4	Average
Modal frequency (Hz)	51.9	76.5	76.5	107.0	
Controlled reduction %	21.6%	17.7%	17.7%	12.4%	17.3%

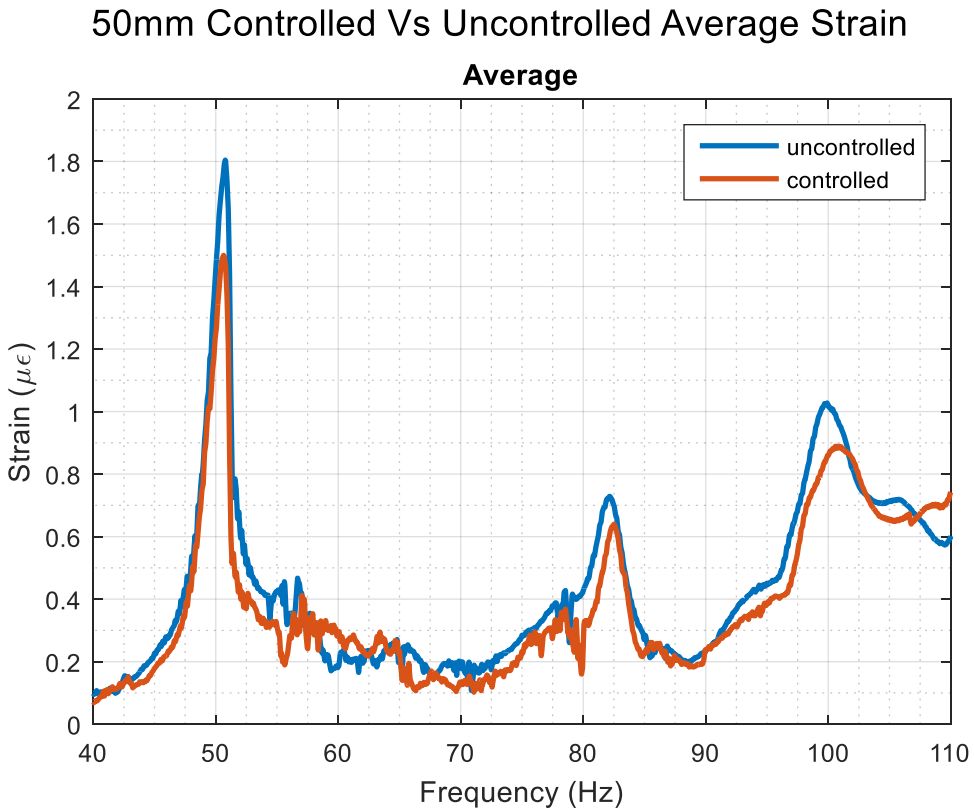

Figure 5.2 – 50mm controlled vs. uncontrolled

For the 50mm water level, the average reduction effectiveness has dropped, with effectiveness at each mode reducing for all modes, except the fourth, which increased slightly. As the water level was still low, the second and third modes are still superimposed onto each other. Other smaller modes, likely caused by plate and water interactions are observed, however only the largest modes are targeted. The controller reduced amplitude of all modes except the first equally, with the first mode being reduced slightly more.

Table 5-2 – 50mm controller effectiveness

	Mode 1	Mode 2	Mode 3	Mode 4	Average
Modal frequency (Hz)	50.8	82.0	82.0	99.5	
Controlled reduction %	19.8%	13.7%	13.7%	13.6%	15.2%

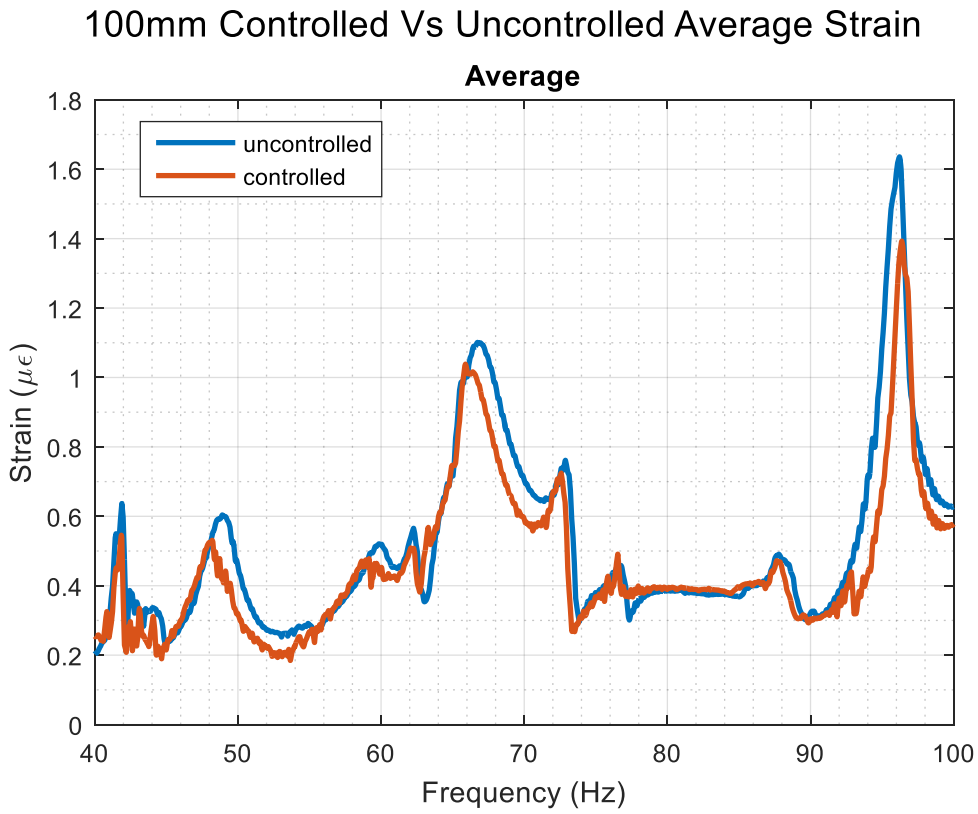

Figure 5.3 – 100mm controlled vs. uncontrolled

At 100mm, average reduction effectiveness is approximately half that of the empty tank, and the lowest overall. This is also the first water level at which the second and third modes begin to become distinct peaks. Modes caused by fluid plate interactions are still visible, but deemed to be of low enough amplitude to be insignificant.

Table 5-3 – 100mm controller effectiveness

	Mode 1	Mode 2	Mode 3	Mode 4	Average
Modal frequency (Hz)	49.0	71.0	76.1	96.2	
Controlled reduction %	11.5%	8.1%	5.3%	9.9%	8.7%

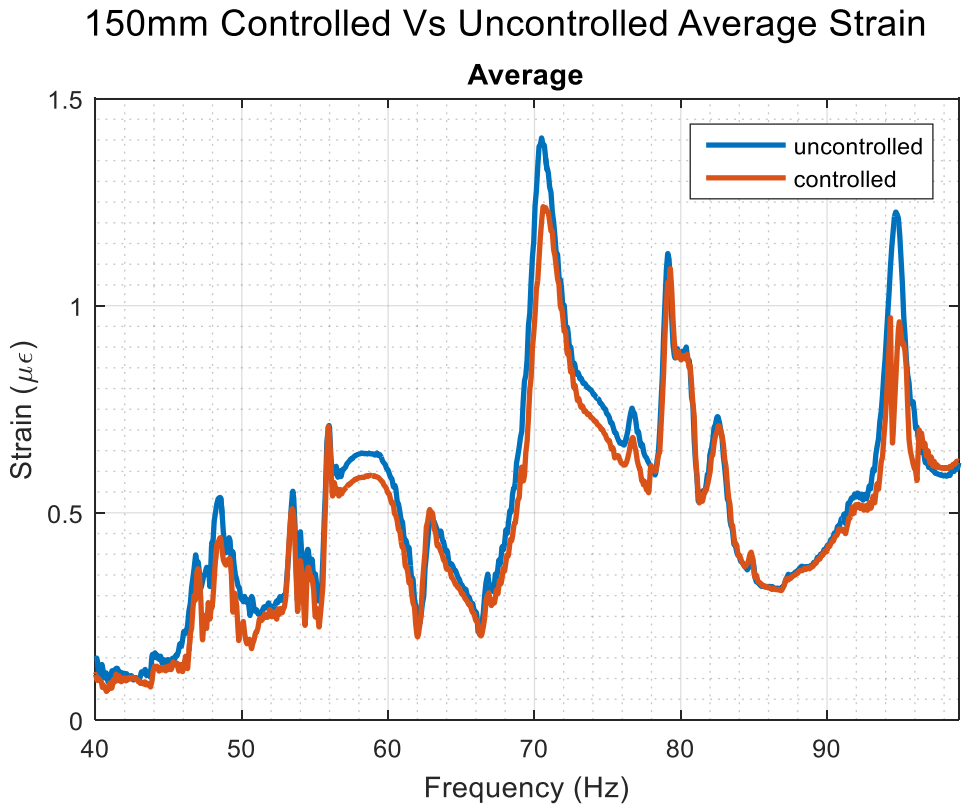

Figure 5.4 – 150mm controlled vs. uncontrolled

Reduction effectiveness for the 150mm water level has increased from 100mm, however is still lower than any other previous levels. For this level, the second and third modes have become completely separate and are thus now controlled independently. The control of the fourth mode has increased to 18%, which is almost as high as the first mode, which has been predominately the highest controlled mode by far until now. Noise from fluid plate interaction is highest at this water level.

Table 5-4 – 150mm controller effectiveness

	Mode 1	Mode 2	Mode 3	Mode 4	Average
Modal frequency (Hz)	48.5	59.0	70.5	94.7	
Controlled reduction %	18.5%	10.3%	12.1%	18.0%	14.3%

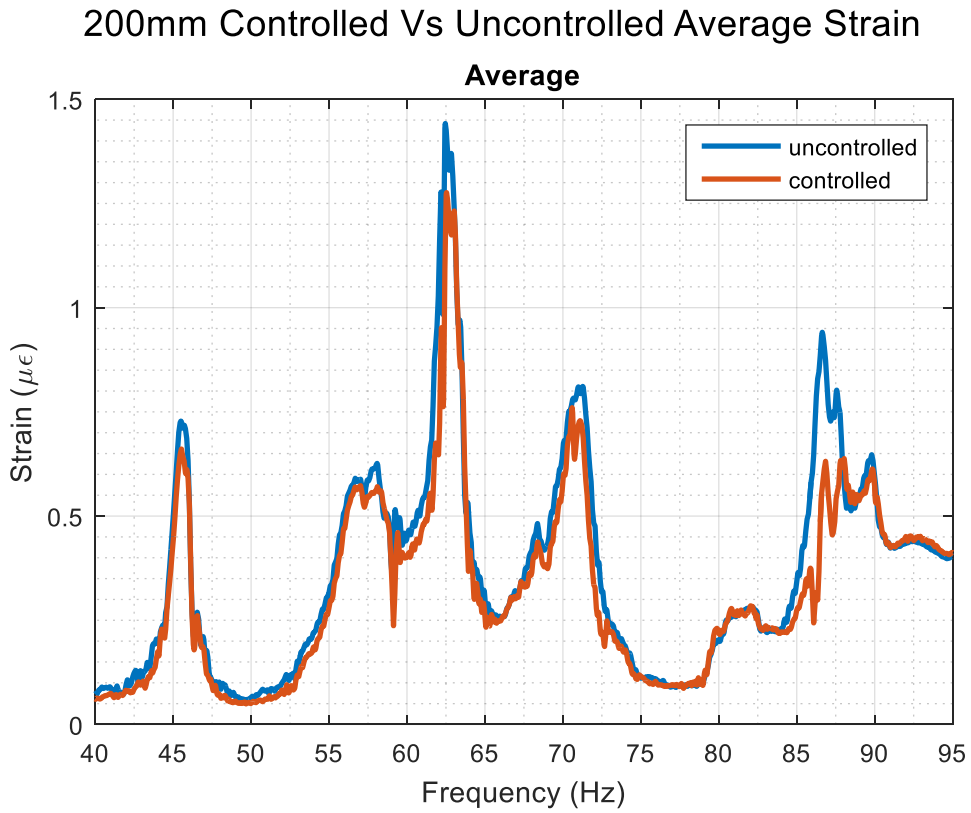

Figure 5.5 – 200mm controlled vs. uncontrolled

The fourth mode, for the 200mm level, has now become the predominately controlled mode, with the other 3 modes at around the same effectiveness. Overall reduction effectiveness has again risen from the 100mm level, and due to the highly controlled fourth mode, was the highest controlled water level tested. Water induced modes have reduced significantly at this water level.

Table 5-5 – 200mm controller effectiveness

	Mode 1	**Mode 2**	**Mode 3**	**Mode 4**	**Average**
Modal frequency (Hz)	45.6	62.5	70.9	87.8	
Controlled reduction %	13.5%	15.2%	13.6%	30.0%	18.1%

5.2 Reduction Effectiveness at each mode

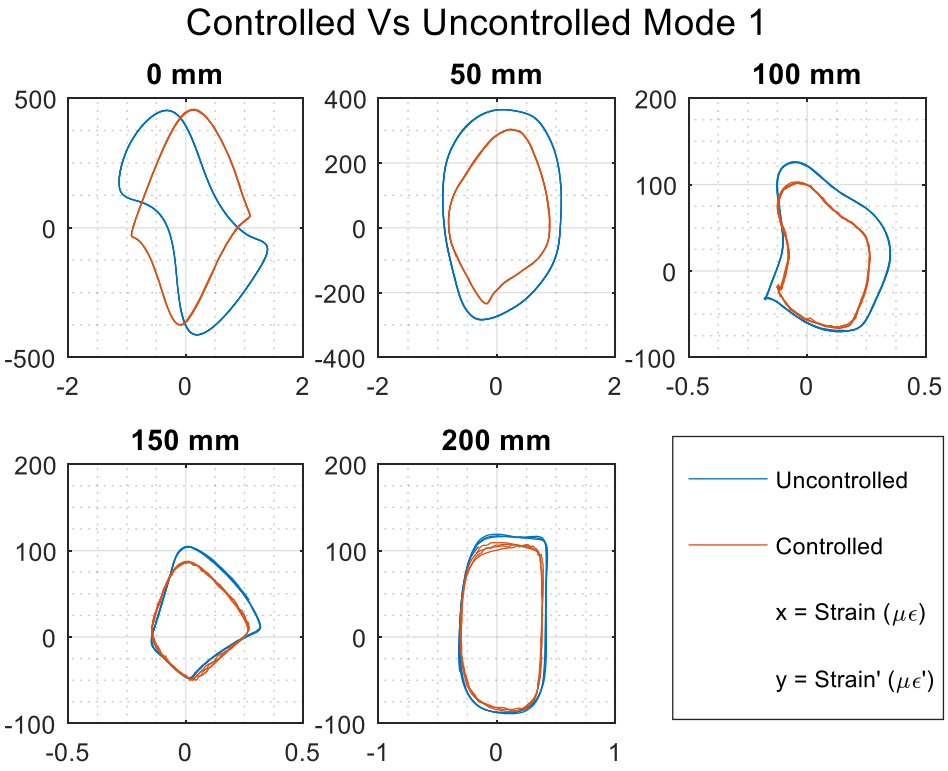

Figure 5.6 – Mode 1 controlled vs. uncontrolled (phase plane)

The first mode was overall the most effectively controlled mode, with the highest overall average, and the highest control in every water level besides the 200mm level.

Table 5-6 –Mode 1 controller effectiveness

	0mm	**50mm**	**100mm**	**150mm**	**200mm**	**Avg.**
Modal frequency (Hz)	51.9	50.8	49.0	48.5	45.6	
Controlled reduction %	21.6%	19.8%	11.5%	18.5%	13.5%	17.0%

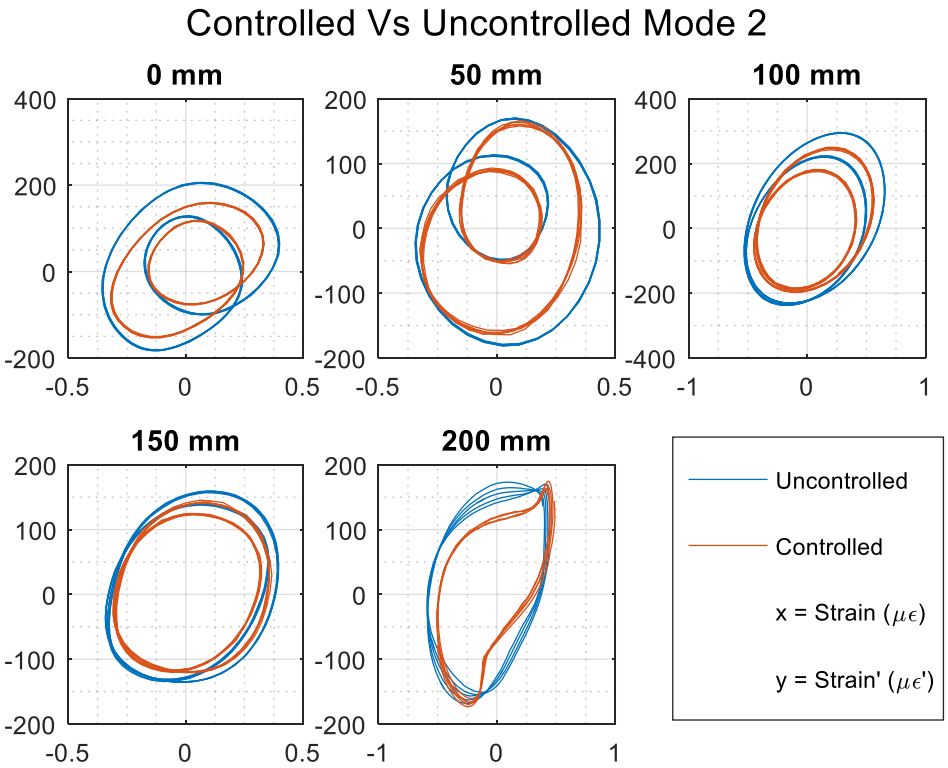

Figure 5.7 – Mode 2 controlled vs. uncontrolled (phase plane)

The second mode follows a trend of falling in efficiency towards 100mm, with efficiency rising either side.

Table 5-7 – Mode 2 controller effectiveness

	0mm	**50mm**	**100mm**	**150mm**	**200mm**	**Avg.**
Modal frequency (Hz)	76.5	82.0	71.0	59.0	62.5	
Controlled reduction %	17.7%	13.7%	8.1%	10.3%	15.2%	13.0%

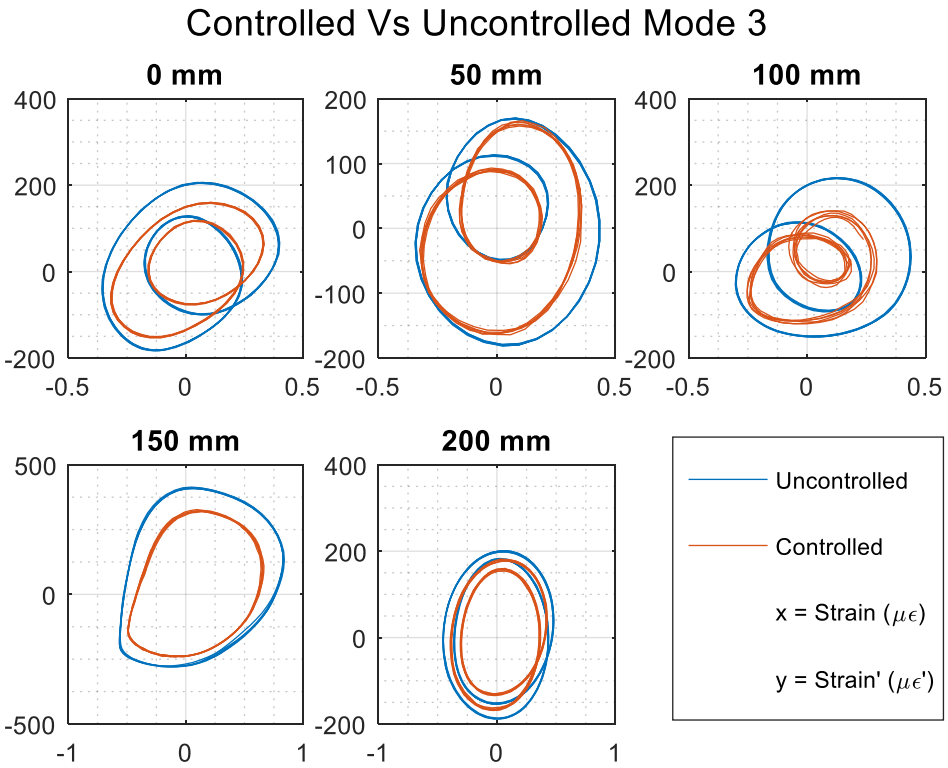

Figure 5.8 – Mode 3 controlled vs. uncontrolled (phase plane)

The third mode follows similar efficiency to the second mode due to their entanglement at the first few water levels, however it is slightly less effective at higher modes.

Table 5-8 – Mode 3 controller effectiveness

	0mm	**50mm**	**100mm**	**150mm**	**200mm**	**Avg.**
Modal frequency (Hz)	76.5	82.0	76.1	70.5	70.9	
Controlled reduction %	17.7%	13.7%	5.3%	12.1%	13.6%	12.5%

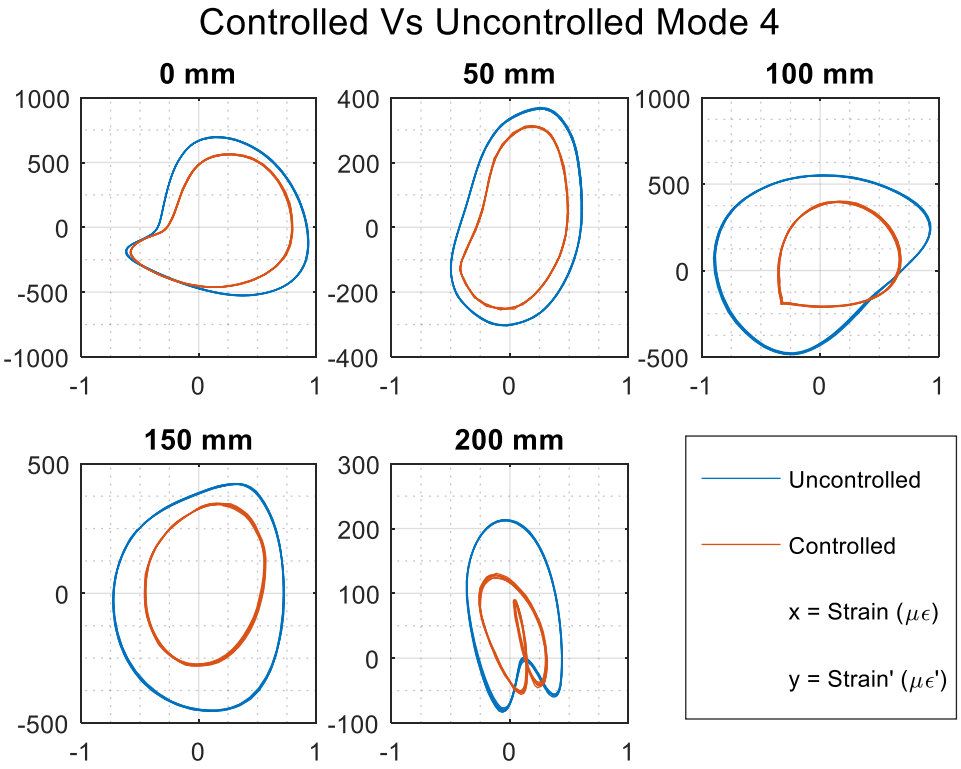

Figure 5.9 – Mode 4 controlled vs. uncontrolled (phase plane)

The forth mode follows the same trend as the other modes, with a decrease in efficiency at 100mm, and an increase either side. The fourth mode is the second most effectively controlled overall, which is mainly due to its greatly increased efficiency in controlling higher modes.

Table 5-9 – Mode 4 controller effectiveness

	0mm	**50mm**	**100mm**	**150mm**	**200mm**	**Avg.**
Modal frequency (Hz)	107.0	99.5	96.2	94.7	87	
Controlled reduction %	12.4%	13.6%	9.9%	18.0%	30.0%	16.8%

5.3 Overall Reduction Effectiveness

Overall it was seen that the controller is most effective at the 200mm water level with an average reduction of 18.1%, which is predominately caused by the relatively high reduction at the fourth mode. Ignoring the fourth mode, however, shows that the 0mm was the most effective consistently across the other 3 modes with an average reduction of 17.3%. The least controlled water level was shown to be 100mm with an average reduction of 8.7%. The overall most controlled mode was the first, which is closely followed by the fourth both at around 17% average reduction, the other 2 modes are also close at around 13% average reduction. Overall the average reduction achieved by the control system was 14.8%.

It was observed that the controller, on average has a higher reduction percentage at the first and last water levels, with a sharp dip focusing at the central water level. The controller also shows that the first and fourth modes, on average, have a higher reduction than the middle two modes, this is likely due to the average larger initial amplitudes of the larger modes, combined with the interference from the smaller, water induced modes visible around the middle modes, which could be interfering with the controller's ability to reduce the targeted mode.

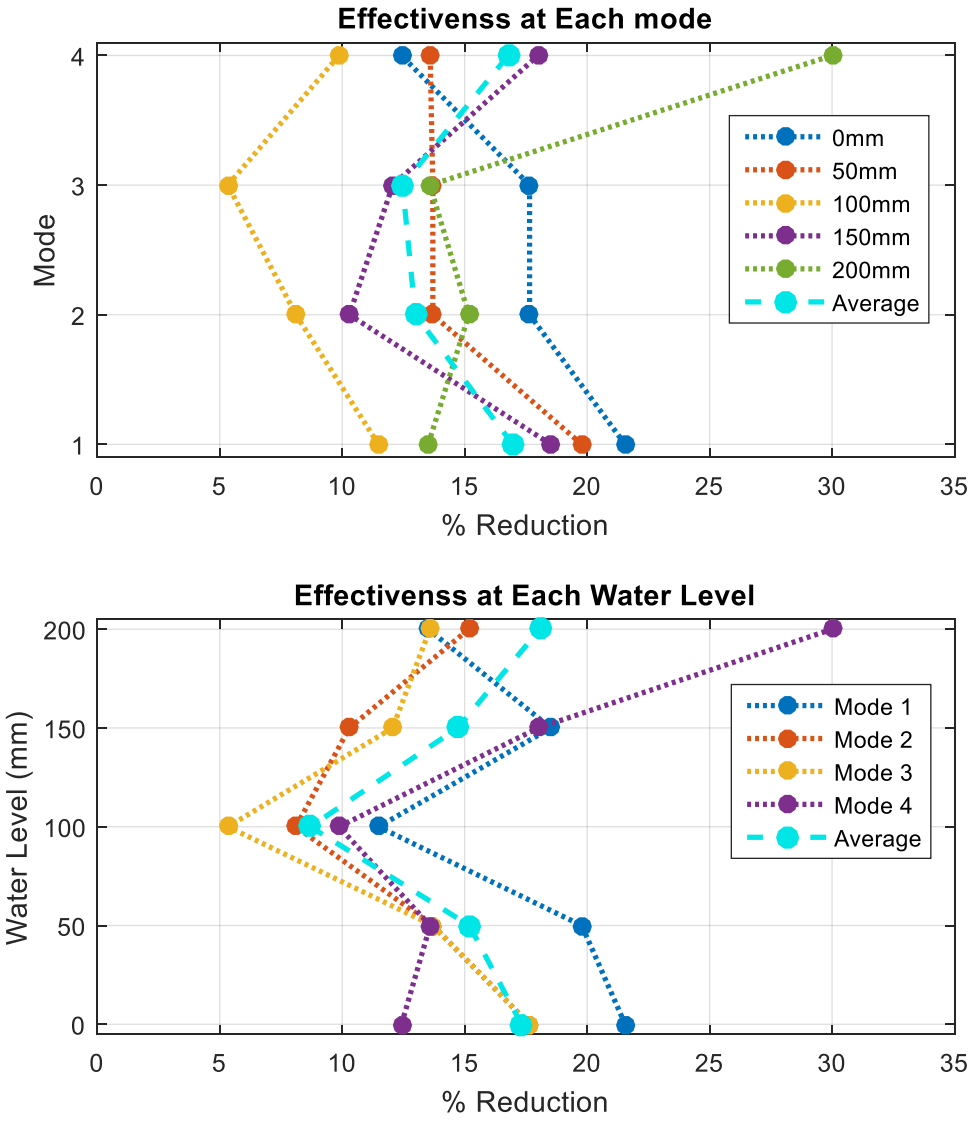

Figure 5.10 – Overall effectiveness comparison

Table 5-10 – Overall control vs. uncontrolled data

Mode #		1	2	3	4	Av
0mm	**Modal frequency (Hz)**	51.9	76.5	76.5	107.0	
	Uncontrolled Strain (με)	2.32	0.68	0.68	1.61	
	Controlled Strain (με)	1.82	0.56	0.56	1.41	
	Controlled reduction %	21.6%	17.7%	17.7%	12.4%	17.3%
50mm	**Modal frequency (Hz)**	50.8	82.0	82.0	99.5	
	Uncontrolled Strain (με)	1.82	0.73	0.73	1.03	
	Controlled Strain (με)	1.46	0.63	0.63	0.89	
	Controlled reduction %	19.8%	13.7%	13.7%	13.6%	15.2%
100mm	**Modal frequency (Hz)**	49.0	71.0	76.1	96.2	
	Uncontrolled Strain (με)	0.61	1.11	0.75	1.52	
	Controlled Strain (με)	0.54	1.02	0.71	1.37	
	Controlled reduction %	11.5%	8.1%	5.3%	9.9%	8.7%
150mm	**Modal frequency (Hz)**	48.5	59.0	70.5	98.7	
	Uncontrolled Strain (με)	0.54	0.68	1.41	1.22	
	Controlled Strain (με)	0.44	0.61	1.24	1.00	
	Controlled reduction %	18.5%	10.3%	12.1%	18.0%	14.7%
200mm	**Modal frequency (Hz)**	45.6	62.3	70.9	87.0	
	Uncontrolled Strain (με)	0.74	1.45	0.81	0.90	
	Controlled Strain (με)	0.64	1.23	0.70	0.58	
	Controlled reduction %	13.5%	15.2%	13.6%	30.0%	18.1%
Avg.	**Controlled reduction %**	17.0%	13.0%	12.5%	16.8%	14.8%

5.4 Comparison of Results with Literature

The proposed modified positive position feedback method (M-PPF) is compared with the reduction effectiveness of the standard positive position feedback method (PPF) from literature to examine their relative efficacy and conclude if M-PPF is a superior or comparative control method.

An experimental study performed by Ferrari et al. [39], and a similar study by Zippo et al. [38] utilise the PPF method in order to control the first five and four modes respectively of a fully free composite plate. Results show that PPF is similarly effective to the proposed M-PPF, however in comparison to these studies, M-PPF gives more precise control at modal frequencies, and less control, and thus less energy expenditure at non modal frequencies. M-PPF achieves this by having multiple variables than can be changed to allow for control only in the desired regions, as detailed in Section 2.1. Less energy is used as the actuators are only on at the precise required intervals, instead of an approximate region as in PPF. This overall makes the M-PPF a more precise and efficient controller

Another study performed by Kwak et al. [53] with a cantilever plate submerged in water, used PPF to control the first 2 modes. Results show again that M-PPF is more precise, as in the aforementioned study, large regions of unwanted amplification are visible, preceding the first mode, which can be avoided using appropriately tuned M-PPF.

Chapter 6 Conclusions and Recommendations for Future Research

The proposed M-PPF control method was successfully implemented for control on a fully clamped liquid impounding plate, with various levels of water.

The dynamics of the plate, in relation to how the first four modal frequencies are affected by changing levels of water are explored. It has been found that, in general, frequencies follow an overall linear decreasing trend as water level increases, which is confirmed in the literature. We conclude that this is likely due to the damping effect the water has on the plate. A clear linear trend is visible for the first and fourth modes, however for the second and third, data trends are less clear. It is concluded this is likely caused by interference from resonances caused by fluid interactions which are prominent in this section of the spectrum.

Strain amplitudes were seen to follow a decreasing trend for the first and fourth mode, and a less prominent, increasing trend for the second and third. Amplitude for all modes after the first seems to vary somewhat sporadically, as oscillation at lower amplitudes, as is the case for these modes, is more readily influenced by the movement of the fluid.

It is shown that the proposed M-PPF method can effectively control the first four modes of the system for various water levels, and it is shown in comparison within the literature, that it can be tuned more accurately and precisely than traditional PPF controllers as hypothesised. The results presented show that the controller varies from highest average reduction of 18.1% at 200mm water, and lowest average reduction of 8.7% at 100mm. We postulate that the overall average amplitude reduction of 14.8% is primarily due to the increase in the effective damping constant of the system.

Assuming that the system behaves like a second order system, for which the magnitude at a resonance frequency is approximately inversely proportional with the damping ratio [63]. Further, we postulate that by using a higher sampling frequency and actuators with a higher force output, the overall reduction can be improved or tailored with a particular application. The first and fourth modes were controlled the most effectively with a ~17% average reduction, the other 2 modes were controlled at a slightly lower average reduction of around 13% average reduction.

M-PPF is inherently more precise than PPF as it has multiple variables that can be tuned to exact frequency and bandwidths. As the actuators are only active, and thus expending energy, only at the defined required intervals, instead of an approximate region as in PPF, it is possible that comparatively more energy can be saved. This overall makes the M-PPF a more precise and efficient controller.

In future the M-PPF method could be applied to other systems where PPF is traditionally used, such as in other vibration control systems, in order to more directly compare the two methods. M-PPF could be applied in more practical systems; such as those where reduced vibration is required at precise frequencies, such as in measuring equipment, where accuracy could be increased by reducing vibration, or in protecting containers of volatile or sensitive substances. Effectiveness of reduction is expected to be increased greatly by using actuators with larger surface areas and higher blocking forces.

References

[1] J. Shan, H.-T. Liu, and D. Sun, "Slewing and vibration control of a single-link flexible manipulator by positive position feedback (PPF)," *Mechatronics,* vol. 15, no. 4, pp. 487-503, 5// 2005.

[2] B. Uğurlu, A. Kutlu, A. Ergin, and M. H. Omurtag, "Dynamics of a rectangular plate resting on an elastic foundation and partially in contact with a quiescent fluid," *Journal of Sound and Vibration,* vol. 317, no. 1–2, pp. 308-328, 10/21/ 2008.

[3] D. S. Cho, B. H. Kim, N. Vladimir, and T. M. Choi, "Natural vibration analysis of rectangular bottom plate structures in contact with fluid," *Ocean Engineering,* vol. 103, pp. 171-179, 7/15/ 2015.

[4] Y. Kerboua, A. A. Lakis, M. Thomas, and L. Marcouiller, "Vibration analysis of rectangular plates coupled with fluid," *Applied Mathematical Modelling,* vol. 32, no. 12, pp. 2570-2586, 12// 2008.

[5] K. Khorshid and S. Farhadi, "Free vibration analysis of a laminated composite rectangular plate in contact with a bounded fluid," *Composite Structures,* vol. 104, pp. 176-186, 10// 2013.

[6] S. Wrona and M. Pawelczyk, "Shaping frequency response of a vibrating plate for passive and active control applications by simultaneous optimization of arrangement of additional masses and ribs. Part II: Optimization," *Mechanical Systems and Signal Processing,* vol. 70–71, pp. 699-713, 3// 2016.

[7] S. Carra, M. Amabili, and R. Garziera, "Experimental study of large amplitude vibrations of a thin plate in contact with sloshing liquids," *Journal of Fluids and Structures,* vol. 42, pp. 88-111, 10// 2013.

[8] R. Manoharan, R. Vasudevan, and A. K. Jeevanantham, "Dynamic characterization of a laminated composite magnetorheological fluid sandwich plate," *Smart Materials and Structures,* vol. 23, no. 2, p. 025022, 2014.

[9] A. W. Leissa, "The free vibration of rectangular plates," *Journal of Sound and Vibration,* vol. 31, no. 3, pp. 257-293, 1973/12/08 1973.

[10] V. Birman, *Plate structures*. Springer Science & Business Media, 2011.

[11] (2016). *Foil-Strain-Gauges.jpg*. Available: http://pimg.tradeindia.com/03043479/b/1/Foil-Strain-Gauges.jpg

[12] Izantux. (2016). *StrainGaugeVisualization*. Available: https://en.wikipedia.org/wiki/File:StrainGaugeVisualization.svg

[13] G. F. Lucas, P. C. McKeighan, and J. S. Ransom, "Nontraditional Methods of Sensing Stress, Strain, and Damage in Materials and Structures: Second Volume," 2001: ASTM.

[14] R. H. Bishop, *Mechatronic systems, sensors, and actuators: fundamentals and modeling*. CRC press, 2007.

[15] Z. Mohamed, J. M. Martins, M. O. Tokhi, J. Sá da Costa, and M. A. Botto, "Vibration control of a very flexible manipulator system," *Control Engineering Practice,* vol. 13, no. 3, pp. 267-277, 3// 2005.

[16] M. Hassan, R. Dubay, C. Li, and R. Wang, "Active vibration control of a flexible one-link manipulator using a multivariable predictive controller," *Mechatronics,* vol. 17, no. 6, pp. 311-323, 7// 2007.

[17] J. Sirohi and I. Chopra, "Fundamental understanding of piezoelectric strain sensors," *Journal of Intelligent Material Systems and Structures,* vol. 11, no. 4, pp. 246-257, 2000.

[18] (9/2016). *Scanning Vibrometer*. Available: http://www.warsash.com.au/products/images/scanning-vibrometers.jpg
[19] (9/2016). *Laser Distance Sensor*. Available: http://epub1.rockwellautomation.com/images/web-proof-large/GL/25483.jpg
[20] (9/2016). *Operation of Optical Distance Sensors*. Available: http://m.eet.com/media/1171626/fig2r.jpg
[21] C. E. Webb and J. D. Jones, *Handbook of Laser Technology and Applications: Laser design and laser systems*. CRC Press, 2004.
[22] F. Alijani, M. Amabili, P. Balasubramanian, S. Carra, G. Ferrari, and R. Garziera, "Damping for large-amplitude vibrations of plates and curved panels, Part 1: Modeling and experiments," *International Journal of Non-Linear Mechanics,* vol. 85, pp. 23-40, 10// 2016.
[23] (9/2016). *PZT sensor*. Available: https://www.fabtolab.com/image/cache/data/Sensors/Pressure/Peizo_sensor-900x700.jpg
[24] (9/2016). *PVDF Sensor*. Available: http://www.imagesco.com/sensors/img/pz-01.jpg
[25] G. Gautschi, *Piezoelectric sensorics: force, stain, pressure, acceleration and acoustic emission sensors, materials and amplifiers*. Springer, 2002.
[26] (09/2016). *Voice Coil Actuators*. Available: https://www.h2wtech.com/Images/General/img-33.jpg
[27] M. Fikar, V. Preda, J. Cieslak, D. Henry, A. Falcoz, and S. Bennani, "Control for Active Vibration Mitigation in High Stability Space Missions: A Comparative Study," *IFAC-PapersOnLine,* vol. 48, no. 14, pp. 88-94, 2015/01/01 2015.
[28] Y.-D. Chen, C.-C. Fuh, and P.-C. Tung, "Application of voice coil motors in active dynamic vibration absorbers," *IEEE Transactions on Magnetics,* vol. 41, no. 3, pp. 1149-1154, 2005.
[29] K. M. Lynch, N. Marchuk, and M. L. Elwin, "Chapter 29 - Other Actuators," in *Embedded Computing and Mechatronics with the PIC32*Oxford: Newnes, 2016, pp. 491-514.
[30] (9/2016). *PZT Actuators*. Available: http://www.piezo.com/prodbm7qmpict760.jpg
[31] D. V. Newton, J. A. Main, E. Garcia, and L. Massengill, "Piezoelectric actuation systems: optimization of driving electronics," in *1996 Symposium on Smart Structures and Materials*, 1996, pp. 259-266: International Society for Optics and Photonics.
[32] Smart-Materials, "Macro Fiber Composite - MFC," *Smart doc # CPRO-V2.1en-0314 Datasheet*.
[33] W. K. Wilkie *et al.*, "Low-cost piezocomposite actuator for structural control applications," in *SPIE's 7th Annual International Symposium on Smart Structures and Materials*, 2000, pp. 323-334: International Society for Optics and Photonics.
[34] H. A. Sodano, G. Park, and D. J. Inman, "An investigation into the performance of macro-fiber composites for sensing and structural vibration applications," *Mechanical Systems and Signal Processing,* vol. 18, no. 3, pp. 683-697, 5// 2004.
[35] A. Kovalovs, M. Wesolowski, E. Barkanov, and S. Gluhihs, "Application of macro-fiber composite (MFC) as a piezoelectric actuator," *Journal of Vibroengineering,* vol. 11, no. 1, 2009.

[36] Q. Q. Zhang, S. J. Gross, S. Tadigadapa, T. N. Jackson, F. T. Djuth, and S. Trolier-McKinstry, "Lead zirconate titanate films for d33 mode cantilever actuators," *Sensors and Actuators A: Physical,* vol. 105, no. 1, pp. 91-97, 6/15/ 2003.
[37] S. Zhang, R. Schmidt, and X. Qin, "Active vibration control of piezoelectric bonded smart structures using PID algorithm," *Chinese Journal of Aeronautics,* vol. 28, no. 1, pp. 305-313, 2// 2015.
[38] A. Zippo, G. Ferrari, M. Amabili, M. Barbieri, and F. Pellicano, "Active vibration control of a composite sandwich plate," *Composite Structures,* vol. 128, pp. 100-114, 9/15/ 2015.
[39] G. Ferrari and M. Amabili, "Active vibration control of a sandwich plate by non-collocated positive position feedback," *Journal of Sound and Vibration,* vol. 342, pp. 44-56, 2015.
[40] W. K. Miao, M. L. Xu, and C. S. Wu, "Active vibration control of cantilever beam using MFC sensor and actuator A2 - Ye, Lin," in *Recent Advances in Structural Integrity Analysis - Proceedings of the International Congress (APCF/SIF-2014)*Oxford: Woodhead Publishing, 2014, pp. 447-452.
[41] I. Boiko, *Non-parametric tuning of PID controllers*. Springer, 2013.
[42] I. Nakić, Z. Tomljanović, and N. Truhar, "Optimal Direct Velocity Feedback," *Applied Mathematics and Computation,* vol. 225, pp. 590-600, 12/1/ 2013.
[43] M. J. Balas, "Direct velocity feedback control of large space structures," *Journal of Guidance, Control, and Dynamics,* vol. 2, no. 3, pp. 252-253, 1979.
[44] M. Serrand and S. J. Elliott, "MULTICHANNEL FEEDBACK CONTROL FOR THE ISOLATION OF BASE-EXCITED VIBRATION," *Journal of Sound and Vibration,* vol. 234, no. 4, pp. 681-704, 2000/07/20 2000.
[45] A. Preumont, *Vibration control of active structures: an introduction*. Springer Science & Business Media, 2011.
[46] P. Gardonio and S. J. Elliott, "Modal response of a beam with a sensor–actuator pair for the implementation of velocity feedback control," *Journal of Sound and Vibration,* vol. 284, no. 1–2, pp. 1-22, 6/7/ 2005.
[47] M. K. Kwak and S. Heo, "Active vibration control of smart grid structure by multiinput and multioutput positive position feedback controller," *Journal of Sound and Vibration,* vol. 304, no. 1–2, pp. 230-245, 7/10/ 2007.
[48] K. Sang-Myeong, W. Semyung, and J. B. Michael, "Comparison of negative and positive position feedback control of a flexible structure," *Smart Materials and Structures,* vol. 20, no. 1, p. 015011, 2011.
[49] J. Fanson and T. K. Caughey, "Positive position feedback control for large space structures," *AIAA journal,* vol. 28, no. 4, pp. 717-724, 1990.
[50] C. C. Fuller, S. Elliott, and P. A. Nelson, *Active control of vibration*. Academic Press, 1996.
[51] C. Goh and T. Caughey, "On the stability problem caused by finite actuator dynamics in the collocated control of large space structures," *International Journal of Control,* vol. 41, no. 3, pp. 787-802, 1985.
[52] M. I. Friswell and D. J. Inman, "The relationship between positive position feedback and output feedback controllers," *Smart Materials and Structures,* vol. 8, no. 3, p. 285, 1999.
[53] M. K. Kwak and D.-H. Yang, "Dynamic modelling and active vibration control of a submerged rectangular plate equipped with piezoelectric sensors and actuators," *Journal of Fluids and Structures,* vol. 54, pp. 848-867, 4// 2015.

[54] H. Zumbahlen, *Linear circuit design handbook*. Newnes, 2011.
[55] A. Williams, *Analog filter and circuit design handbook*. McGraw Hill Professional, 2013.
[56] K. Uchino, "Introduction to piezoelectric actuators and transducers," DTIC Document2003.
[57] B. Jaffe, *Piezoelectric ceramics*. Elsevier, 2012.
[58] J.-J. Tzen, S.-L. Jeng, and W.-H. Chieng, "Modeling of piezoelectric actuator for compensation and controller design," *Precision Engineering,* vol. 27, no. 1, pp. 70-86, 1// 2003.
[59] E. Hughes, J. Hiley, K. Brown, and I. M. Smith, *Hughes electrical and electronic technology*. Pearson education, 2008.
[60] M. Plonus, "Chapter 4 - Semiconductor Diodes and Transistors," in *Electronics and Communications for Scientists and Engineers*San Diego: Academic Press, 2001, pp. 111-153.
[61] K.-H. Jeong and J.-W. Kim, "Free vibration analysis of liquid-filled open rectangular containers," *Ocean Engineering,* vol. 99, pp. 72-84, 5/1/ 2015.
[62] M. P. Paidoussis, *Fluid-structure interactions: slender structures and axial flow*. Academic press, 1998.
[63] K. Ogata, *System dynamics*. Prentice Hall New Jersey, 1998.

Appendix - I. Detailed LabVIEW Program

This appendix details the entire LabVIEW program developed to conduct experimentation. In the following figures, sub-Vis have their icon in the corner of the figure, for identification in their respective top level VIs. The main 2 top level VIs are the data collection and user interface VI, running on the main computer, and the control system VI, running on the cRIO FPGA.

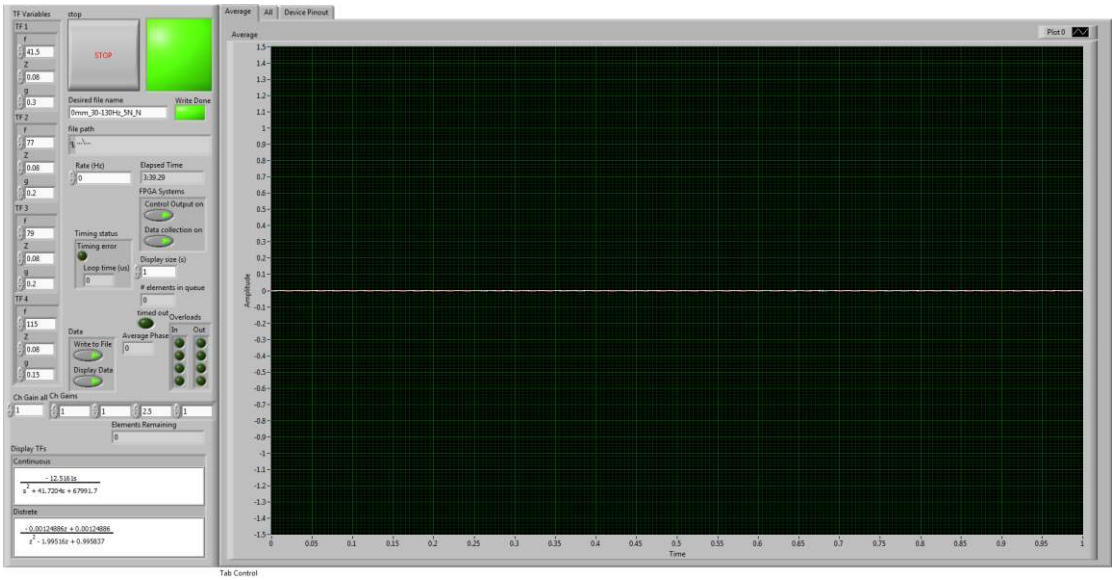

Appx Figure I-1 – Data collection and front end - User interface

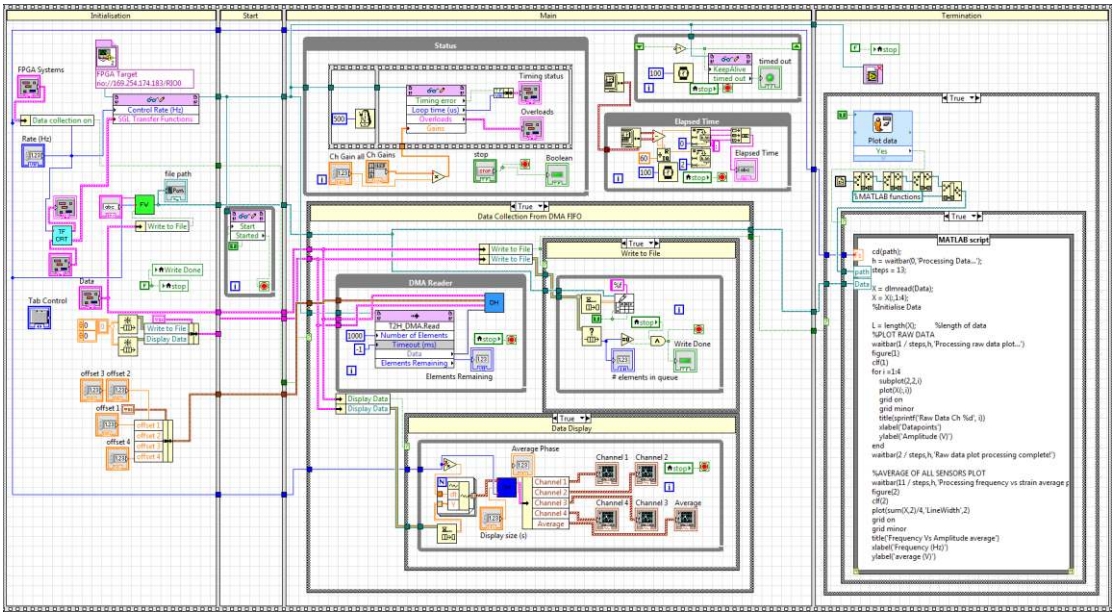

Appx Figure I-2 – Data collection and front end – entire top level program

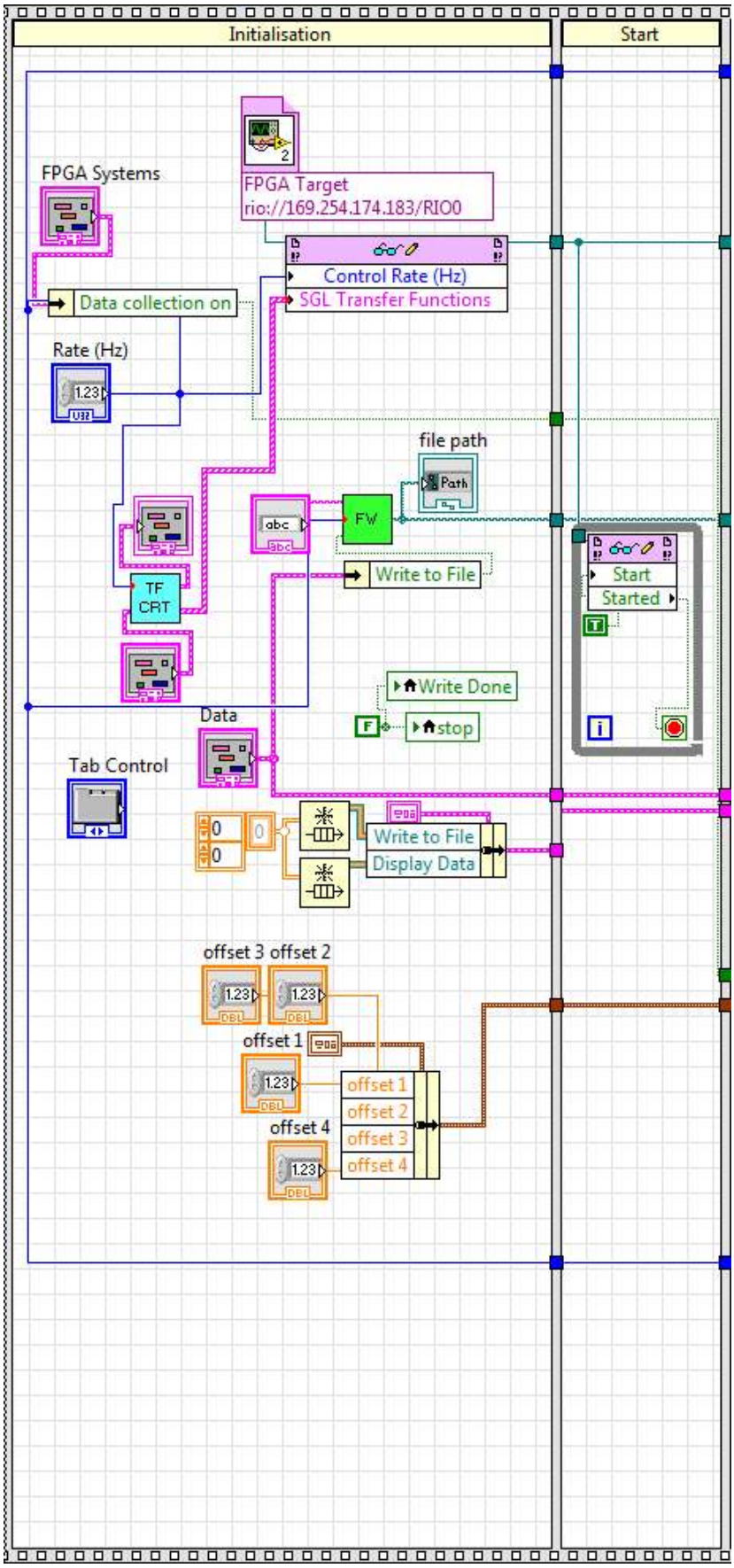

Appx Figure I-3 – Data collection and front end – Initialisation frames

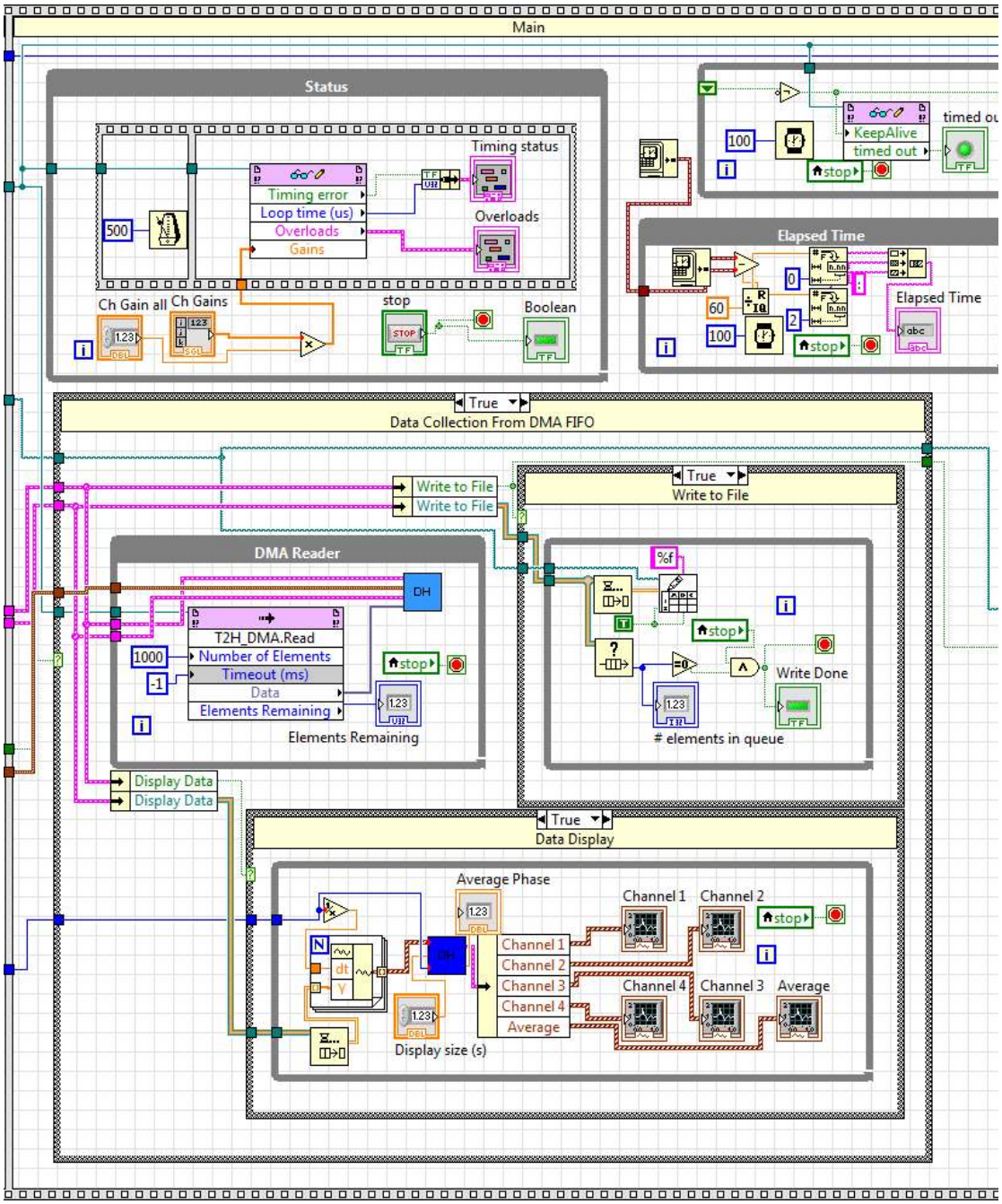

Appx Figure I-4 – Data collection and front end – Main frame

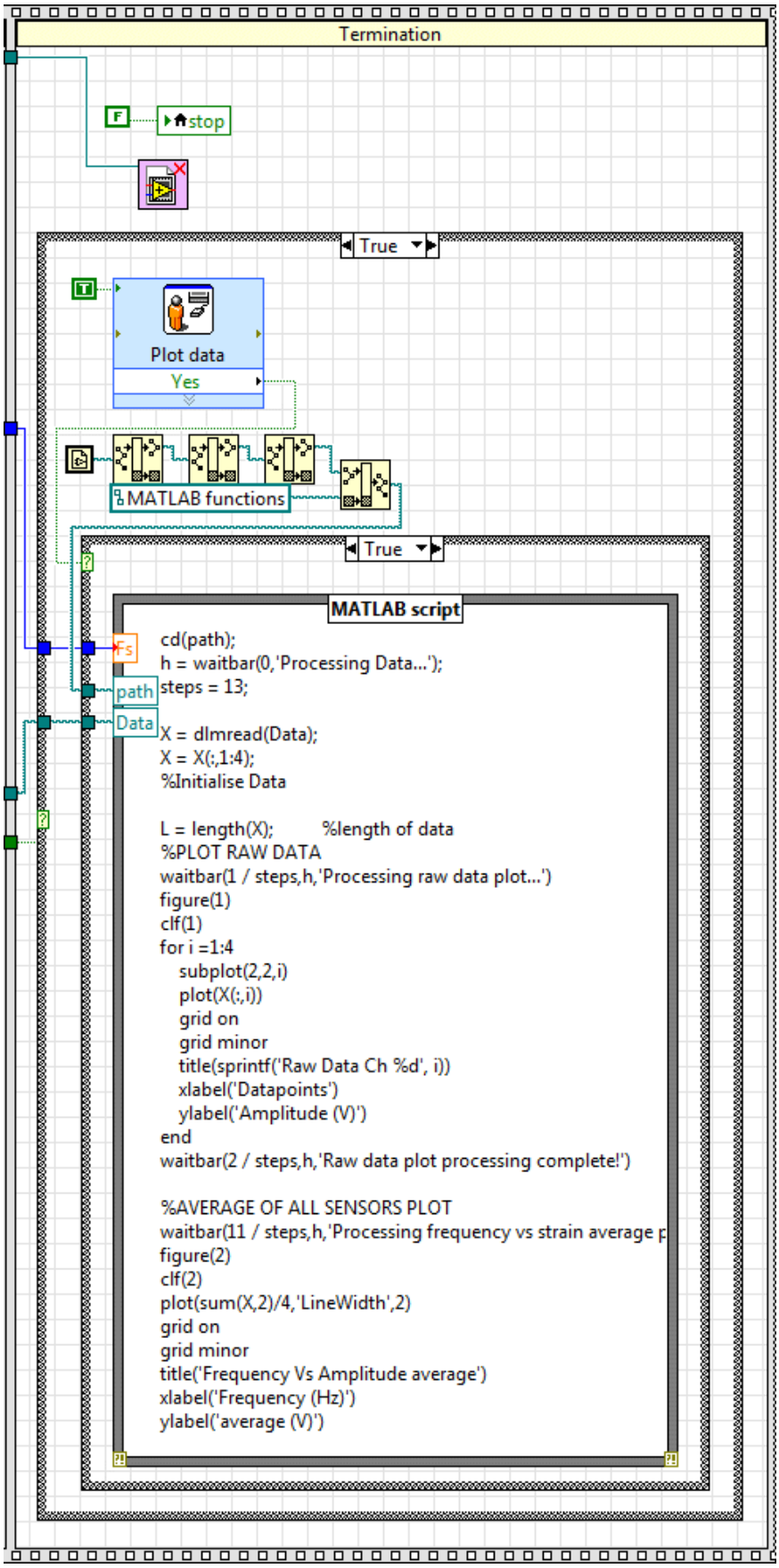

Appx Figure I-5 – Data collection and front end – Termination frame

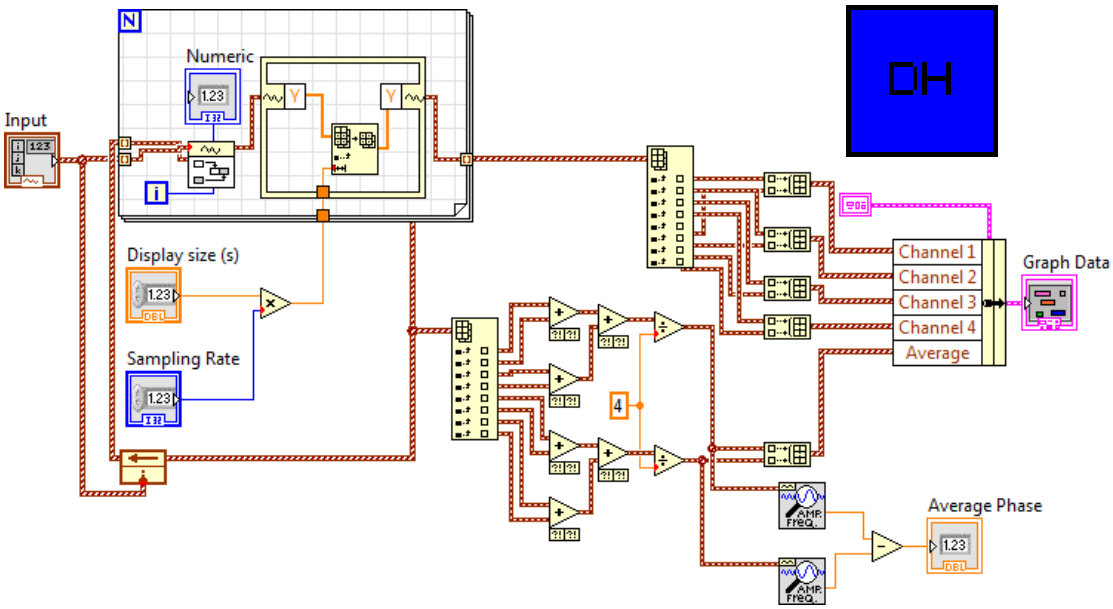

Appx Figure I-6 – Data collection and front end – Display handler SubVI

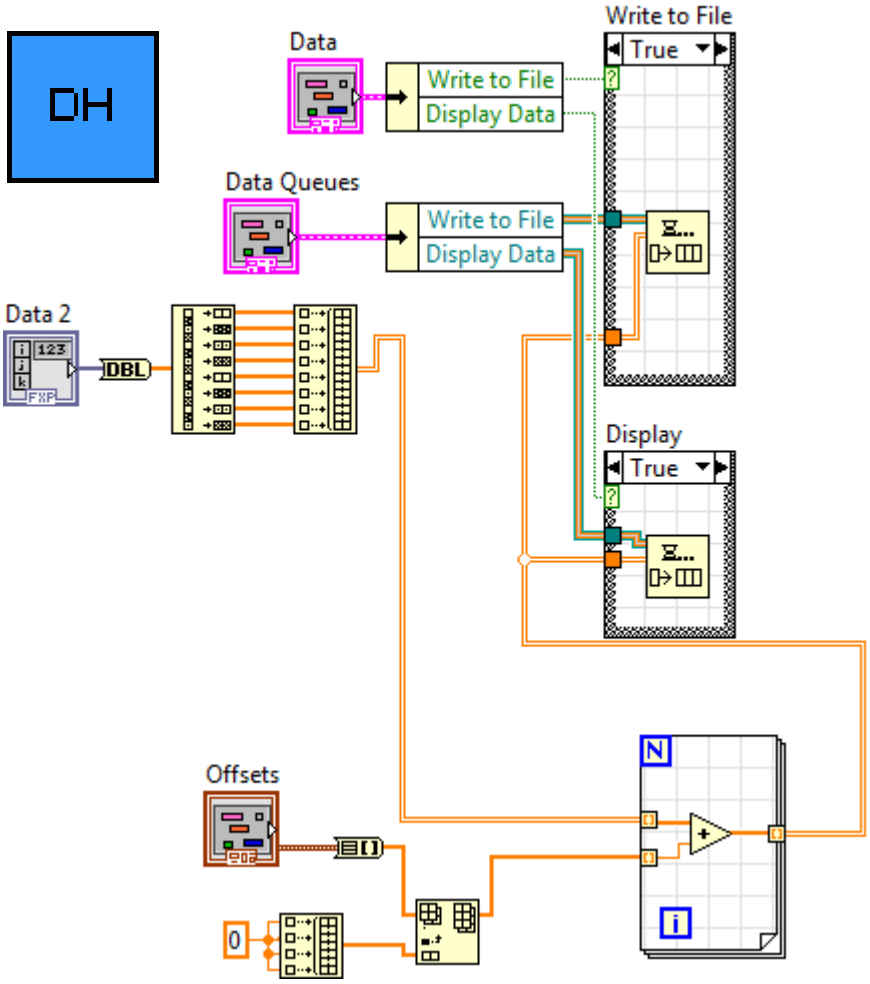

Appx Figure I-7 – Data collection and front end – Data handler SubVI

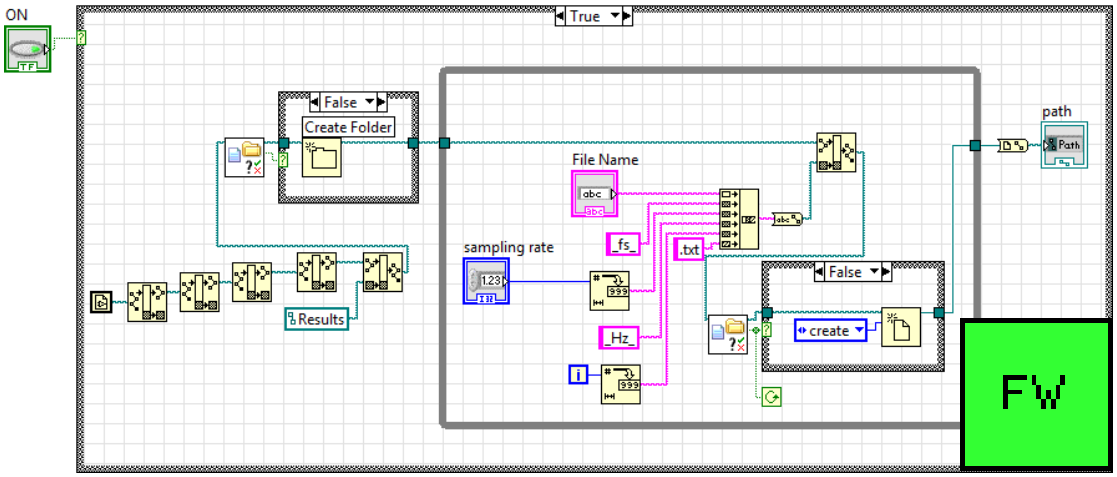

Appx Figure I-8 – Data collection and front end – File writing initialiser

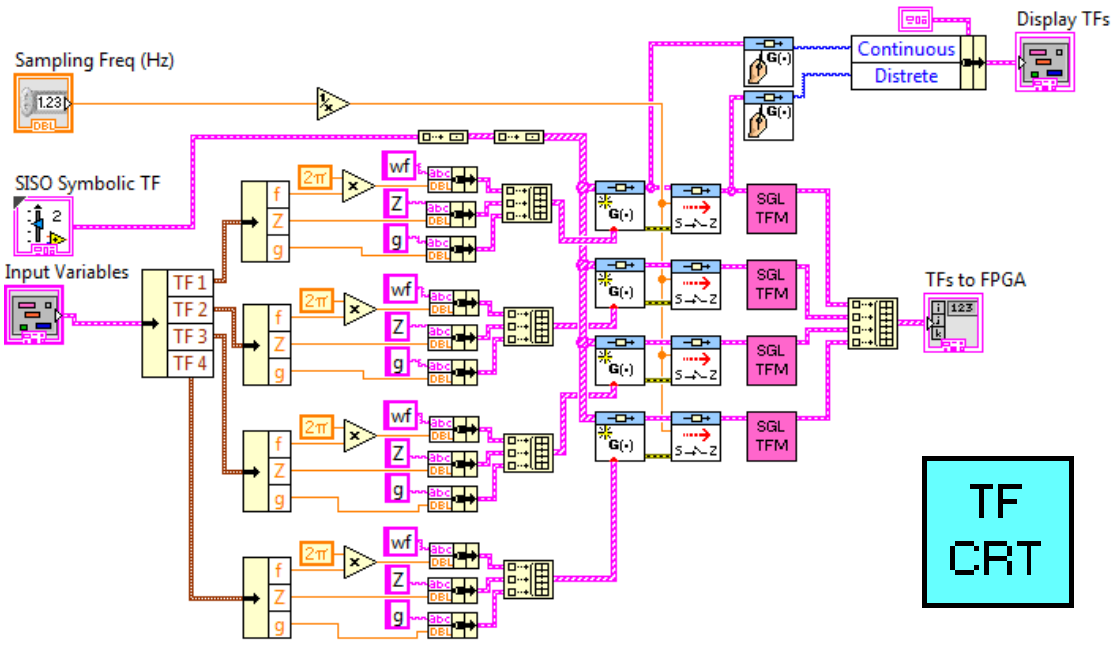

Appx Figure I-9 – Data collection and front end – Transfer function builder

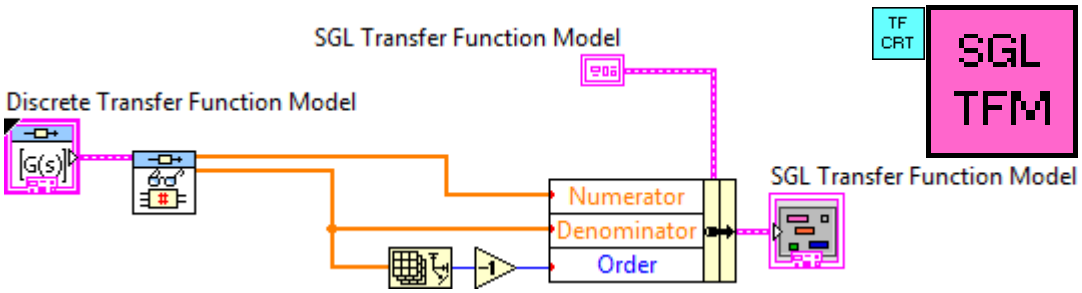

Appx Figure I-10 – Data collection and front end – Transfer function parsing

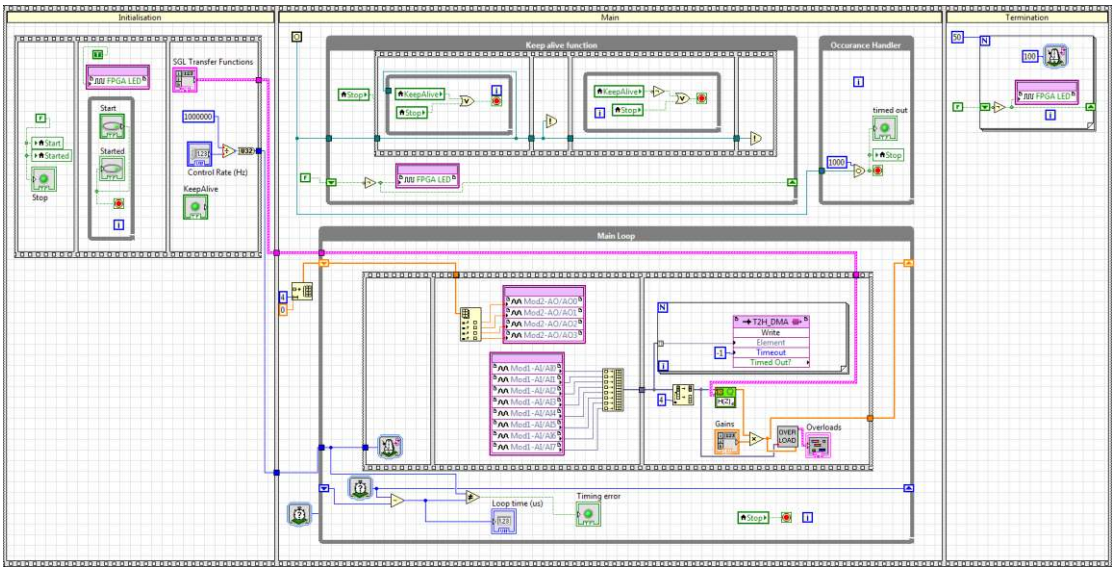

Appx Figure I-11 – Control system – Entire top level program

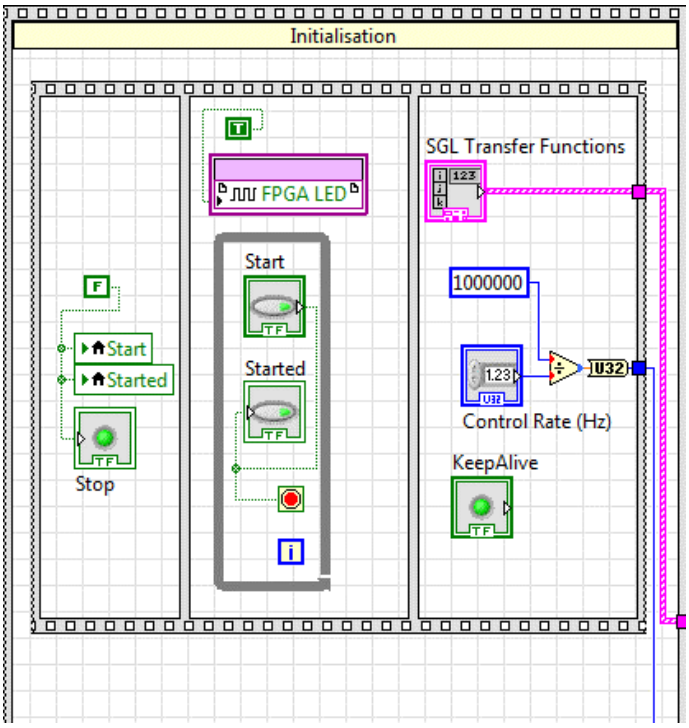

Appx Figure I-12 – Control system – Initialisation frame

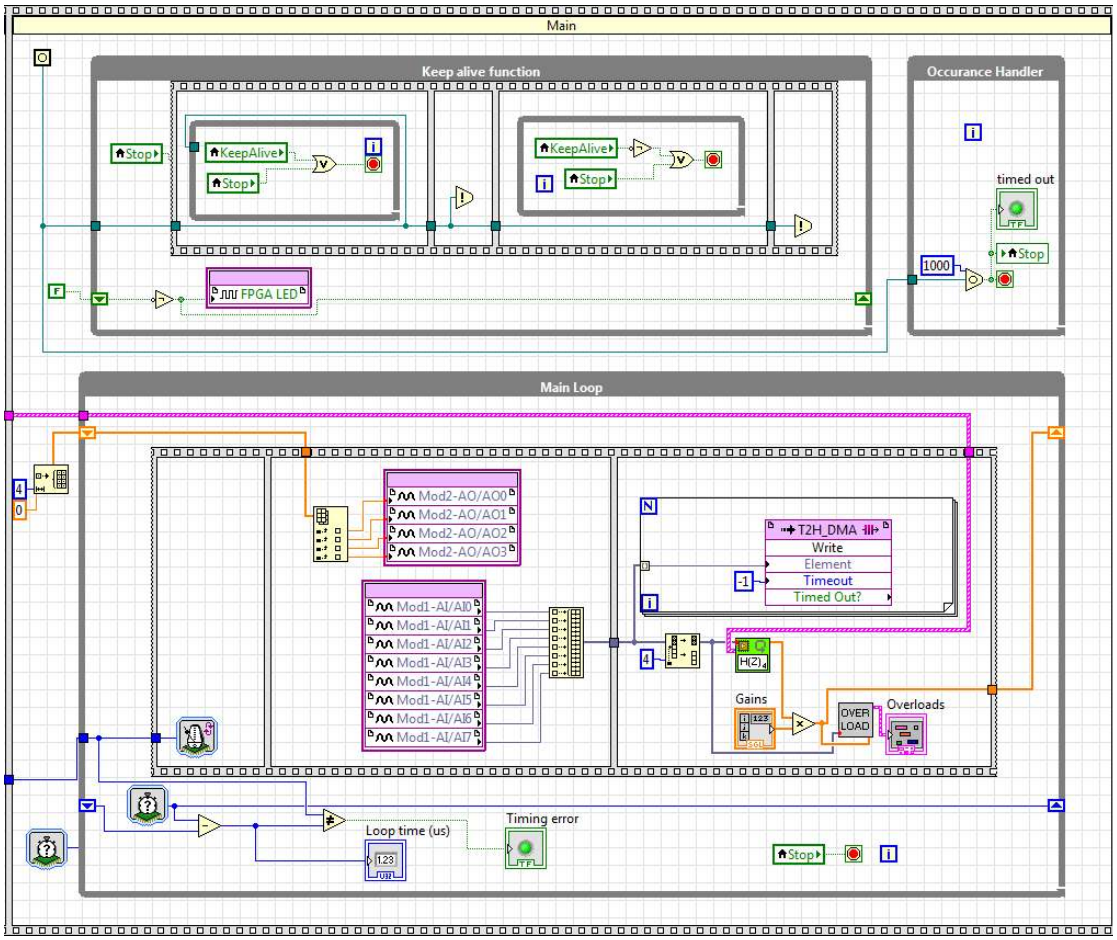

Appx Figure I-13 – Control system – Main frame

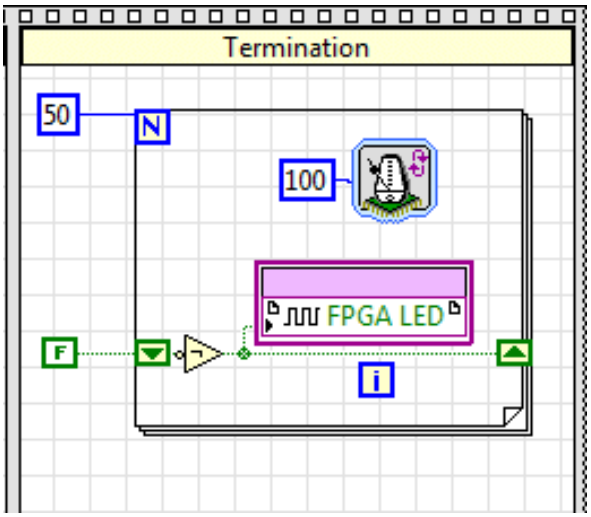

Appx Figure I-14 – Control system – Termination frame

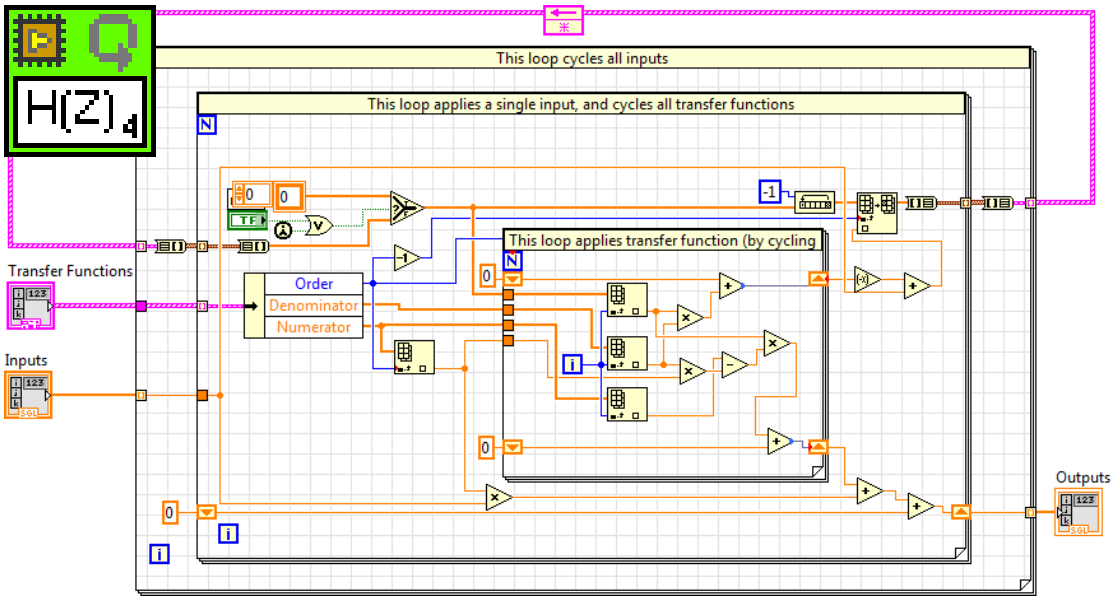

Appx Figure I-15 – Control system – Iterative MIMO transfer function application

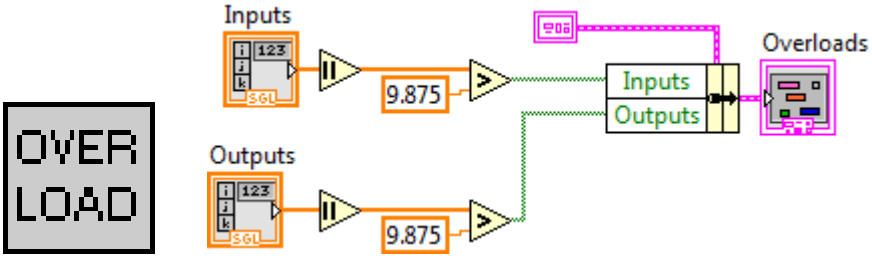

Appx Figure I-16 – Control system – Data overload handler

Appendix - II. Detailed MATLAB Program

In this appendix all relevant MATLAB code used to process the raw data is detailed. This includes the 'Main' program and all relevant subsequent functions. It can be noted that some of the functions called in Main are not included, as their functionality was not used directly in calculations or plotting for this thesis, for succinctness they were not included.

Main Function – Data processing and plotting

```
%% MAIN PROGRAM FOR DATA PROCESSING AND PLOTTING
tic
display('Preparing environment...')
addpath('C:\Users\jc763\Google Drive\Uni-Masters\LabVIEW\Results');
display('Done')
%check if data exists, prompt user to reload data or use existing
if (exist('X','var') || exist('Y','var'))
    InputCheck = 0;
    while (InputCheck == 0)
        Reload = input('Data Loaded. Reload Data? (Y/N)? \n','s');
        InputCheck = strcmpi(Reload,'n') || strcmpi(Reload,'y');
    end
else
    Reload = 'y';
end

%load and calculate all data
if (strcmpi(Reload,'y'))
    %Load in data from experiment
    [X,Y] = LoadData;
    toc
    %Set frequency range for plots
    Freq = FreqRange(X,Y);
    toc
    %Find Magnitudes from data
    [MagX,MagXav,MagXavS,MagY,MagYav,MagYavS,StrainFactor] =
MagCalc(X,Y);
    toc
    %phase plane calculations
    [PPX,PPY] = PhasePlaneCalc(X,Y,Freq);
    toc
end
close all
InputCheck = 0;
    while (InputCheck ~= 1:9)

        TxtInput{1} =  '1: Raw vs Freq, All chans & av \n';
        TxtInput{2} =  '2: Volt Vs Freq, All chans & av \n';
        TxtInput{3} =  '3: Strain Vs Freq Av \n';
        TxtInput{4} =  '4: Phase plane (Level Plots) \n';
        TxtInput{5} =  '5: Phase plane (Mode Plots) \n';
        TxtInput{6} =  '6: PDF  \n';
        TxtInput{7} =  '7: Dynamics Comparsison \n';
```

```
        TxtInput{8} =  '8: Effectiveness overall \n';
        TxtInput{9} =  '9: Mode movements \n';
        TxtInputFull = '';
        for i = 1:9
        TxtInputFull = strcat(TxtInputFull,TxtInput{i});
        end
        PlotType = input(strcat('Select Data to
Plot:\n',TxtInputFull));
        InputCheck = strcmpi(Reload,'n') || strcmpi(Reload,'y');
    end

    switch PlotType
        case 1
            %Plots Raw Data if user requests
            RawDataPlot(X, MagX, MagXav, Y, MagY, MagYav, Freq)
        case 2
            %plot magnitute vs frequency and all channels
            MagVFreqPlot(MagX, MagXav, MagY, MagYav, Freq)
        case 3
            %plot frequency vs average strain ((used in thesis))
            StrainVFreq(MagXavS, MagYavS,Freq)
        case 4
            %plot phase plane (water levels)
            PhasePlanePlot(PPX,PPY,StrainFactor)
        case 5
            %plot phase plane (modes collected) ((used in thesis))
            PhasePlanePlot2(PPX,PPY,StrainFactor)
        case 6
            % Plot PDF
            PDFplot(PPX,PPY,StrainFactor)
        case 7
            % Plot Dynamics comparison ((used in thesis))
            DynamicsPlot(MagXavS,Freq)
        case 8
            % Plot Overall Effectivenss ((used in thesis))
            Overall_Effectiveness
        case 9
            % Plot Mode Movement ((used in thesis))
            Mode_Movement
    end
display('Program complete!')


function [Uncontrolled,Controlled] = LoadData()
%LoadData
% Loads Data into Workspace
display('Loading data...')
load('Raw_Data_30to150Hz_10N_0to200mm_Sweep_at_5000Hz.mat')
display('Done!')
end

%EOF
```

Calculation Function – Magnitude calculation

```
function [MagX,MagXav,MagXavS,MagY,MagYav,MagYavS,StrainFactor] =
MagCalc(X,Y)
%MAGCALC Calculates Magnitudes of Data
%   finds all peaks then sets all values to peaks
%preallocate and initialise variables
MagData = cell(1,9);
AvMagData =cell(1,9);
AvStMagData = cell(1,9);

Cp = 3;
VoltRatio = 5/3;
d33 = 4.6E2;
Yc = 30.336;
lc = 85;
bc = 14;

display('Calculating Magnitude Data')
%cycle through X then Y data
for DataSetSelect = 1:2
    switch DataSetSelect
        case 1;             Data = X;
        case 2;             Data = Y;
    end

    %cycle through all water levels
    for WaterLevel = 1:9
        %check if data exists
        if ~isempty(Data{WaterLevel})
            %cycle through data channels
            for DataChannel = 1:4
                DataSet = Data{WaterLevel}(:,DataChannel);
                Mag = MagPks(DataSet);
                MagData{WaterLevel}(:,DataChannel) = Mag;
            end
            %calculate average
            AvData = sum((Data{WaterLevel}(:,1:4)),2)/4;
            AvMagData{WaterLevel} = MagPks(AvData);
            %calculate average strain
            TrueVolts = AvMagData{WaterLevel}*VoltRatio;
            Sq = d33*Yc*lc*bc;
            Strain = (TrueVolts*Cp)/Sq;
            StrainFactor = Cp/Sq*10E6;
            AvStMagData{WaterLevel} = Strain*10E6;
        end
    end
    switch DataSetSelect
        case 1
            MagX = MagData;
            MagXav = AvMagData;
            MagXavS = AvStMagData;
        case 2
            MagY = MagData;
            MagYav = AvMagData;
            MagYavS = AvStMagData;
    end
    clear Data MagData
end
```

```
display('Done')

end

function Mag = MagPks(Data)
%MAGPks Calculates Magnitudes of Data
%   finds all peaks then sets all values to peaks
L = length(Data);
for iFindPeaks = 1:2           %itterate 2 times for smoother results
    [pks,locs] = findpeaks(abs(Data));      %find location of peaks
    data_i = 1;                             %set data index to 1
    for peak_i = 1:length(locs)             %index peaks
        for data_i = data_i:locs(peak_i);   %set all values up to
peak as peak
            Data(data_i) = pks(peak_i);
        end
    end
    for data_i = data_i:L;
        Data(data_i) = pks(peak_i);
    end
end
Mag = Data;
for iSmoothing  = 1:4         %itterate 2 times for smoother results
Mag = smooth(Mag,700);        %smooth data
end
end
 %EOF
```

Calculation Function – Frequency range data

```
function Freq = FreqRange(X,~)
%FREQRANGE Set frequency range based off experimental data
%   Detailed explanation goes here
Freq = cell(1,9);
Frange{1} = [36.6, 122];    %0mm
Frange{2} = [39, 112.3];    %25mm
Frange{3} = [38.5, 112.3];  %50mm
Frange{4} = [41, 115];     %75mm
Frange{5} = [24, 122.5];    %100mm
Frange{6} = [40, 120];     %125mm
Frange{7} = [30, 99];    %150mm
Frange{8} = [23, 111];       %175mm
Frange{9} = [34, 100];       %200mm

for n = 1:9
Freq{n} = linspace(min(Frange{n}), max(Frange{n}), length(X{n}));
end
```

Calculation Function – Phase plane calculation

```
function [PPX,PPY] = PhasePlaneCalc(X,Y,Freq)
% the 2 datasets, then an average frequency set
PPData = cell(4,9);
display('Calculating Phase Plane Data')
%get mode data
ModeData = ModeDataTable();
%cycle through X then Y data
for DataSetSelect = 1:2
    switch DataSetSelect
        case 1
            Data = X;
        case 2
            Data = Y;
    end

    %cycle through all water levels
    for WaterLevel = 1:size(Data,2)
        %set modal frequencies for each water level
        w(1:4) = ModeData.Loc(WaterLevel,:);

        %check if data exists
        if ~isempty(Data{WaterLevel})
            %cycle through data channels
            f = Freq{WaterLevel};
            for DataChannel = 1:4
                DataSet = Data{WaterLevel}(:,DataChannel);
                [PP] = PhasePlane(DataSet,w,f);
                PPData{DataChannel,WaterLevel} = PP;
            end
        end
    end
    clear Data
    switch DataSetSelect
        case 1
            PPX = PPData;
        case 2
            PPY = PPData;
    end
    clear Data FreqData
end
display('Done')
%EOF
end

function [PP] = PhasePlane(DataSet,w,FreqSet)
%Phase Plane calculations for each dataset
WinSize = 200;
PP = cell(4,2);
%find windowed data for phase plane of mode 1-4 from given freq
for Mode = 1:4
    index = find(FreqSet>=w(Mode),1);
    Data = DataSet((index-WinSize):(index+WinSize));
    freq = FreqSet((index-WinSize):(index+WinSize));

    Fs = 5000;
    Ts = 1/Fs;
    time = zeros(1,length(Data));
```

```
    time(1) = 0;
    for i = 2:length(Data)
        time(i) = time(i-1)+Ts;
    end

    avg = 0;
    DataCor = Data-avg;

    %FRF plot, phase planes, timetraces
    velocity = zeros(1,length(Data));
    for i = 1:length(freq)
        %range = round(i*n_points-((n_points-1))):round(i*n_points);
        range = i;
        velocity(range) = DataCor(range)*2*pi*freq(i);
    end
    num_vel = diff(DataCor)./diff(time');

    [acor,lag] = xcorr(num_vel,velocity);
    [~,I] = max(abs(acor));
    lagDiff = abs(lag(I));
    DiffXCor = velocity(lagDiff:end);

    PP{Mode,1} = DataCor;
    PP{Mode,2} = DiffXCor;
end
end
 %EOF
```

Calculation Function – Modal data table

```
function ModeData = ModeDataTable()
%MODELOCS Table of data
%
ModeData.Loc(1,:) = [51.9     76.5    76.5    107     ];  %0mm
ModeData.Loc(2,:) = [51.1     73.0    73.0    103.5   ];  %25mm
ModeData.Loc(3,:) = [50.8     82.0    82.0    99.5    ];  %50mm
ModeData.Loc(4,:) = [50.1     75.4    82.4    97.8    ];  %75mm
ModeData.Loc(5,:) = [49.0     71.0    76.1    96.2    ];  %100mm
ModeData.Loc(6,:) = [48.7     67.8    77.0    95      ];  %125mm
ModeData.Loc(7,:) = [48.5     59.0    70.5    94.7    ];  %150mm
ModeData.Loc(8,:) = [47.8     68.1    73.4    91.9    ];  %175mm
ModeData.Loc(9,:) = [45.6     62.5    70.9    87      ];  %200mm

ModeData.Val(1,:) = [2.32   0.68    0.68    1.61];  %0mm
ModeData.Val(2,:) = [1.71   0.68    0.68    1.17];  %25mm
ModeData.Val(3,:) = [1.82   0.73    0.73    1.03];  %50mm
ModeData.Val(4,:) = [1.36   0.53    0.97    0.92];  %75mm
ModeData.Val(5,:) = [0.61   1.11    0.75    1.52];  %100mm
ModeData.Val(6,:) = [0.50   0.57    0.95    0.77];  %125mm
ModeData.Val(7,:) = [0.54   0.68    1.41    1.22];  %150mm
ModeData.Val(8,:) = [0.63   0.56    0.77    1.05];  %175mm
ModeData.Val(9,:) = [0.74   1.45    0.81    0.90];  %200mm

%EOF
```

Plotting Function – Strain vs. frequency plots

```
function StrainVFreq(MagXavS, MagYavS,Freq)
%STRAINVFREQ
% plot frequency vs average strain
%RAWPLOT plots all 4 chanels of data, and averages
%   Detailed explanation goes here
%DATA PLOTTING%
display('Plotting all data chans and average')
%cycle all levels
for LevelNum = 1:9
    %set water levels for each index for legend naming, and axis
limits
    switch LevelNum
        case 1;             Level = 0;       Lim{LevelNum} = [40 120];
        case 2;             Level = 25;      Lim{LevelNum} = [40 110];
        case 3;             Level = 50;      Lim{LevelNum} = [40 110];
        case 4;             Level = 75;      Lim{LevelNum} = [35 85];
        case 5;             Level = 100;     Lim{LevelNum} = [40 100];
        case 6;             Level = 125;     Lim{LevelNum} = [50 92];
        case 7;             Level = 150;     Lim{LevelNum} = [40 99];
        case 8;             Level = 175;     Lim{LevelNum} = [40 85];
        case 9;             Level = 200;     Lim{LevelNum} = [40 95];
    end

    %set changing variable to current datasets
    MgXavS = MagXavS{LevelNum};
    MgYavS = MagYavS{LevelNum};
    Fq = Freq{LevelNum};

    %check if controlled data is empty, then set name
    if mod(LevelNum,2)
        FigTitle = (sprintf('%dmm Controlled Vs Uncontrolled Average
Strain',Level));
    else
        FigTitle = (sprintf('%dmm Uncontrolled Average
Strain',Level));
    end
    figure('Name',FigTitle,'NumberTitle','off');
    suptitle(FigTitle)

    %plot averages
    plot(Fq,MgXavS,'LineWidth',2)
    if mod(LevelNum,2)
        hold on
        plot(Fq,MgYavS,'LineWidth',2);
        hold off
        legend('uncontrolled','controlled')
    end
    xlim(Lim{LevelNum})
    title('Average')
    xlabel('Frequency (Hz)')
    ylabel('Strain (\mu\epsilon)')
    grid on
    grid minor
end

display('All plots complete!')
%EOF
end
```

Plotting Function – Phase plane plots at each mode

```
function PhasePlanePlot2(PPX,PPY,StrainFactor)
%PHASEPLANEPLOT Summary of this function goes here
display('Plotting Phase Plane Data')
%cycle control type
%cycle water levels (and figures)
for WaterLevel = 1:9
    %initialise and name plot
    switch WaterLevel
        case 1;             Level = 0;
        case 2;             Level = 25;
        case 3;             Level = 50;
        case 4;             Level = 75;
        case 5;             Level = 100;
        case 6;             Level = 125;
        case 7;             Level = 150;
        case 8;             Level = 175;
        case 9;             Level = 200;
    end
    %cycle mode shapes (and subplots)
    for Mode = 1:4
        %initialise data size for plot
        DataL = zeros(2,4);

        for Channel = 1:4
            DataL(1,Channel) =
length(PPX{Channel,WaterLevel}{Mode,2});
            DataL(2,Channel) =
length(PPY{Channel,WaterLevel}{Mode,2});
        end
        DataSize = min(min(DataL));
        %cycle controlled and uncontrolled
        for Control = 1:2
            if (Control == 2 && mod(WaterLevel,2)) || Control == 1
                switch Control
                    case 1
                        PPdata = PPX;
                    case 2
                        PPdata = PPY;
                        hold on
                end
                AvStrain = 0;
                AvDStrain = 0;
                %cycle data channel
                for Channel = 1:4
                    Strain =
PPdata{Channel,WaterLevel}{Mode,1}*StrainFactor;
                    DStrain =
PPdata{Channel,WaterLevel}{Mode,2}*StrainFactor;
                    AvStrain = AvStrain + Strain(1:DataSize);
                    AvDStrain = AvDStrain + DStrain(1:DataSize);
                end
                AvStrain = AvStrain/4;
                AvDStrain = AvDStrain/4;

                PPplot{WaterLevel,Mode,Control}.AvS = AvStrain;
                PPplot{WaterLevel,Mode,Control}.AvSD = AvDStrain;
```

```
            end
        end
    end
 end
for Mode = 1:4
    FigTitle = (sprintf('Controlled Vs Uncontrolled Mode %d',Mode));
    figure('Name',FigTitle,'NumberTitle','off');
    PlotNum = 0;

    for WaterLevel = 1:9

        switch WaterLevel
            case 1;                 Level = 0;
            case 2;                 Level = 25;
            case 3;                 Level = 50;
            case 4;                 Level = 75;
            case 5;                 Level = 100;
            case 6;                 Level = 125;
            case 7;                 Level = 150;
            case 8;                 Level = 175;
            case 9;                 Level = 200;
        end

        if mod(WaterLevel,2)
            PlotNum = PlotNum +1;
            switch PlotNum
                case 1; subplot(2,3,1)
                case 2; subplot(2,3,2)
                case 3; subplot(2,3,3)
                case 4; subplot(2,3,4)
                case 5; subplot(2,3,5)
            end
            for Control = 1:2
                x = PPplot{WaterLevel,Mode,Control}.AvS;
                y = PPplot{WaterLevel,Mode,Control}.AvSD;
                plot(x,y)
                hold on
            end
            hold off
            title(sprintf('%d mm',Level))
            if PlotNum == 5
                hold on
                plot(0,'w-')
                plot(0,'w-')
                hold off
                xax = 'x = Strain (\mu\epsilon)';
                yax = 'y = Strain'' (\mu\epsilon'')';
                Lh = legend('Uncontrolled','Controlled',xax,yax);
            end
            grid on
            grid minor
        end
    end
    suptitle(FigTitle)
     Sh=subplot(2,3,6);
     Sp=get(Sh,'position');
     set(Lh,'position',Sp);
     delete(Sh);
```

```
end
```

Plotting Function – Dynamics shifting plot

```
function DynamicsPlot(MagXavS,Freq)
%DYAMICSPLOT Summary of this function goes here
%   Detailed explanation goes here
%DATA PLOTTING%
display('Plotting all data chans and average')
%cycle all levels

for FigNum = 1:7

    if FigNum == 1
        iNum = 1:5;
        FigTitle = ('%Water Levels 0mm-100mm');
        figure('Name',FigTitle,'NumberTitle','off');
    elseif FigNum == 2
        iNum = 6:9;
        FigTitle = ('%Water Levels 125mm-200mm');
        figure('Name',FigTitle,'NumberTitle','off');
    else
        iNum = 1:9;
        if      FigNum == 3;   FigTitle = ('Water Levels 0mm-200mm');
        elseif  FigNum == 4;   FigTitle = ('Water Levels 0mm-200mm
Mode 1');
        elseif  FigNum == 5;   FigTitle = ('Water Levels 0mm-200mm
Mode 2');
        elseif  FigNum == 6;   FigTitle = ('Water Levels 0mm-200mm
Mode 3');
        elseif  FigNum == 7;   FigTitle = ('Water Levels 0mm-200mm
Mode 4');
        end
        figure('Name',FigTitle,'NumberTitle','off');
    end

    for LevelNum = iNum
        Colour  = Colourselect(LevelNum);
        MgXavS  = MagXavS{LevelNum};
        Fq      = Freq{LevelNum};
        DtRange = FindRange(Fq,LevelNum);


plot(Fq(DtRange),MgXavS(DtRange),'LineWidth',3,'color',Colour)
        hold on
    end
    hold off

    if FigNum == 1;         legend('0mm','25mm','50mm','75mm','100mm')
    elseif FigNum ==2;      legend('125mm','150mm','175mm','200mm')
    else

legend('0mm','25mm','50mm','75mm','100mm','125mm','150mm','175mm','20
0mm')
        if FigNum == 3;            xlim([41 115])    %all modes
        elseif FigNum == 4;        xlim([41 55])     %mode 1
        elseif FigNum == 5;        xlim([55 85])     %mode 2
        elseif FigNum == 6;        xlim([65 85])     %mode 3
        elseif FigNum == 7;        xlim([84 115])    %mode 4
        end
    end
```

```
    ModeData = ModeDataTable();
    ModeLoc = ModeData.Loc;

    hold on
    for LevelNum = iNum
        Colour = Colourselect(LevelNum);
        Modes = FigModeSelect(FigNum);

        for ModeNum = Modes
            plot([ModeLoc(LevelNum,ModeNum)
ModeLoc(LevelNum,ModeNum)],[0 2.5],':','linewidth',2,'color',Colour)
        end
    end
    hold off
    title(FigTitle)
    xlabel('Frequency (Hz)')
    ylabel('Strain (\mu\epsilon)')
    grid on
    grid minor
end

display('All plots complete!')
%EOF
end
function DtRange = FindRange(Fq,LevelNum)
switch LevelNum
    case 1; Range = [41, 120];  %0mm
    case 2; Range = [41, max(Fq)];  %25mm
    case 3; Range = [41, max(Fq)];  %50mm
    case 4; Range = [41, 105];  %75mm
    case 5; Range = [45, 100];  %100mm
    case 6; Range = [41, 102];  %125mm
    case 7; Range = [41, max(Fq)];  %150mm
    case 8; Range = [41, 97];  %175mm
    case 9; Range = [41, max(Fq)];  %200mm
end
DtRange = find(Fq >= Range(1),1):find(Fq >= Range(2),1);
end
function Colour = Colourselect(LevelNum)
switch LevelNum
    case 1; Colour = [0   0   1  ];  %0mm
    case 2; Colour = [0.5 1   0  ];  %25mm
    case 3; Colour = [1   0.5 0  ];  %50mm
    case 4; Colour = [0.5 0   1  ];  %75mm
    case 5; Colour = [1   0   0  ];  %100mm
    case 6; Colour = [0   1   1  ];  %125mm
    case 7; Colour = [0   0   0.5];  %150mm
    case 8; Colour = [0.5 0   0  ];  %175mm
    case 9; Colour = [0   0.5 0  ];  %200mm
end
end
function Modes = FigModeSelect(FigNum)
switch FigNum
    case {1,2,3}; Modes = 1:4;
    case 4; Modes = 1;
    case 5; Modes = 2;
    case 6; Modes = 3;
    case 7; Modes = 4;
```

```
end
end
```

Plotting Function – Overall effectiveness at modes and water levels

```
function Overall_Effectiveness
WL(1,:) =   [21.55  17.65   17.65   12.42];   %0mm
WL(2,:) =   [19.78  13.70   13.70   13.59];   %50mm
WL(3,:) =   [11.48  8.11    5.33    9.87];    %100mm
WL(4,:) =   [18.52  10.29   12.06   18];   %150mm
WL(5,:) =   [13.51  15.17   13.58   30.00];   %200mm
for Mode = 1:4
    for dataNum = 1:5
        MD(Mode,dataNum) = WL(dataNum,Mode);
    end
end


FigTitle = 'Effectivenss at Each mode';
subplot(2,1,1)
for Level = 1:5
    plot(WL(Level,:),[1 2 3 4],':.','MarkerSize',25,'LineWidth',2)
    hold on
end
plot(mean(WL),[1 2 3 4],'-
-.','MarkerSize',30,'LineWidth',2,'color',[0 0.9 0.9])
hold off
legend('0mm','50mm','100mm','150mm','200mm','Average')
xlim([0 35])
ylim([0.9 4.1])
set(gca, 'YTick', [1 2 3 4])

title(FigTitle)
xlabel('% Reduction')
ylabel('Mode')
grid on

FigTitle = 'Effectivenss at Each Water Level';
subplot(2,1,2)
for Mode = 1:4
    plot(MD(Mode,:),[0 50 100 150
200],':.','MarkerSize',25,'LineWidth',2)
    hold on
end
plot(mean(MD),[0 50 100 150 200],'-
-.','MarkerSize',30,'LineWidth',2,'color',[0 0.9 0.9])
hold off
legend('Mode 1','Mode 2','Mode 3','Mode 4','Average')
xlim([0 35])
ylim([-5 205])
set(gca, 'YTick', [0 50 100 150 200])

title(FigTitle)
xlabel('% Reduction')
ylabel('Water Level (mm)')
grid on

%EOF
end
```

Plotting Function – Overall movement of modes

```
function Mode_Movement
%MODE_MOVEMENT Summary of this function goes here
%   Detailed explanation goes here
ModeData = ModeDataTable();
ModeLoc = ModeData.Loc;
ModeVal = ModeData.Val;

FigTitle = 'Modal Frequency Vs Water Level';
figure('Name',FigTitle,'NumberTitle','off');
for Mode = 1:4

plot(linspace(0,200,9),ModeLoc(1:9,Mode),':.','MarkerSize',25,'LineWi
dth',2)
    hold on
end
legend('Mode 1','Mode 2','Mode 3','Mode 4')
%xlim([0 35])
%ylim([0.9 4.1])
set(gca, 'XTick', linspace(0,200,9))
set(gca, 'YTick', linspace(40,110,15))
set(gca, 'YMinorGrid','on')
title(FigTitle)
ylabel('Frequency (Hz)')
xlabel('Water Level (mm)')
grid on

FigTitle = 'Modal Amplitude Vs Water Level';
figure('Name',FigTitle,'NumberTitle','off');
for Mode = 1:4

plot(linspace(0,200,9),ModeVal(1:9,Mode),':.','MarkerSize',25,'LineWi
dth',2)
    hold on
end
legend('Mode 1','Mode 2','Mode 3','Mode 4')
%xlim([0 35])
%ylim([0.9 4.1])
set(gca, 'XTick', linspace(0,200,9))
%et(gca, 'YTick', linspace(40,110,15))
set(gca, 'YMinorGrid','on')
title(FigTitle)
ylabel('Strain (\mu\epsilon)')
xlabel('Water Level (mm)')
grid on
%EOF
end
```

Appendix - III. Amplifier Case CAD Drawings

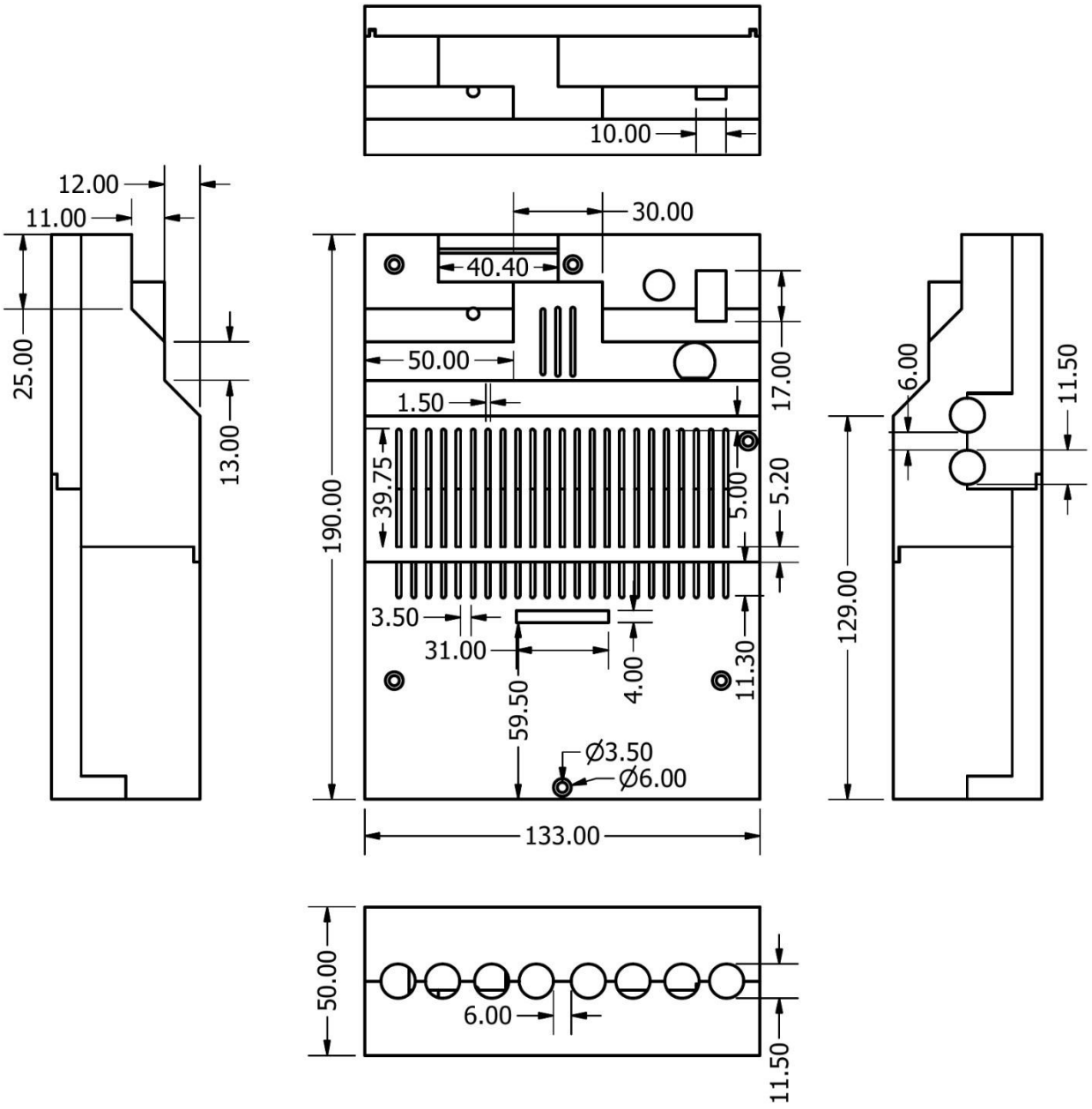

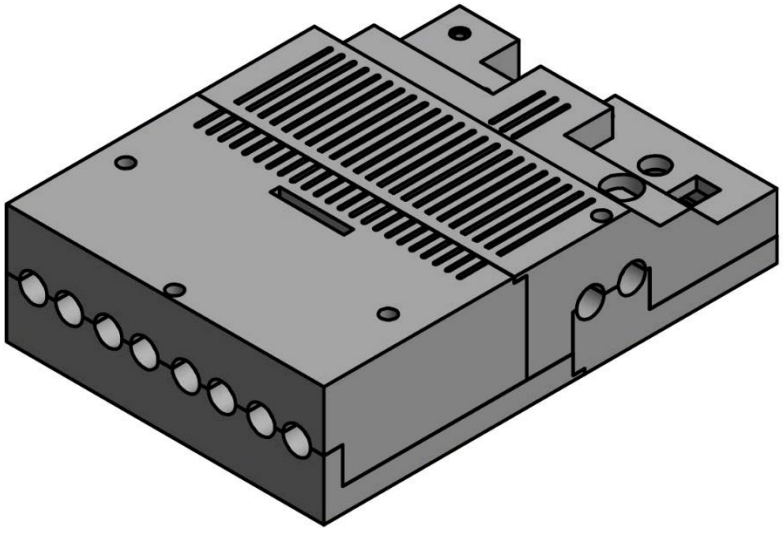

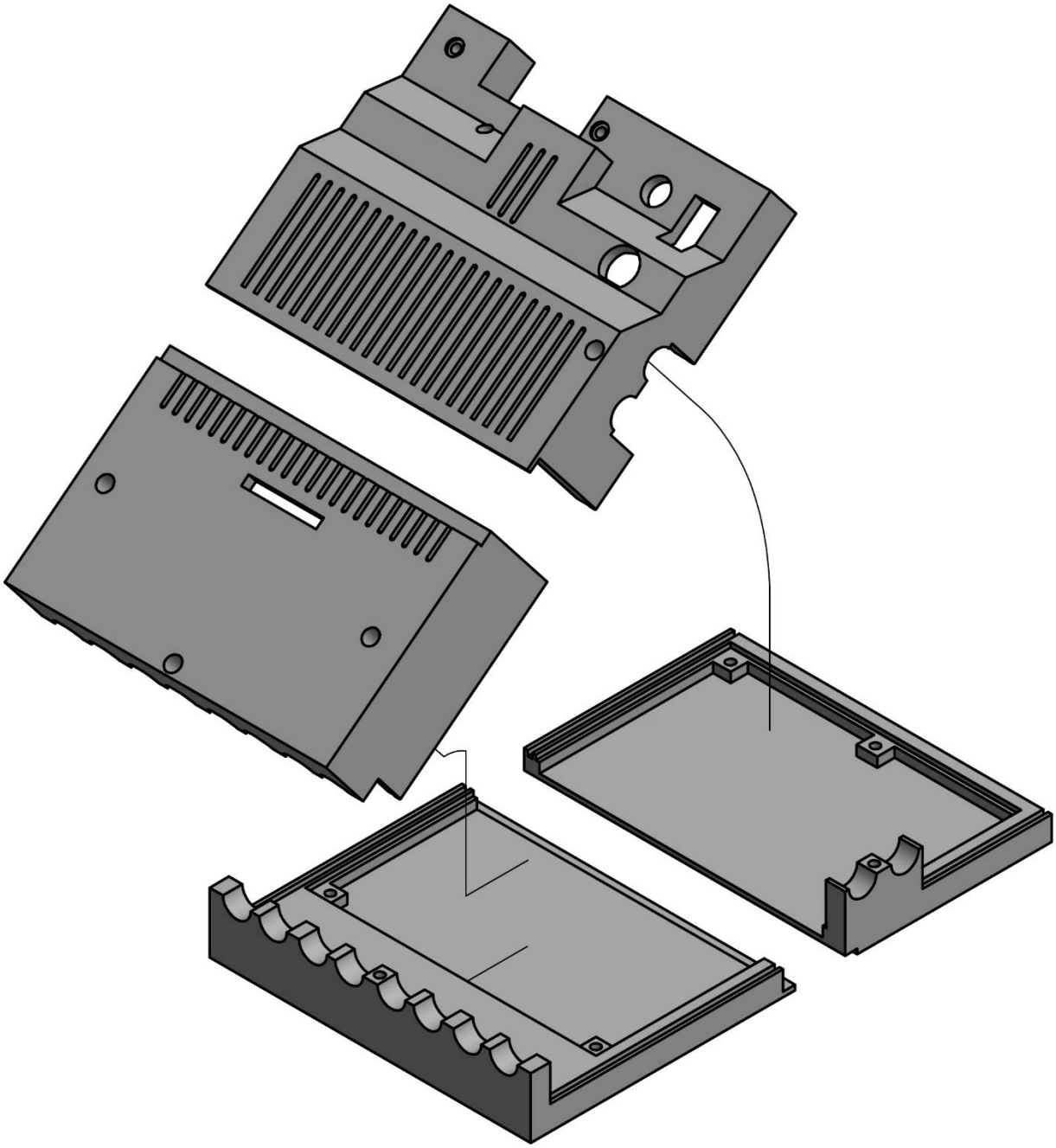

Appendix - IV. Amplifier PCB CAD Layout

PCB layout of amplifier designed to power piezoelectric patches, and connection diagrams.

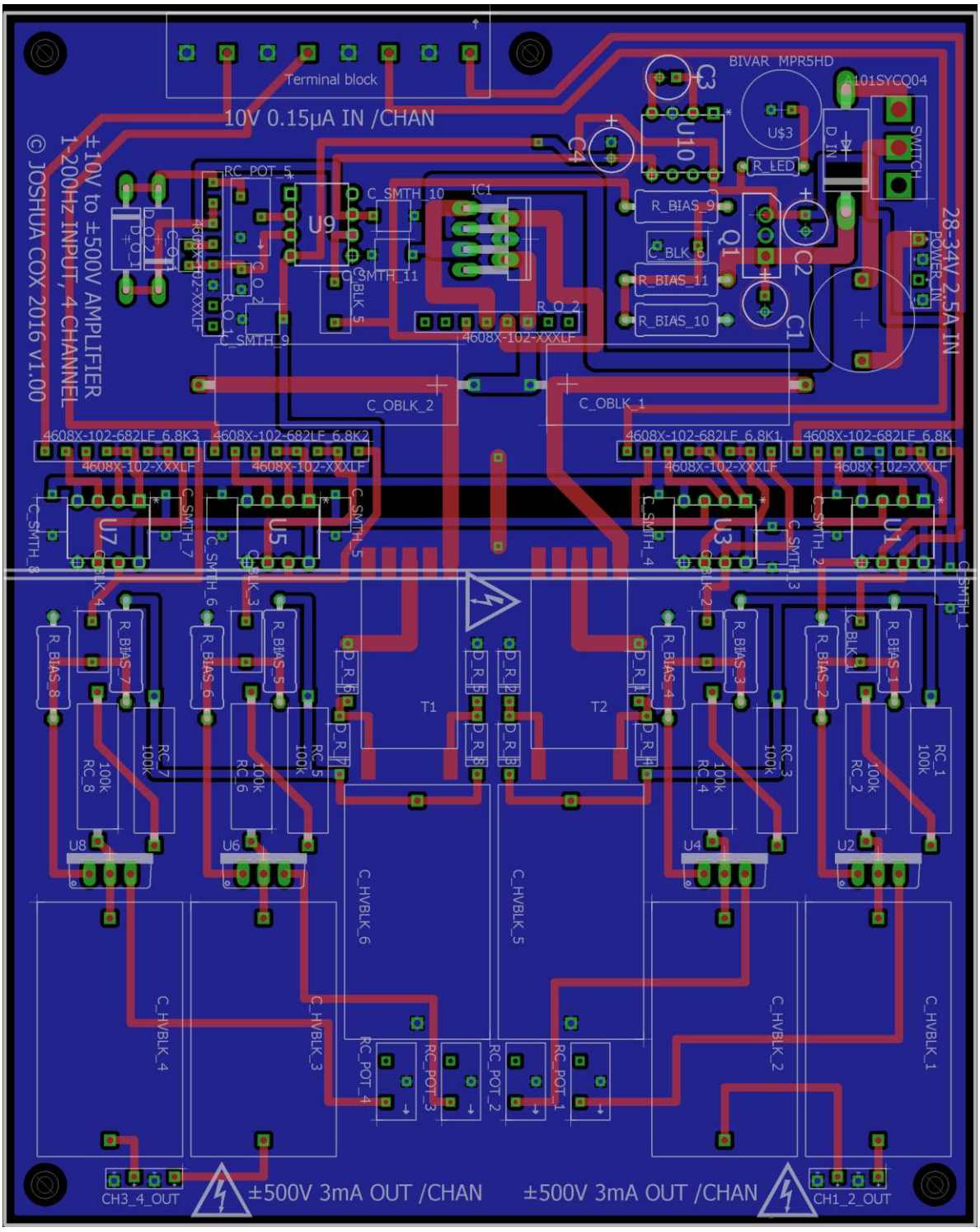

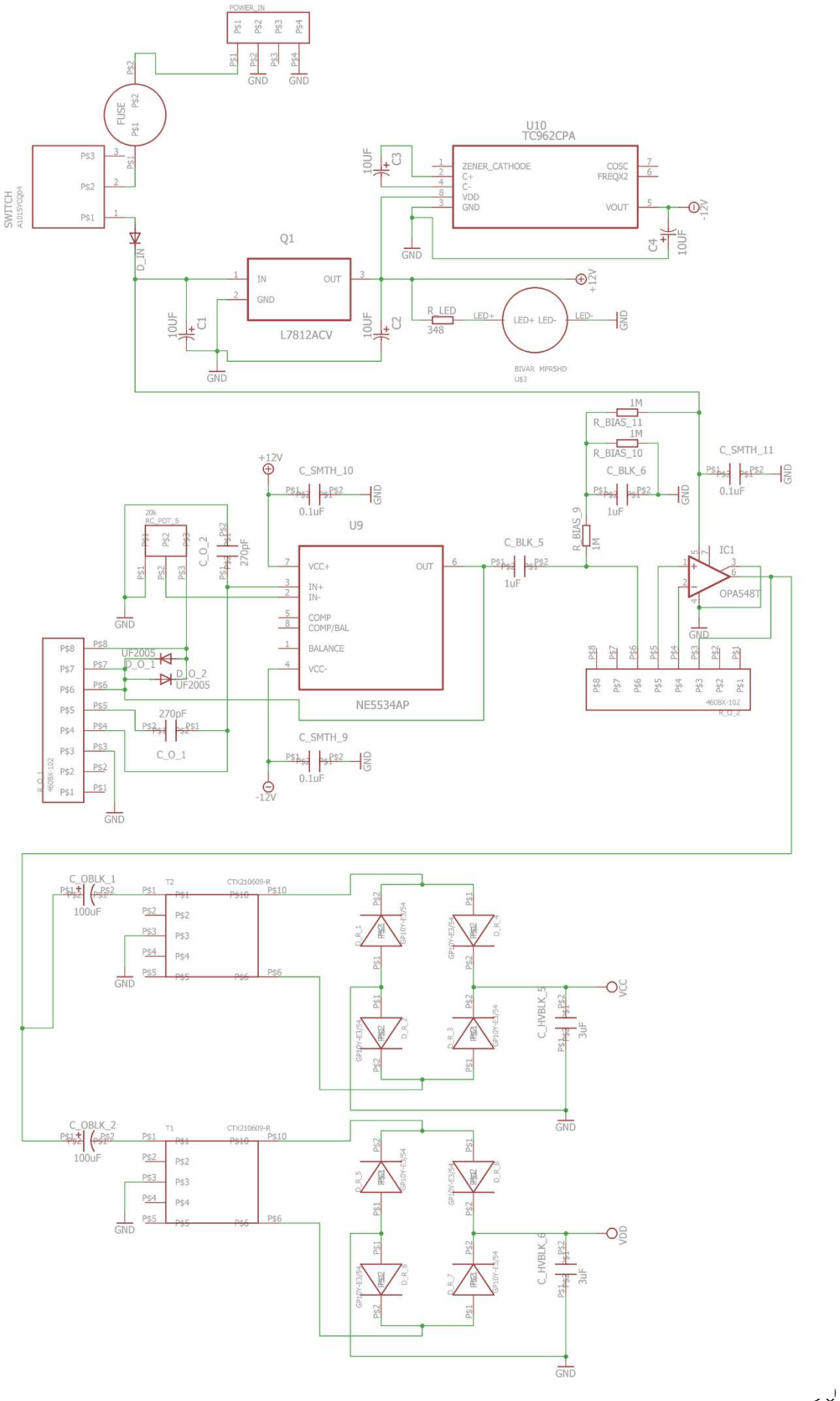
POWER_IN
FUSE
SWITCH
D_IN
Q1
L7812ACV
U10
TC962CPA
ZENER_CATHODE
COSC
FREQX2
VOUT
-12V
+12V
R_LED
348
BIVAR_MPR5HD
U$3
U9
NE5534AP
VCC+
OUT
IN+
IN-
COMP
COMP/BAL
BALANCE
VCC-
IC1
OPA548T
R_BIAS_11
R_BIAS_10
R_BIAS_9
C_BLK_6
C_BLK_5
C_SMTH_10
C_SMTH_11
C_SMTH_9
C_O_1
C_O_2
270pF
UF2005
D_O_1
D_O_2
20k
RC_POT_5
C_OBLK_1
C_OBLK_2
100uF
T1
T2
CTX210609-R
C_HVBLK_5
C_HVBLK_6
3uF
VCC
VDD
GND

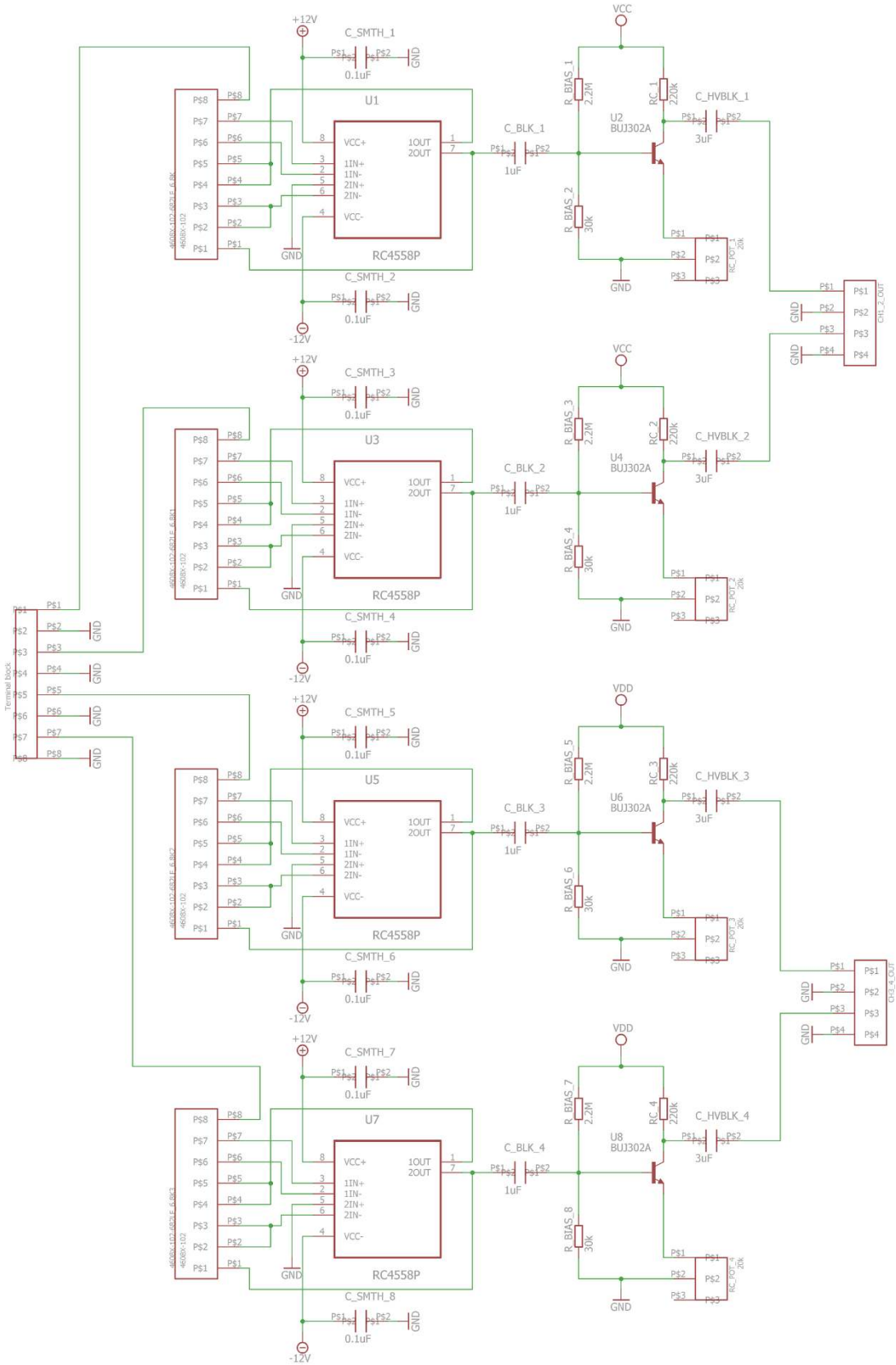
+12V
C_SMTH_1
0.1uF
GND
U1
RC4558P
VCC+
1OUT
2OUT
1IN+
1IN-
2IN+
2IN-
VCC-
C_SMTH_2
-12V
VCC
R_BIAS_1
2.2M
RC_1
220k
C_HVBLK_1
3uF
U2
BUJ302A
C_BLK_1
1uF
R_BIAS_2
30k
RC_POT_1
20k
CH1_2_OUT
C_SMTH_3
U3
C_SMTH_4
R_BIAS_3
RC_2
C_HVBLK_2
U4
C_BLK_2
R_BIAS_4
RC_POT_2
C_SMTH_5
U5
C_SMTH_6
VDD
R_BIAS_5
RC_3
C_HVBLK_3
U6
C_BLK_3
R_BIAS_6
RC_POT_3
CH3_4_OUT
C_SMTH_7
U7
C_SMTH_8
R_BIAS_7
RC_4
C_HVBLK_4
U8
C_BLK_4
R_BIAS_8
RC_POT_4
Termite block